4-28-1984

Proceedings of the 14th Annual Biochemical Engineering Symposium

Rakesh K. Bajpai
University of Missouri–Columbia

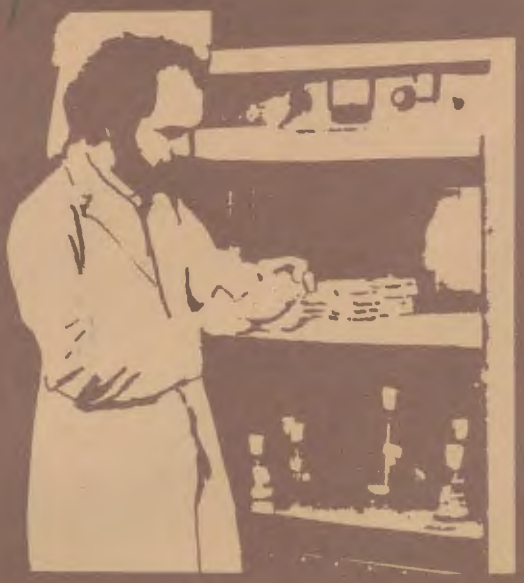

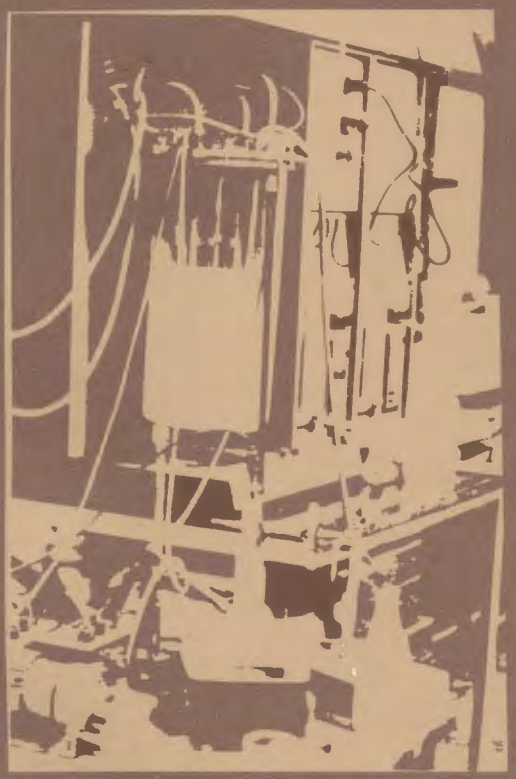

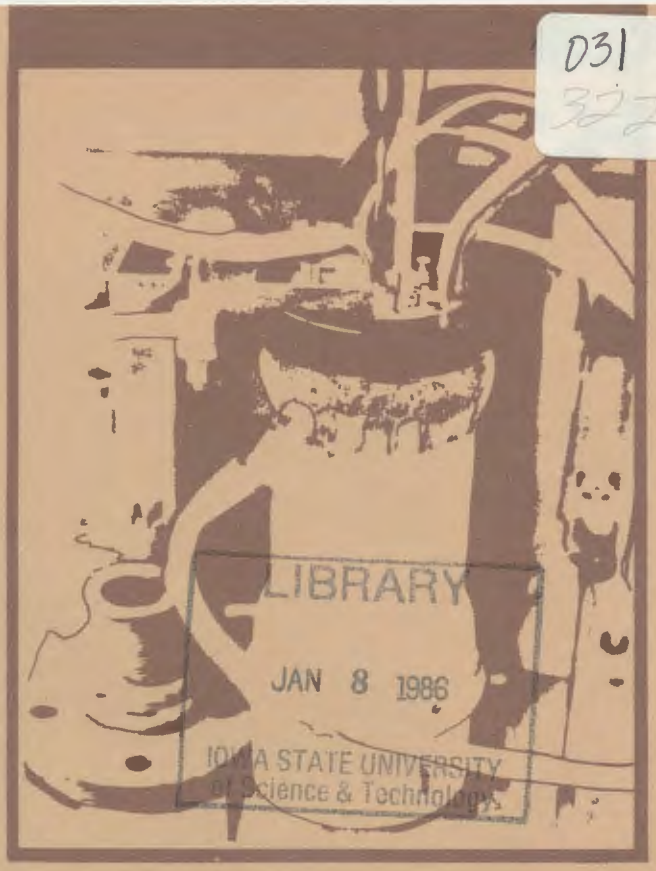

Proceedings of the 14th Annual

Biochemical Engineering Symposium

April 28, 1984
Department of Chemical Engineering
University of Missouri-Columbia

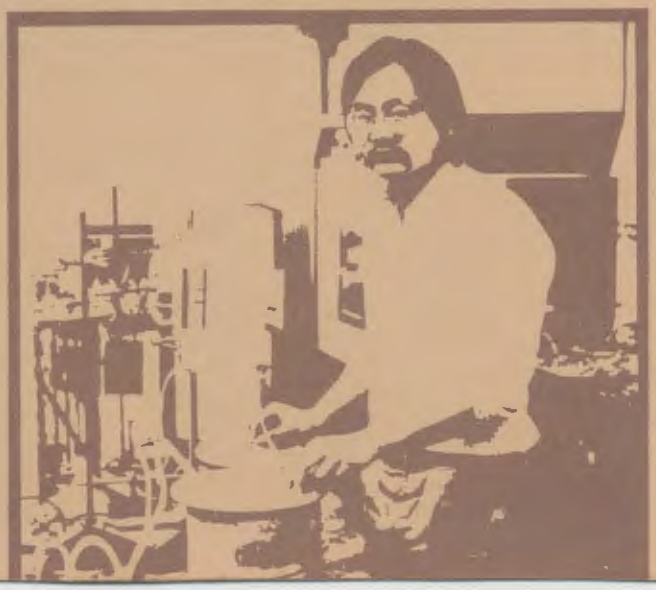

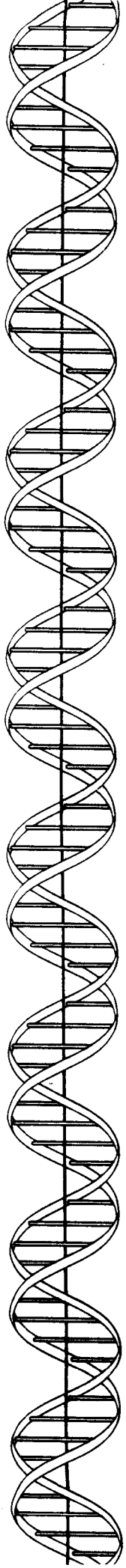

Proceedings of the 14th Annual

Biochemical Engineering Symposium

Rakesh K. Bajpai, Editor
April 28, 1984
Department of Chemical Engineering
University of Missouri-Columbia

PROCEEDINGS OF THE FOURTEENTH ANNUAL BIOCHEMICAL ENGINEERING SYMPOSIUM

The Annual Biochemical Engineering Symposium series is devoted to presentations by students on their research topics. The fourteenth event, held in 1984, was organized at the University of Missouri-Columbia. It was attended by the biochemical engineering faculty and the students from Colorado State University, Iowa State University, Kansas State University, University of Missouri-Columbia, University of Missouri-Rolla and Washington University, St. Louis. The names of the attendees appear on the last page of this proceedings. Enquiries on the research conducted at these schools should be directed to professors Jim Linden, Peter J. Reilly, Larry E. Erickson, Rakesh K. Bajpai, Oliver Sitton or Eric Dunlap.

We would like to thank Dr. George Preckshot (Chairman, Department of Chemical Engineering at U.M.C.) and Samuel Watson (President, Energen Inc.) for their sponsorship of this symposium and assistance in preparation and publication of these proceedings.

Rakesh K. Bajpai
Editor

Fourteenth Annual Biochemical Engineering Symposium

University of Missouri-Columbia

Columbia, MO 65211

Saturday, April 28, 1984

ESTIMATION OF PRODUCT FORMATION KINETIC AND MICROBIAL YIELD PARAMETERS FOR ANAEROBIC ORGANIC ACID AND SOLVENT PRODUCTION

Mehmet D. Oner

Department of Chemical Engineering
Kansas State University
Manhattan, Kansas 66506

INTRODUCTION

Methods for the estimation of product formation kinetic and microbial yield parameters for anaerobic organic acid and solvent production are described in this work.

The available electron balance [1,2,3], the covariate adjustment method [4,5,6], and the Luedeking and Piret product formation kinetic model [7,8] are used together to estimate product formation kinetic parameters, maintenance coefficient and true growth yield. It was found that yield and kinetic parameters are directly related to each other. Thus, the thermodynamic and biochemical pathway limitations for the true growth yield also provide constraints on the numerical values of the corresponding parameter in the product formation kinetic model.

THEORY

In anaerobic organic acid and solvent production, ATP generation is well coupled to extracellular product formation.

If the available electrons that are transferred from organic substrate to products are viewed as being expended to provide energy for growth and maintenance, based on Pirts model [9], the following equations are derived [2];

$$\frac{\mu}{\eta} = \frac{\mu}{\eta_{max}} + m_e \tag{1}$$

$$\frac{\mu(\eta+\xi_p)}{\eta} = \frac{\mu}{\eta_{max}} = m_e \tag{2}$$

$$\frac{\mu(y_c+z+d)}{\eta} = \frac{\mu}{\eta_{max}} = m_e \tag{3}$$

where μ is the specific growth rate, hr^{-1}, y_c, z and d are fractions of substrate carbon in biomass, extracellular product(s), and carbon dioxide, respectively, η and ξ_p are fractions of substrate available electrons converted to biomass and extracellular products, respectively, m_e is the rate of organic substrate consumption for maintenance, g equiv. of available electrons per g equiv. of available electrons in biomass (hr), and η_{max} is "true" biomass available electron yield, dimensionless. For the details of theory refer to Oner et al. [10].

DISCUSSION AND RESULTS

Several sets of data from literature have been analyzed to estimate the true growth yield, η_{max}, maintenance coefficient, m_e, and the product formation kinetic parameters, α_e and β_e. These results are given in Tables I and IV. Also some information related to consistencies of these data sets are shown on these tables and Table II.

Estimated yield parameters, m_e and η_{max}, and the kinetic parameters α_e and β_e, from the data of Reilly [11] for anaerobic growth of Lactobacillus delbrueckii on glucose and yeast extract, are shown on Table I. During lactic acid production this organism uses the EMP pathway and produces 2 moles of ATP per mole glucose consumed when the only product is lactic acid [12]. When yeast extract is used to provide amino acids and other biochemicals for cell growth, Stouthamer [13] reports that $Y_{ATP}^{max} = 31.9$ g dry biomass/g mole ATP, is the estimated theoretical maximum value based on biochemical pathway analysis. Table III gives three different values of η_{max} for three different values of Y_{ATP}^{max}. The results in Table I and the results of Luedeking and Piret [7] and Hanson and Tsao [15], as analysed in Table IV, show that the estimated values of η_{max} are similar in magnitude to this theoretical value. Average values of η_{max} are 0.347 for the data of Reilly [11], 0.279 for the data of Luedeking and Piret [7] and 0.339 for the data of Hanson and Tsao [14]. The average of these values is slightly higher than the theoretical maximum expected value of 0.305. There may be several reasons for obtaining higher than expected values of η_{max}. It could be due to incorrect conversion factor used to convert optical density to biomass dry weight (0.75 mg/UOD). Also there could be small amount of aerobic growth due to imperfect anaerobic conditions applied. Analysis of the batch data of Reilly [11] shows that the fraction of available electrons of glucose supplied which are converted to lactic acid averages 0.776. So, there is possibility that parts of remaining fraction, 0.224, may have been converted to some other products, or some may be transferred to oxygen as well as biomass. Chance of having partly aerobic growth is the most probable reason for these results. Equations [1] and [2] are used with the covariate adjustment method to estimate the parameters in Table IV for the data of Hanson and Tsao [14]. In Equation [2] the quantity of consumed substrate is based on the amount of glucose utilized. The analysis of data consistency in Table IV indicates that some significant measurement errors may have occurred in this work. The results of Reilly [11], Luedeking and Piret [7] and Hanson and Tsao [14] show that the growth yield is relatively large for this organism and that the average maintenance coefficient of 0.145 hr^{-1} from the data of Reilly and 0.132 hr^{-1}, reported by Rees et al. [15] and the values for some other organisms in Table I and IV. If lactic acid production is the desired goal, the development of organisms with higher maintenance coefficient and lower true growth yields would be desirable.

Relatively large values of η_{max} are obtained from the data of De Vries et al. [16] (also see Table IV). The products, lactate, acetate, ethanol and formate are treated as one product based on the sum of the available electrons of the individual products and used with equations [1] and [2]. Using δ = 10.43 eq. of avail. electrons per mole of ATP produced from ADP and their value of $m_{ATP} = 0.00152$ moles ATP/g cell (hr), one obtains $m_e = 0.096$. Thus, the results from the two different methods are reasonably consistent as one would expect.

These methods also have been applied to some other data sets from the literature. Some results for Lactobacillus bulgaricus, Lactobacillus plantarum, Clostridium acetobutylicum and Butyribacterium methylotrophicum are published elsewhere. [10]

The results for anaerobic solvent production, which are described in reference 10, include studies in which acetone, butanol, and butyrate are produced.

In Table V, maintenance coefficient and true growth yields, based on free energy, for the data of Reilly [11] are given. The calculational procedure is described in detail elsewhere [10]. The values of the true growth yield η , should lie between the limits zero and one. All of the point estimates and all of the confidence intervals are within these limits; however, in Table V, several relatively large values are reported (theoretically estimated maximum values, based on known biochemical pathways, are shown in Table III).

The values of the true growth yield, η , for the lactic acid fermentations are consistently relatively high. This appears to be due to the relatively efficient production of ATP from ADP in lactic acid fermentations.

CONCLUSIONS

Methods have been developed to estimate true growth yields, maintenance coefficients, and product formation kinetic parameters for anaerobic fermentaions where product formation is coupled to the bioenergetics of growth and maintenance. These methods have been applied to organic acid and solvent production.

The covariate adjustment techniques may be applied to estimate kinetic parameters as well as energetic parameters.

When product formation is the desired goal, the maintenance coefficient should be as large as possible. Both product yield and specific rate of product formation increase with increasing values of the maintenance coefficient. Small values of true growth yield are desired when product formation is the objective.

ACKNOWLEDGEMENT

This work was supported in part by National Science Foundation GRANT CPE 81-20039

REFERENCES

1. Erickson, L.E., J. Ferment. Technol. 58, 531 (1980).

2. Erickson, L.E. and M.D. Oner, Ann, N.Y. Acad. of Sci., 413, 99 (1983).

3. Erickson, L.E., I.G. Minkevich, and V.K. Eroshin, Biotechnol. Bioeng., 21, 575 (1979).

4. Oner, M.D., L.E. Erickson, and S.S. Yang, Biotechnol. Bioeng. 25, 631 (1983).

5. Solomon, B.O., M.D. Oner, L.E. Erickson, and S.S. Yang, "Estimation of Parameters Where Dependent Observations Are Related by Equality (Constraints, "AIChE Los Angeles Meeting (No, 1982), AIChE Journal (1983).

6. Yang, S.S., B.O. Solomon, M.D. Oner, and L.E. Erickson, "Estimation and Testing Common Parameters for Multiresponse Models Associated with Microbial Growth and Bioenergetics". Technometrics, In Press. (1984).

7. Luedeking, R. and E.L. Piret, J. of Biochem. and Microbiol. Technol. Eng., Vol. I, No. 4, pp. 393 (1959).

8. Luedeking, R., "Fermentation Process Kinetics" In Biochemical and Biological Engineering Science, Vol. I, 181, Academic Press (1967).

9. Pirt, S.S., Proc. Royal Soc. B 163, 224 (1965).

10. Oner, M.D., L.E. Erickson and S.S. Yang, "Estimation of Yield, Maintenance and Product Formation Kinetic Parameters in Anaerobic Fermentations", Biotechnol. Bioeng., In Press (1984).

11. Reilly, P.J., "Kinetics of Lactic Acid and Gluconic Acid Fermentations," Ph.D. Thesis, University of Pennsylvania (1964).

12. Decker, K., K. Jungermann, and R.K. Thauer, "Eng. Production in Anaerobic Organisms," Angew. Chem. Internat. Edit., Vol. 9, No. 2, pp. 138 (1979).

13. Stouthomer, A.H., "The Search for Correlation Between Theoretical and Experimental Growth Yields, "International Review of Biochemistry 21, 1 (1970).

14. Hanson, T.P. and G. T. Tsao, Biotechnol. Bioeng. 14, 233 (1972).

15. Rees, J.F. and S. J. Pirt, J. Chem. Techn. Biotechnol. 29, 591 (1979).

16. DeVries, W., W.M.C. Kapteijn, E.G. VonDer Beek and A.H. Stouthomer, J. Gen. Microbiol. 63, 333 (1970).

Table I. Point and 95% confidence interval estimates of m_e, η_{max}, α_e and β_e from the data collected during anaerobic growth of Lactobacillus delbrueckii NRRL B-445.*

Form of equation	m_e and β_e (hr^{-1})	η_{max}	α_e	
I	-0.097[-0.263, 0.068]	0.203[0.156, 0.291]	3.928[2.435, 5.421]	Run # 7
II	0.164[-0.362, 0.689]	0.280[0.179, 0.638]	2.571[0.568, 4.574]	(Batch culture)
I	0.078[0.006, 0.220]	0.281[0.234, 0.351]	2.558[1.845, 3.271]	Run # 9
II	0.196[-0.143, 0.536]	0.339[0.242, 0.566]	1.948[0.765, 3.129]	(Batch culture)
I	0.112[0.057, 0.166]	0.308[0.264, 0.371]	2.243[1.696, 2.791]	Run # 10
II	0.178[-0.035, 0.392]	0.351[0.274, 0.491]	1.845[1.038, 2.652]	(Batch culture)
I	0.115[0.072, 0.196]	0.329[0.295, 0.373]	2.036[1.684, 2.388]	Run # 11
II	0.204[0.011, 0.397]	0.376[0.309, 0.478]	1.660[1.093, 2.228]	(Batch culture)
I	0.134[0.125, 0.144]	0.312[0.286, 0.342]	2.209[1.926, 2.493]	Run # 12 (Batch culture, points 1, 6, 7, 8, 9 are excluded)
II	0.162[0.133, 0.192]	0.351[0.325, 0.380]	1.853[1.630, 2.075]	
I	0.288[0.274, 0.302]	0.418[0.385, 0.457]	1.394[1.188, 1.600]	Run # 14
II	0.287[0.191, 0.383]	0.424[0.373, 0.492]	1.357[1.033, 0.680]	(Batch culture)
I	0.013[-0.075, 0.100]	0.306[0.251, 0.392]	2.270[1.552, 2.988]	Run # 15
II	0.205[-0.173, 0.582]	0.394[0.269, 0.737]	1.537[0.357, 2.717]	(Batch Culture)
I	0.057[0.037, 0.077]	0.329[0.303, 0.360]	2.042[1.781, 2.303]	Run # 16
II	0.071[-0.070, 0.211]	0.334[0.288, 0.398]	1.995[1.516, 2.473]	(Batch culture)
I	0.143[0.118, 0.168]	0.399[0.381, 0.419]	1.503[1.382, 1.624]	Run # 17
II	0.156[0.101, 0.212]	0.408[0.381, 0.440]	1.450[1.272, 1.628]	(Batch culture)
I	0.172[0.081, 0.263]	0.402[0.338, 0.497]	1.487[1.013, 1.962]	Run # 18
II	0.159[0.053, 0.267]	0.393[0.333, 0.479]	1.545[1.089, 2.000]	(Continuous culture)

*Data of Reilly [11] σ_b = 0.462 and 4.291 were used in the analysis. The media contained 5% glucose and 3% yeast extract except that 1% yeast extract was used in Run 12, 2% yeast extract was used in Run 14, and 2.5% glucose was used in Run 15.

Table II. Available electron balances for the data of Reilly [11].

	No. of data points	$n + \xi_p$
Run 7	20	1.045
Run 9	22	1.122
Run 10	20	1.023
Run 11	16	1.048
Run 12	26	0.951
Run 14	17	0.987
Run 15	12	1.198
Run 16	18	1.048
Run 17	15	1.047
Run 18	5	---

Table III. Theoretical values of true growth yield for anaerobic lactic acid fermentations by Lactobacillus delbrueckii for given values of δ and Y_{ATP}^{max}

δ	Y_{ATP}^{max}	η_{max}	η_{th}^{max}
1.2	10.5	0.126	0.744
	28.8	0.284	0.868
	31.9	0.305	0.876

Table IV. Point and 95% confidence interval estimates of m_e, η_{max}, α_e, β_e, and available electron balances for some literature data for lactic acid producing organisms.

Form of Equations	m_e and β_e (hr^{-1})	η_{max}	α_e	Microorganisms	Substrate	Product(s)	Source of Data
I	0.491[0.453, 0.530]	0.267[0.247, 0.290]	2.750[2.453, 3.049]	Lactobacillus delbrueckii NRRL - B445	Glucose	Lactic Acid	Luedeking and Piret [7] (Batch Culture)
II	0.569[0.457, 0.681]	0.291[0.268, 0.318]	2.439[2.144, 2.734]				
I	0.123[-0.032, 0.288]	0.336[0.255, 0.494]	1.976[1.024, 2.922]	Lactobacillus delbrueckii NRRL - B445	Glucose	Lactic Acid	Hanson and Tsao [14] (continuous culture)
II	0.145[-0.080, 0.370]	0.342[0.247, 0.555]	1.924[0.802, 3.049]				
I	-0.005[-0.142, 0.132]	0.287[0.238, 0.362]	2.484[1.762, 3.202]	Lactobacillus casei L3	Glucose	Lactate, acetate ethanol, formate	De Vries et al. [16] (continuous culture)
II	-0.060[-0.260, 0.139]	0.269[0.288, 0.328]	2.717[2.049, 3.386]				

Data	No. of Data Points	$\eta + \xi_p$ Mean and 95% CI		Std. Dev.
1st	22	1.073	-----	
2nd	19	1.002	(-0.169, 2.173)	0.557
3rd	6	1.354	(1.230, 1.479)	0.048

Table V. Point and 95% confidence interval estimates for true growth yield, η_{th}^{max}, and maintenance coefficient, m_{th}, in free energy units for lactic acid production data of Reilly [11].

Form of Equations	m_{th}	η_{th}^{max}	Source of data
I	-0.004(-0.012, 0.003)	0.814(0.770, 0.864)	Run # 7
II	0.008(-0.017, 0.032)	0.859(0.794, 0.935)	
I	0.004(0.0003, 0.010)	0.859(0.835, 0.885)	Run # 9
II	0.009(-0.007, 0.025)	0.881(0.840, 0.926)	
I	0.005(0.003, 0.008)	0.870(0.851, 0.890)	Run # 10
II	0.008(-0.02, 0.018)	0.885(0.856, 0.916)	
I	0.005(0.003, 0.009)	0.878(0.865, 0.891)	Run # 11
II	0.010(0.0005, 0.019)	0.892(0.871, 0.914)	
I	0.0063(0.0059, 0.0068)	0.872(0.861, 0.882)	Run # 12
II	0.0076(0.0063, 0.009)	0.885(0.876, 0.893)	
I	0.0136(0.0129, 0.0142)	0.902(0.894, 0.910)	Run # 14
II	0.0135(0.009, 0.018)	0.903(0.891, 0.916)	
I	0.0006(-0.0035, 0.0047)	0.870(0.845, 0.896)	Run # 15
II	0.0096(-0.008, 0.027)	0.896(0.854, 0.943)	
I	0.0027(0.0017, 0.0036)	0.878(0.868, 0.887)	Run # 16
II	0.0033(-0.0033, 0.0099)	0.879(0.861, 0.897	
I	0.0067(0.0056, 0.0079)	0.897(0.891, 0.902)	Run # 17
II	0.0073(0.0047, 0.010)	0.900(0.893, 0.906)	
I	0.0081(0.0038, 0.0124)	0.898(0.881, 0.917)	Run # 18
II	0.0075(0.0025, 0.0126)	0.896(0.878, 0.914)	

CHARACTERIZATION OF SOY PROTEIN TEXTURIZATION IN A COMPLEX BIOREACTOR

J. L. Ibave
Department of Agricultural and Chemical Engineering
Colorado State University
Fort Collins, Colorado 80523

INTRODUCTION

The modern food industry relies extensively on extrusion technology for the processing of raw materials such as cereals, oilseeds, and protein flours and meals. Despite widespread use, it is well known that very little scientific knowledge is available to accurately describe extrusion texturization of soy protein flours (Harper, 1981). Knowledge of rheological and physical properties of protein doughs is essential for adequate modeling of extrusion texturization process (Harper, 1979 and Jao *et al.*, 1978). In place of mechanistic models, researchers have been conducting studies correlating product characteristics with variables intrinsic to the extruder used (Aguilera and Kosikowski, 1976, Maurice and Stanley, 1978 and Owusu *et al.*, 1982), and the resulting models are equipment specific and cannot be extrapolated to other process equipment due to the nonlinearity of the variables.

A food extruder could be modeled as a continuous flow reactor. The key performance characteristics which are important in defining the reaction conditions in the extruder are the residence time, the thermal conditions inside the extruder channel and the deformation of dough which can align molecules and cause reactive sites to become close in proximity. Models involving both rheological and kinetic behaviours, and above all, variables extrinsic to the equipment in combination with physical properties of the texturized dough will hopefully describe the texturization process of soy protein doughs.

MATERIALS AND METHODS

A 19 mm diameter, single-screw Brabender extruder (Model 2003) equipped with a Plasticorder Torque Rheometer (Model PL-V500) and a constant tapered screw having a 3:1 compression ratio was used in this study and previously described by Holay and Harper (1982). To make it possible to change the residence time in the extruder independently of the screw speed, two separate heated die plates were used (Figure 1). Individual dies of varying diameters and lengths were screwed into the die plates as part of the experimental design.

The following operating conditions were varied in a ½ replicate of a 2^5 factorial design: (a) die diameter, 0.35 cm, 0.25 cm; (b) die length/diameter ratio (L/D), 1:1 and 1:2; (c) die plate, long and short; (d) screw speed 80 rpm, 120 rpm; and, (e) extrudate temperature 150°C, 160°C. The feed material was a defatted soy flour obtained from Archers Daniels Midland, Chicago, Illinois with a proximal analysis listed in Table 1. The desired moisture level of 36% dry basis in the feed was achieved by adding water during dough preparation prior to extrusion.

Product Characterization

Bulk density and water absorption measurements were performed on extrudate samples that had been roller-milled and sieved to a particle size between 2-3.35 mm in diameter. Forty grams of sieved product were placed in a 250 ml graduated cylinder and tapped gently 50 times to settle the samples. The product bulk density was obtained by dividing the mass by the final volume. After completing the bulk density measurements, the samples were soaked in 200 ml water and then drained to obtain the volume of water (V) not absorbed by the sample in order to calculate the absorption percentage as:

$$A\ (\%) = \frac{200 - V}{40} \times 100$$

The Kramer Shear Press was used to determine the force (N/g) required to shear hydrated textured soy samples.

A fluorescent dye (Rhodamine B) was used to measure residence time distribution of the product in the extruder. About 5 mg of dye were mixed with dough to form a small pellet, which was introduced at the feed hooper once steady state operation was reached. Extrudate was collected and cut representing one second time intervals. These were soaked in water over-night to extract the dye. The samples were then blended and centrifuged. The supernatant was excited with a Turner Spectrofluorometer (Model 430) at 493 nm and the fluorescence measured at 585 nm. From these data it was possible to estimate an exit age distribution, E(t), which shows the concentration of dye in the supernatant as a function of time.

CALCULATIONS

Machine Independent Correlating Parameters

Temperature-time History Function.

The evaluation of the temperature-time history function

$$\psi(t,T) = \int_0^t \text{EXP}\left[- \Delta E_d/RT(t) \right] dt$$

where $T(t) \geq T_d$ for all t, $T_d = 70^0C$

$\psi(t,T) = 0$ for $T(t) < T_d$

ΔE_d = activation energy of denaturation determined by differential scanning calorimetry (DSC) Bouchard-Daniels Kinetic Analysis as 114 kJ/g-mole.

R = gas law constant

can be done using the residence time distribution data gathered experimentally with knowledge of the dough temperature distribution along the barrel. To automate the calculation of $\psi(t,T)$, it is necessary to mathematically describe the exit age distribution curves E(t) for the experimental run under consideration. The experimental residence time data for a single screw extruder shows a tail which extends to long times due to material held in dead spaces within the extruder. The model for distributions with extended tails is described as follows (Levich et al., 1967):

In the region $t < \eta/\lambda$ (less than maximum peak height)

$$E(t) = (1-\eta\nu/\lambda) \frac{\lambda}{\sqrt{2\pi\eta}} \text{EXP} \left[- \frac{(\lambda(t) - \eta)^2}{2\nu} \right] + \frac{\eta\nu\gamma}{4} \cdot \left[1-\text{ERF}\left(\frac{\eta-\lambda(t)}{\sqrt{2\eta}}\right)\right]$$

In the region $t > \eta/\lambda$ (more than maximum peak height)

$$E(t) = (1-\eta\nu/\lambda) \frac{\lambda}{\sqrt{2\pi\eta}} \text{EXP} \left[- \frac{(\lambda(t)-\eta)^2}{2\nu} \right] + \frac{\eta\nu\gamma}{\lambda} \text{EXP} (-\gamma(t))$$

The parameters η, ν, λ, and γ were calculated using a derivative-free nonlinear regression which estimates the parameters of the nonlinear function by least squares and can be used to compute maximum likelihood estimates (BMDPAR Statistical Program). To reflect the impact of the exit age distribution E(t) on the temperature-time function calculations, the value of this function was calculated for different fractions of the sample, each having a specific residence time [F(t) function], then becomes:

$$\psi(t,T) \simeq \text{EXP} \left[-\Delta E_d / RT(t) \right] F(t)$$

Strain.

The nominal shear strain can be described as:

$$\bar{\gamma}_N = \sum_{I=0}^{n} \gamma(I) \cdot t(I)$$

where $\bar{\gamma}_N$ = nominal shear strain

$\dot{\gamma}$ = $\pi DN/H$, nominal shear rate in channel

$\dot{\gamma}$ = $4Q/\pi r^3$, nominal shear rate in die plate

Q = volumetric flow rate

r = radius of die section

N = speed of the screw

H = channel depth

t(I) = $[v(I)/V]\ \bar{t}$

v(I) = segment volume

v = total volume

$\bar{t}$ = mean residence time

The normalized strain was calculated according to Bigg and Middleman (1974).

$$\bar{\gamma} = \bar{\gamma}^* \cdot \bar{\gamma}_N$$

where $\bar{\gamma}^*$ = normalized shear strain

$\bar{\gamma}$ = actual shear strain

Shear Rate at the Die

$$\dot{\gamma}_{ap} = \frac{4Q}{\pi r_d^3}$$

where Q = volumetric flow rate

r_d = radius of die

Vapor Pressure

The vapor pressure was determined at the discharge temperature of the dough since it is responsible to some extent to the degree of product expansion.

Regression Analysis

Regression Analysis was performed using the extrudate product characteristics as dependent variables against the above independent ones with the BMDP9R Statistical Program. The resulting machine-independent correlating equations are given in the Appendix.

RESULTS AND DISCUSSION

Density has been used as a criteria to differentiate samples of textured soy protein. To produce samples of low density, they must first have the characteristic layered and cross-linked structure that can expand with the release of internal steam pressure when the product passes through the die. It was postulated that increasing shear strain within the extruder aligns the partially denatured protein molecules in the streamline of flow, thereby exposing reactive sites along the length of the molecules and enhancing protein-protein cross-linking capability. The extent of cross-linking reactions may be correlated with the time-temperature history of the sample. The cross-linked material expands upon exiting the extruder as a result of the vapor pressure exerted by the free moisture within the samples. As shown in Figure 2, the greater vapor pressure values occurring at the higher discharge temperatures resulted in a decrease in bulk density.

The extent of final product expansion is also related to the degree of cross-linking and the presence of structural fissures. In all cases, increasing the time-temperature shear strain function, $\psi\bar{\gamma}$, results in lower density product (Figure 3). In the range of conditions studied, increasing the dough temperature by increasing the barrel wall temperature or increasing residence time by adding to the void volume at the extruder discharge would have the effect of reducing the density of the product. In contrast, increases in apparent shear rate at the die caused by increased flow or reduced die size may create disruptions within the soy protein matrix described as mechanical fissures. Thus, these conditions may prevent uniform expansion in the final product resulting in density increases (Figure 4).

Water absorption and density are inversely related. Generally, the effects of the correlating variables showed the opposite trends to those observed with density Under conditions of greater values of vapor pressure or the time-temperature, strain function, $\psi\bar{\gamma}$, an increase of water absorption due to the greater expansion of the product resulted (Figure 5). Increasing the apparent shear rate at the die decreased the water retention probably due to the formation of cracks in the final product which increased the ease of water to escape from the product (Figure 6). However, greater shear strain resulted in lower water holding capacity due to denser layered structure within the samples that inhibits diffusion of water.

Finally, samples which showed significant expansion and a well layered structure required lower shear force and less work of shearing (Figure 7). Although increased shear rate

at the die is related to increases in bulk density, these same samples showed a decrease in both shear strength and work of shearing because of mechanical fissures within their microstructure which apparently created weak spots.

CONCLUSIONS

Procedures were developed for combining residence time distributions and temperature profiles into a time-temperature history function, ψ, which appears to correlate with the extent of denaturation in extruded soy protein doughs.

Increased ψ and $\bar{\gamma}$ within the extruder resulted in samples having lower density, shear strength and larger water absorption. As the level of these parameters increased, samples were characterized by a greater extent of ordered cross-linking which formed a readily expandable matrix. The same conclusion may be drawn when water vapor is taken into consideration.

Increased apparent shear rate at the die, $\dot{\gamma}_{ap}$, apparently causes the formation of small mechanical fissures in the matrix which result in a non-uniform expanded product.

Finally, and most importantly, the machine-independent correlating parameters and the procedures for their calculation proposed in this study will serve as a starting point for the modeling and scale-up of extrusion process.

APPENDIX: Correlating Equations

Density

$$\rho, \text{ g/cc} = 1.2712 - .001632\ P_v + .0002678\ \dot{\gamma}_{ap} - .0008085\ \bar{\gamma}$$

Mallow's "cp" = 2.73 R^2=0.80

$$\rho, \text{ g/cc} = 0.368 - 7.43\times10^{8}\ \psi\bar{\gamma} - 2.67\times10^{-4}\ \dot{\gamma}_{ap} + 8.4\times10^{-4}\ \tau_w$$

Mallow's "cp" = 2.14 R^2=0.83

Water Absorption

$$A, \% = -201.764 + 0.7837\ P_v - 0.0753\ \dot{\gamma}_{ap} - 0.0166\ \bar{\gamma}$$

Mallow's "cp"=3.95 R^2=0.72

$$A, \% = 162 + 3.23\times10^{11}\ \psi\bar{\gamma} + 0.127\ \dot{\gamma}_{ap} - 0.351\ \tau_w$$

Mallow's "cp"=2.08 R^2=0.86

Shear Strength

$$S, \text{ N/g} = 795.321 - 1.058\ P_v - 0.144\ \dot{\gamma}_{ap}$$

Mallow's "cp"=1.08 R^2=0.65

$$S, \text{ N/g} = 988 - 0.479\ \bar{\gamma} - 0.428\ \dot{\gamma}_{ap} + 0.363\ \tau_w$$

Mallow's "cp"=2.82 R^2=0.75

Work of Shearing

$$W, \text{ Nm/g} = 6.5875 - 0.0088\ P_v - 0.0013\ \dot{\gamma}_{ap}$$

Mallow's "cp"=2.01 R^2=0.65

REFERENCES

Aguilera, J. M. and F. V. Kosikowski. 1976. Soybean extruded product: a response surface analysis. J. Food Sci. 41:647.

Bigg, D. and S. Middleman. 1974. Mixing in a screw extruder. A model for residence time distribution and strain. Ind. Eng. Chem. Fundamentals. 13(1):66.

Harper, J. M. 1979. Extruder not prerequisite for texture formation. J. Food Sci. 44(3):11.

Harper, J. M. 1981. Food Extrusion, Vols. 1 and 2. CRC Press, Boca Raton, Florida.

Holay, S. H. and J. M. Harper. 1982. Influence of the extrusion shear environment on plant protein texturization. J. Food Sci. 47(6):1869.

Jao, Y. C., D. L. Chen and W. E. Irwin. 1978. Engineering analysis of soy dough rheology in extrusion. J. Food Proc. Eng. 2(1):97.

Levich, V. G., V. S. Markin and Y. A. Chismadzhen. 1967. On hydrodynamic mixing in a model of a porous medium with stagnant zones. Chem. Eng. Sci. 22:1357.

Maurice, T. J. and D. W. Stanley. 1978. Texture-structure relationships in texture soy protein. IV. Influence of process variables on extrusion texturization. Can. Inst. Food Sci. Technol. 11(1):1.

Owusu-Ansah, J., F. R. Van de Voort and D. W. Stanley. 1982. Effect of extrusion variables on product moisture and extrusion crystallinity of corn starch. Can. Inst. Food Sci. Technol. 15(4):257.

Wolf, W. J. and F. L. Baker. 1975. Scanning electron microscopy of soybeans, flours, protein concentrates and protein isolates. Cereal Chem. 52:387.

Table 1. Proximal analysis of defatted soy flour.

	%
Moisture	6.45
Fat	1.15
Ash	7.05
Fiber	2.90
Protein	51.84
Carbohydrates	30.61

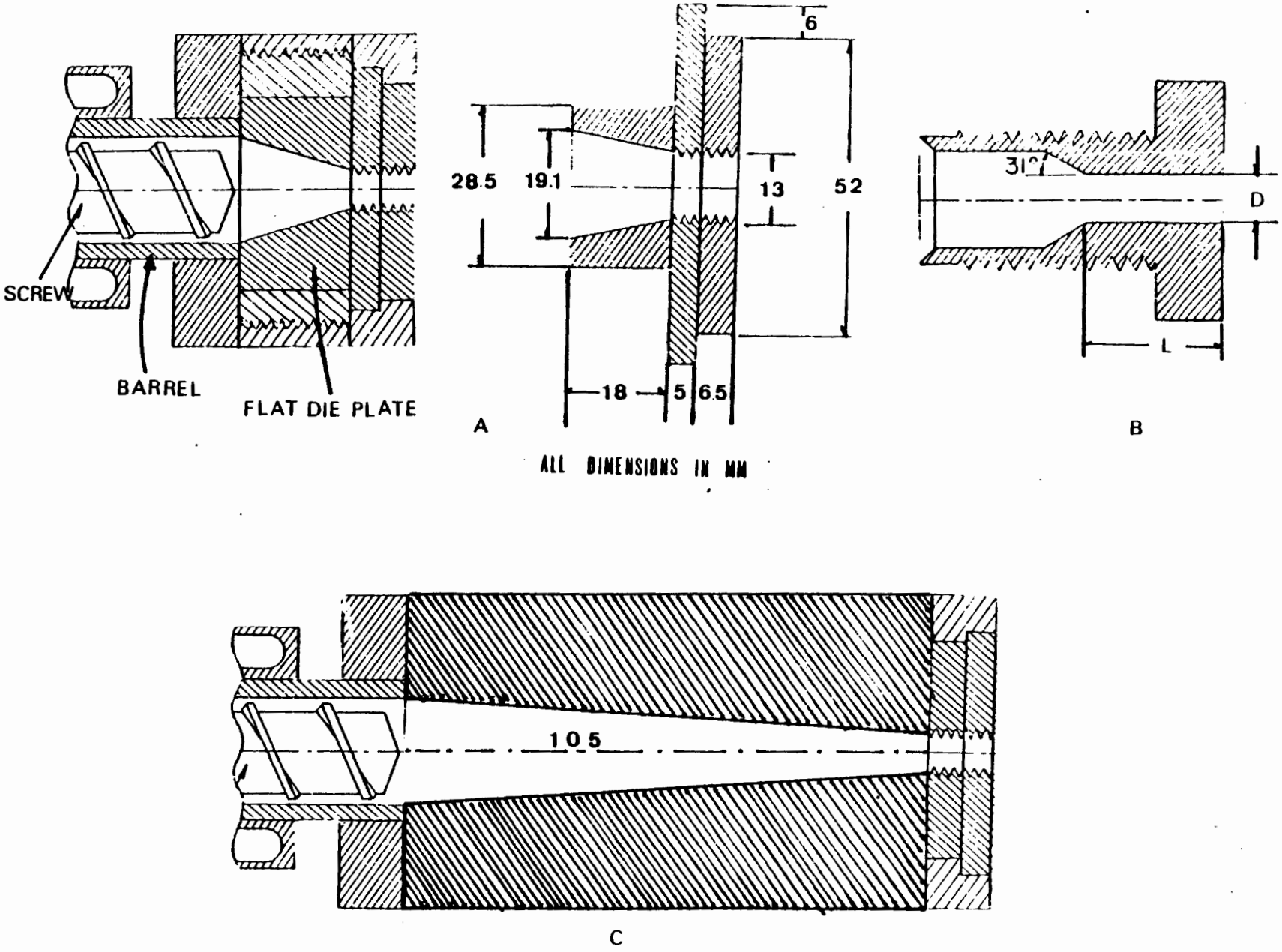

Figure 1. Cross-sectional view of short die plate (A), die insert (B), and long die plate (C).

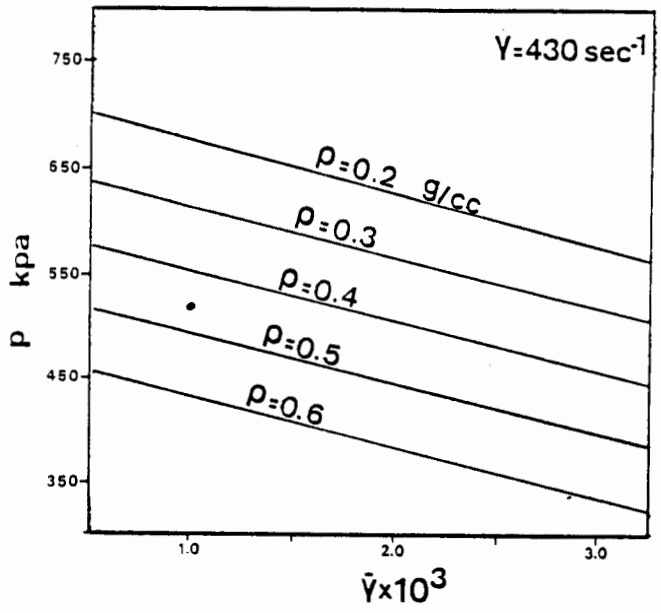

Figure 2. Effect of different shear environments and vapor pressure on bulk density.

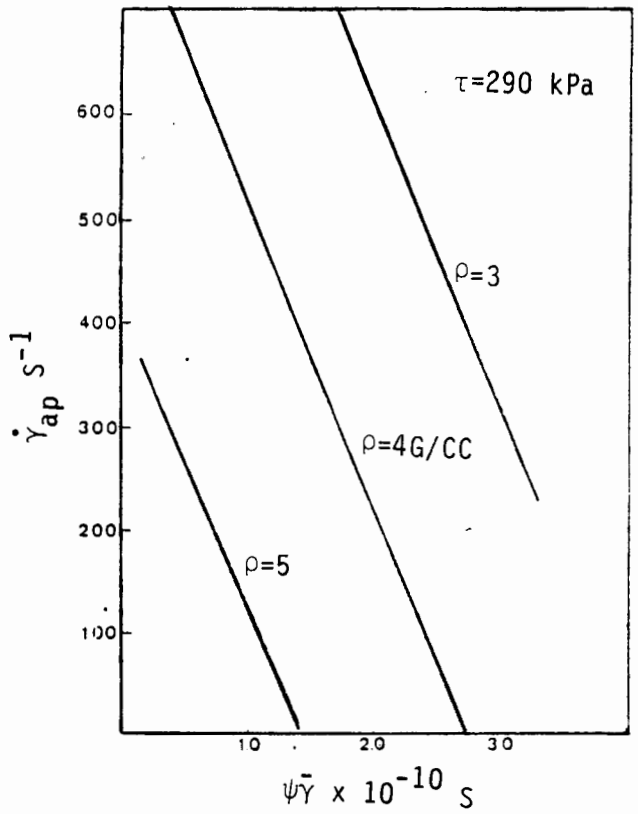

Figure 3. Textured soy product density as influenced by $\psi\bar{\gamma}$ and $\dot{\gamma}_{ap}$.

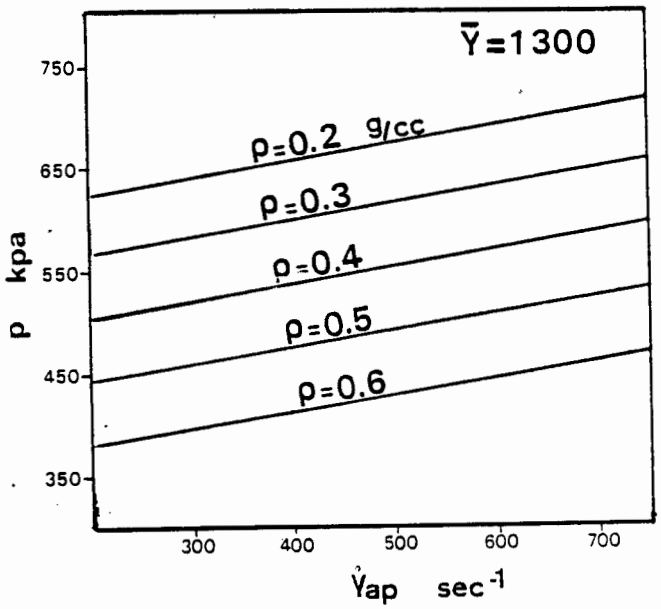

Figure 4. Effect of apparent shear rate at the die environment and vapor pressure on bulk density.

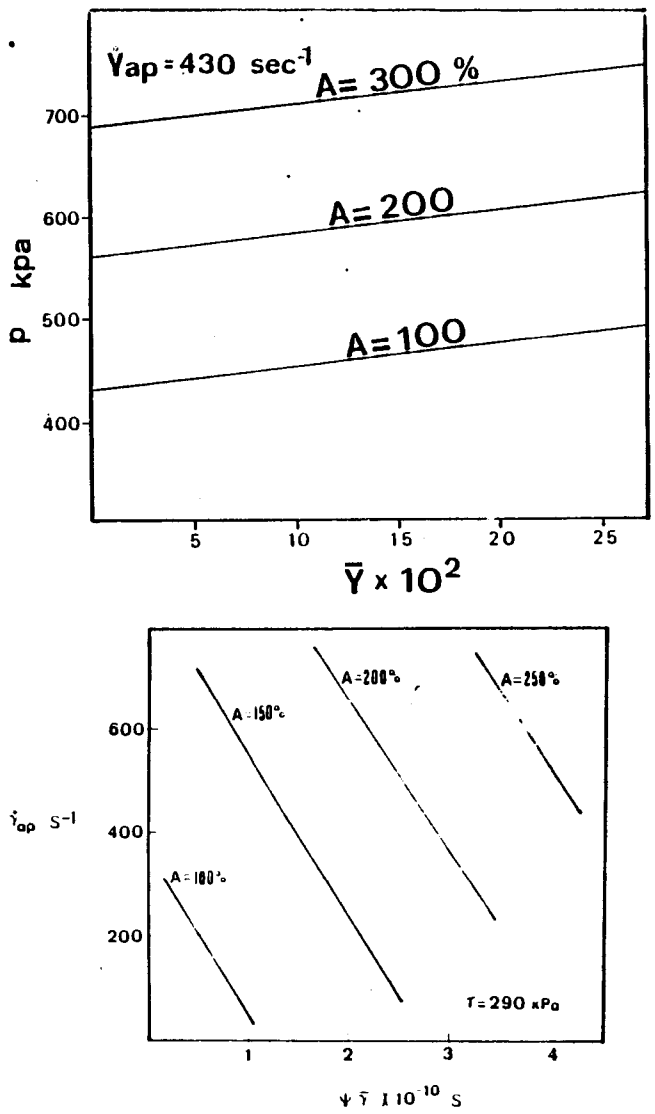

Figure 5. Water absorption of textured soy samples as a function of the time-temperature history function-strain correlation ($\psi\gamma$), vapor pressure (P_v) and apparent shear rate at the die ($\dot{\gamma}_{ap}$).

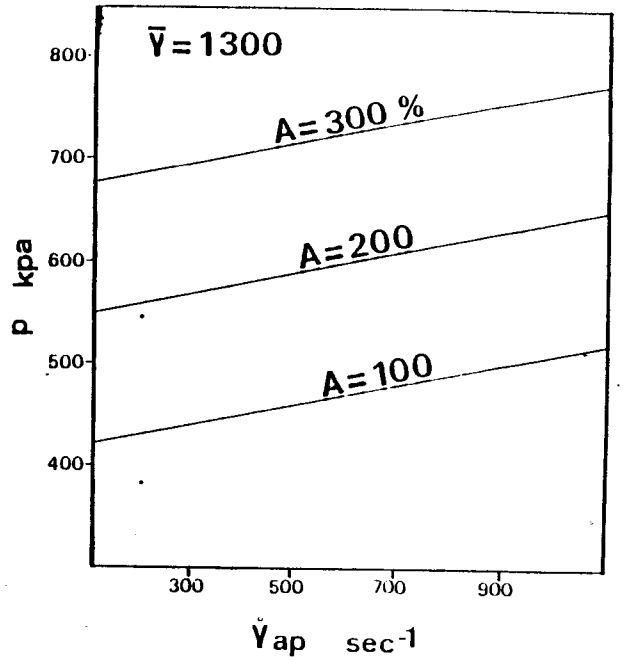

Figure 6. Effect of vapor pressure and shear on water holding capacity.

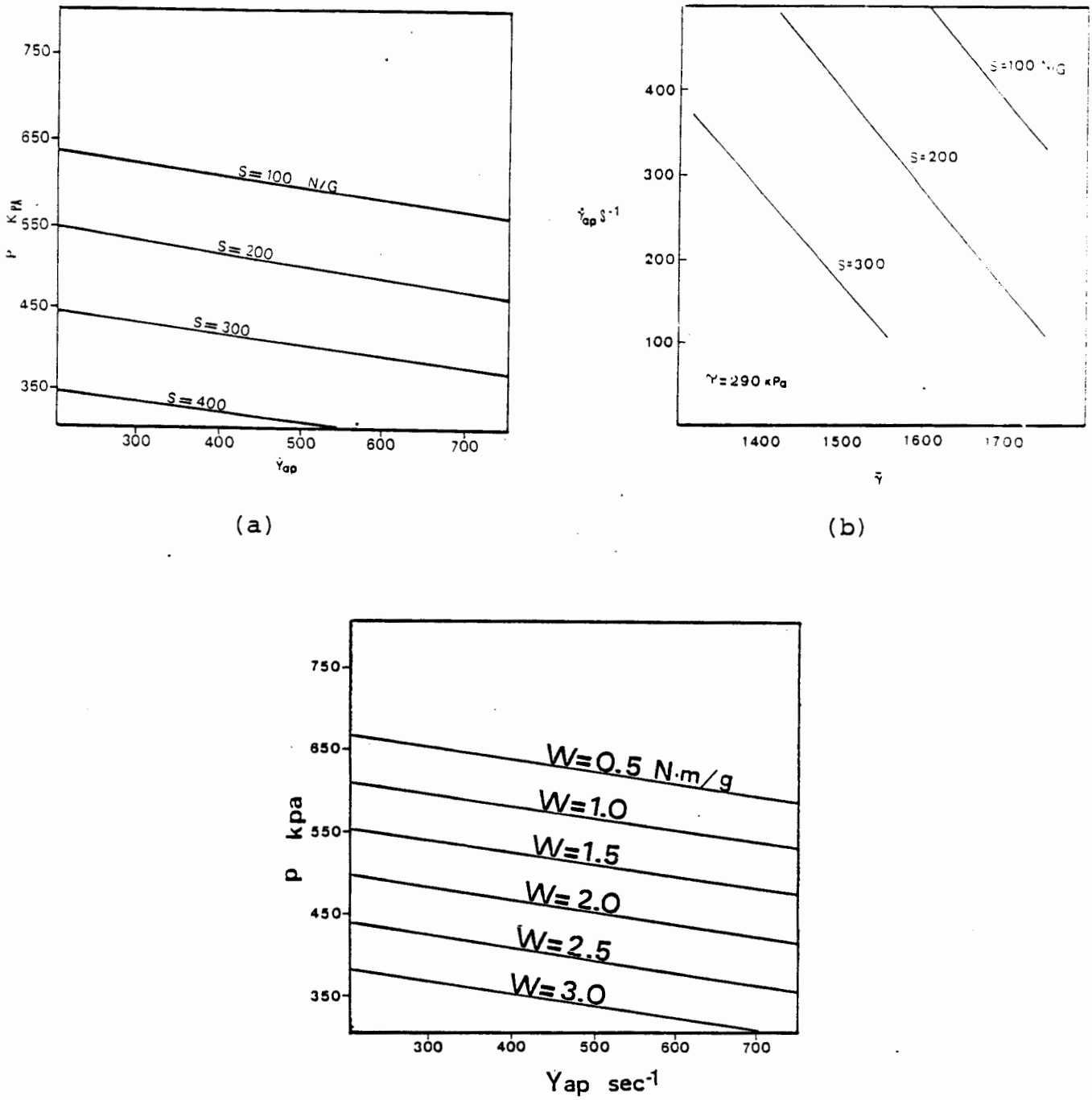

Figure 7. (a) Effect of vapor pressure and shear on product shear strength. (b) Maximum force required to shear hydrated samples as a function of strain, $\bar{\gamma}$ and apparent shear rate at the die, $\dot{\gamma}_{ap}$. (c) Effect of vapor pressure at discharge temperature and apparent shear rate at the die on product work of shearing.

ACID AND SOLVENT FERMENTATIONS USING MIXED CULTURES

D. Stevens, S. Alam, and R. K. Bajpai

Department of Chemical Engineering
University of Missouri - Columbia
Columbia, Missouri 65211

INTRODUCTION

Cheese whey, a by-product of cheese manufacture, is a waste stream containing fermentable sugars and is a current waste disposal problem. Whey is left after the milk has been curdled and the cheese curd removed. Missouri ranks third behind Wisconsin and Minnesota in total production in the United States, contributing about 1.5×10^6 metric tons/year of whey (1). Cheese whey is difficult to dispose of due to its high BOD (30,000 - 60,000 ppm) and constitutes a major dilemma for the dairy industry. In two plants (2), (3) in the vicinity of Columbia, Missouri, disposal of unconcentrated whey is accomplished by trucking to a hog feed manufacturing facility or applying as fertilizer to local farms.

The production of acetone and butanol from clostridial fermentations has also been subject to new research using cheese whey as a sustrate (4), (5). Lactose levels of 4.5-5% (w/v) in unsupplemented and untreated whey can support solvent production to the extent of 1-1.5% (w/v). These are in the range of maximum concentrations of solvents that can be achieved by clostridial fermentations due to the end-product toxicity. Of the fermentation products, butanol and acetone have generally been the products of choice, although the simultaneous formation of acids opens up the possibility of subsequent ester formation.

In the present study, the main products of interest were butanol and butyric acid. Industrial strains, supplied by the Biodiesel Refiners Corporation of Iowa, were investigated to determine their capacity to

ferment cheese whey. A further objective of the study was to establish the kinetics of production of butanol and butyric acid by these strains.

MATERIALS AND METHODS

Microorganisms

The pure culture of C. beijerinckii as well as its coculture with B. cereus were supplied by the Biodiesel Refiners Corporation of Iowa.

Medium

Acid cheese whey was obtained from the Mid. America Dairy in Kirksville, Missouri. The whey was collected after the curd-removal was completed and before it was subjected to reverse osmosis. The pH of the raw whey was between 4.25 and 4.5, and it contained 50-65 g/ℓ sugar. pH was adjusted by addition of 5N NaoH.

Fermentation Methods

All the operations were conducted under anaerobic conditions. To activate the spore cultures, 1 ml of the respective spore stock solution was added to 10 mls of Reinforced Clostridial Medium (RCM, osoid Ltd.) in a Hungate tube using a hypodermic syringe. The inoculated RCM medium was then heat-shocked for 45 seconds in a water bath at 100^{o}c and then immediately cooled under running water. Maximum optical density was observed after incubation at 37^{o}c for 20-24 hours. The growing cultures in RCM were then used to inoculate a cheese whey medium in Hungate tubes and subsequently in cheese whey inoculum flasks (300 mlc). Fermentations were performed in a 14 liter (6 liters cheese whey) New Brunswick Microferm fermenter at 37^{o}c. The pH was maintained at the desired valve by automatic addition of 5N NaoH.

Analytical Methods

Reducing sugars were measured by the Nelson-Somagi method (6). Samples

were prepared by centrifugation at 12,000 rpm for 15 minutes and filtration through a 0.45 micron filter to remove interfering solids. Lactose was used as the standard sugar.

Concentrations of acids (butyric and acetic) and solvent (butanol) present in the fermentation samples were determined using a Varian 1520 gas chromatograph with a flame ionization detector. Separations were carried out in a 6' teflon coated stainless steel column filled with chromosorb WAW 80/100 having 1% AT 1000.

Results: Pure culture of C. beijerinckii

The kinetics of a batch fermentation of cheese whey using the pure culture of C. beijerinckii at a constant broth pH of 5.5 is shown in Figure 1. A total product concentration of 17.9 g/ℓ was obtained with a sugar consumption of 55.1 g/ℓ. 1.8 g/ℓ of sugar remained unutilized. 12.4 g/ℓ butyric acid, 3.5 g/ℓ acetic acid and 1.1 g/ℓ butanol were present in the broth. The overall yield of products (grams products produced/grams sugar consumed) was 30.8%. Biomass concentration was not measured as the cheese whey contained a substantial amount of solids (protein) in it. During the fermentation, butyric and acetic acids were formed first, their levels increasing rapidly from the start. Butanol appeared in the broth after a lag of 43 hours. Butyric acid levels increased linearly at a rate of 0.188 g/ℓ hr for the first 55 hours. The level of sugar also fell in nearly linear fashion. Acetic acid and butanol concentrations rose during this time, although at a much lower rate. The slow-down of metabolic activity may be attributed to product inhibition (14 g/ℓ total product) as 15 g/ℓ sugar still remained in the broth at that time.

Additional fermentations, conducted at lower (4.5, 5.0) as well as higher (6.3, 6.0) constant controlled broth pH values, showed that a pH

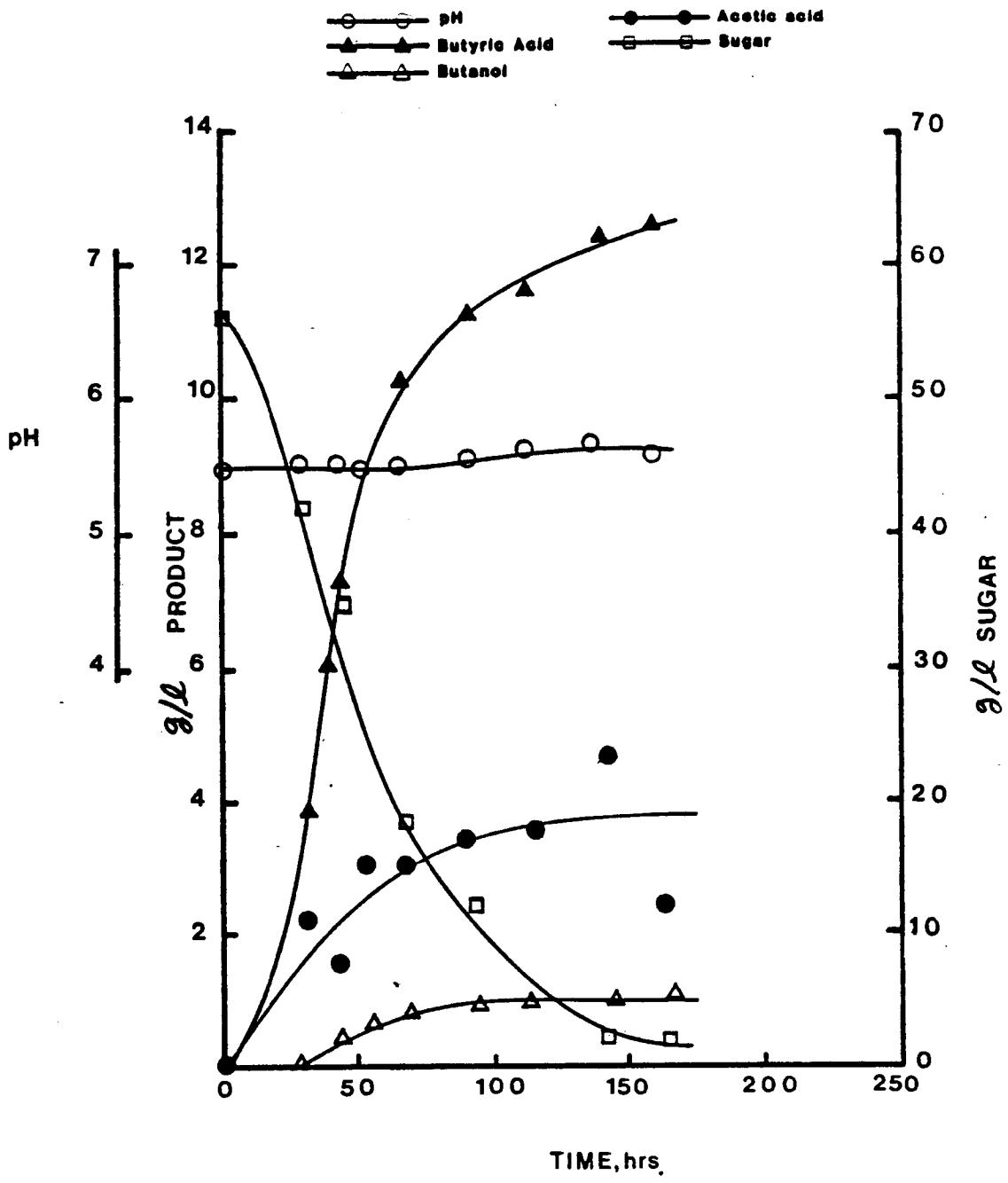

Figure 1. Batch Fermentation of cheese whey using C. beijerinckii: Initial pH of 3.5; pH controlled at 5.5.

of 5.5 was the optimal value for both the final concentration and the production rate of butyric acid; however, in each case butanol levels were quite low.

Literature (7) reports that a high initial pH favors growth and a lower final pH favors solvent production. An experiment was, therefore, conducted with an initial pH of 6.14. The pH was not controlled for the rest of this run. The kinetics is shown in Figure 2, which shows a typical 'butyric' formation. It can be concluded that this strain of clostridium beijerinckii is not a butanol producer. The low pH values do not stimulate butanol production in this strain. These, in fact, affect the overall metabolism adversely.

Results: Mixed culture of B. cereus and C. beijerinekii

The kinetics of a batch fermentation of cheese whey using the mixed culture is shown in Figure 3. The time-course observed was considerably different from that of the pure culture (Figure 1): acetic acid concentration decreased and the pH rose during the final phases of fermentation. Also, considerably more butanol was produced with the mixed culture. In both the fermentations, there were similarities in the microbial activities, butyric acid levels and sugar consumption patterns. Each fermentation resulted in high levels of butyric acid (> 11 g/ℓ) in less than 150 hours and completely utilized all of the available sugars in the broth. A total of 21.9 g/ℓ of products were formed with a sugar consumption of 63.52 g/ℓ. Acetic acid and butyric acid were present at levels of 3.7 g/ℓ and 11.7 g/ℓ, respectively. The level of butanol was 7.0 g/ℓ, which was almost seven times the amount formed in the pove culture C. beijerinckii fermentation on cheese whey.

The presence of the Bacillus was apparently increasing the level of butanol produced during the fermentations. Acetic acid consumption could

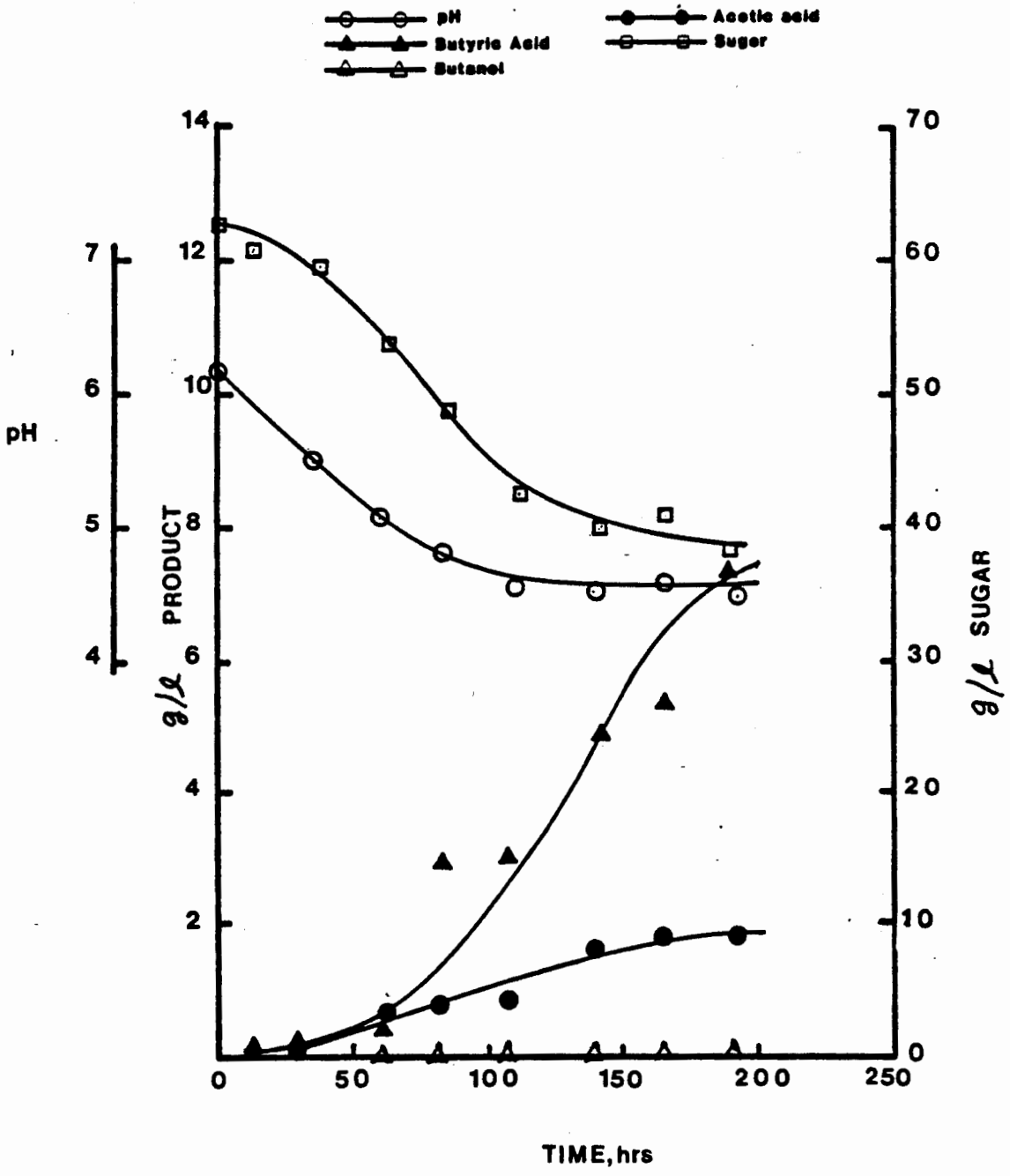

Figure 2. Batch Fermentation of cheese whey using C. beijerinckii: Initial pH of 6.14; uncontrolled pH.

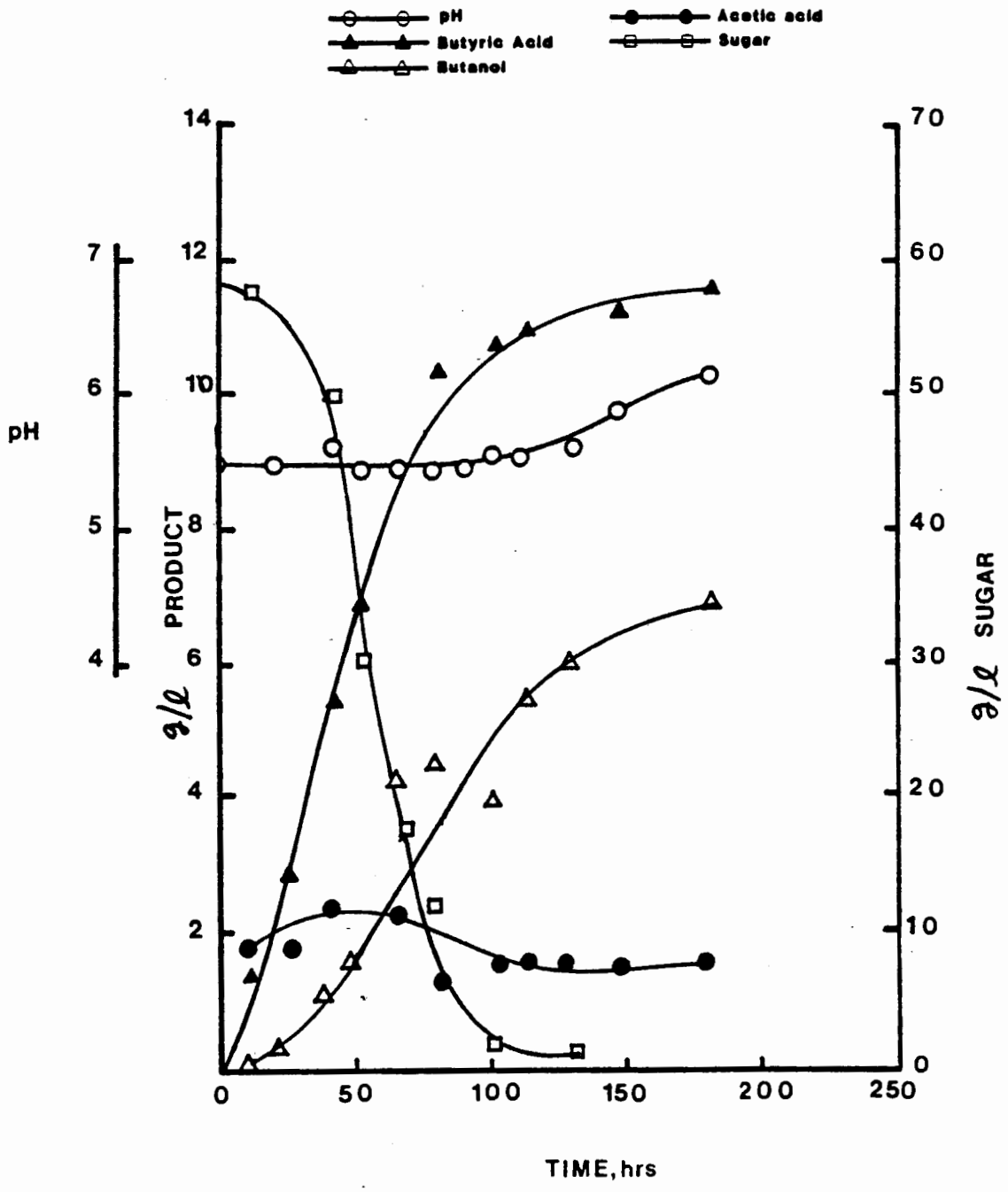

Figure 3. Batch Fermentation of cheese whey using the mixed culture: Initial pH of 5.5; pH controlled at 5.5.

not be associated with formation of any other product nor was any decrease in butyric acid level observed. The rise in pH may be due to the Bacillus, as this species is known to produce proteases which could attack the proteins present in the whey to form alkaline amides (8).

The kinetic profile (mixed culture on cheese whey) observed when the pH was initially held at 6.5 for 24 hours and then allowed to fall to 5.5 is shown in Figure 4. Under these conditions, the Bacillus apparently consumed large amounts of sugar without forming products. The fermentation activity ceased due to substrate limitation, as the sugar level fell to near zero in 50 hours. Very little products were found in the broth.

Experiments conducted at an initial pH of 6.3 and controlled at 5.5 and 5.0, respectively, gave less than optimal results in comparison to case of constant pH of 5.5. Under these conditions, the product levels were similar to these in the pure culture, except that production rates in the mixed culture were much higher. At a control pH of 5.0, the presence of Bacillus was not observed (as indicated by the similarities of yield to the pure culture). The influence of Bacillus, in increasing the butanol concentrations, is most noticeable at a constant pH of 5.5.

DISCUSSION: Bacillus Effect

The presence of B. cereus in C. beirjerinckii fermentations resulted in higher productivities, higher butanol levels and enhanced butanol to butyric acid ratios. A decrease in acetic acid levels and a rise in pH towards the end typified these fermentations. Figure 5 shows the effect of mixed culturing upon the maximum butyric acid production rate as a function of the control pH. At each pH value investigated, the butyric acid production rate was higher for the mixed culture than the pure culture of C. beijerinckii. A maximum rate is observed in both the cases at a control pH of 5.5.

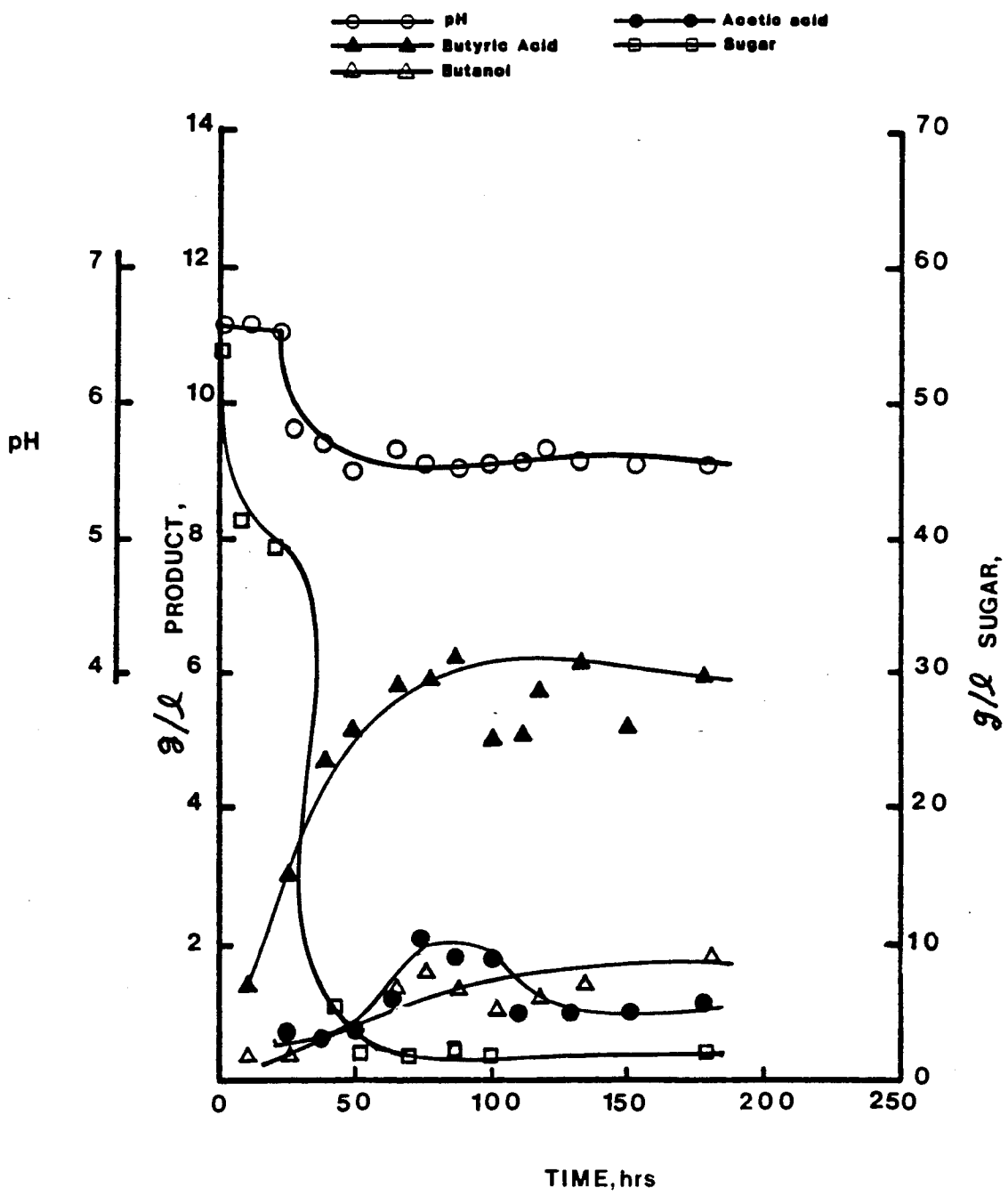

Figure 4. Batch Fermentation of cheese whey using the mixed culture: Initial pH 6.5; held for 24 hours; pH controlled at 5.5.

The effect of coculturing on sugar consumption as a function of the control of pH is shown in Figure 6. The theoretical sugar consumption values were calculated from the amount of lactose consumed to form the experimentally observed product concentrations using theoretical yield coefficients (9). For the pure culture of clostridium, the differences between the experimentally observed and the theoretically calculated values of substrate consumption were nearly constant at 4 g/ℓ.

In case of the mixed culture, the difference increases at higher control pH values. The increase is attributed to additional biomass formation (possibly Bacillus). At low pH (i.e. 5.0), the difference was nearly the same as that in the pure culture of clostridium. The total amount of sugar consumed in the case of the mixed culture, increased with an increase in control pH. However, for the pure culture of clostridium, the maximum was observed at a pH of 5.5.

Exact causes of these effects are not known; however, some speculation can be made about the effect of the presence of a Bacillus in a clostridium culture. Bacillus species are facultative anaerobes. Clostridium, on the other hand, are strict anaerobes. Attainment of strict anaerobic conditions, due to the Bacillus consuming oxygen in the broth, could allow the Clostridum to grow better. The strict anaerobic conditions might also divert butyric acid to butanol. There also exists the possiblity of a more complex interaction, such as a growth factor exchange. In conclusion, the mixed cultures are not uncommon in nature and the observation that a mixed culture is more productive than a mono-culture is not unrealistic.

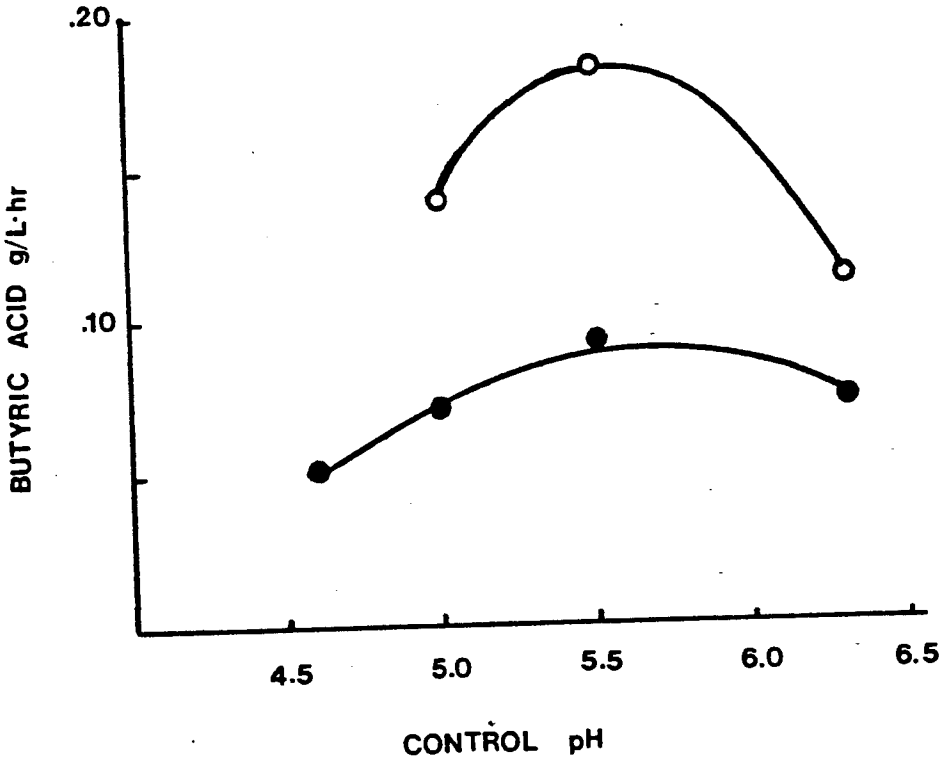

Figure 5. Maximum Butryci Acid Production Rate as a function of the control pH (Initial Broth pH 6.1-6.5)

o Mixed culture

● Pure culture

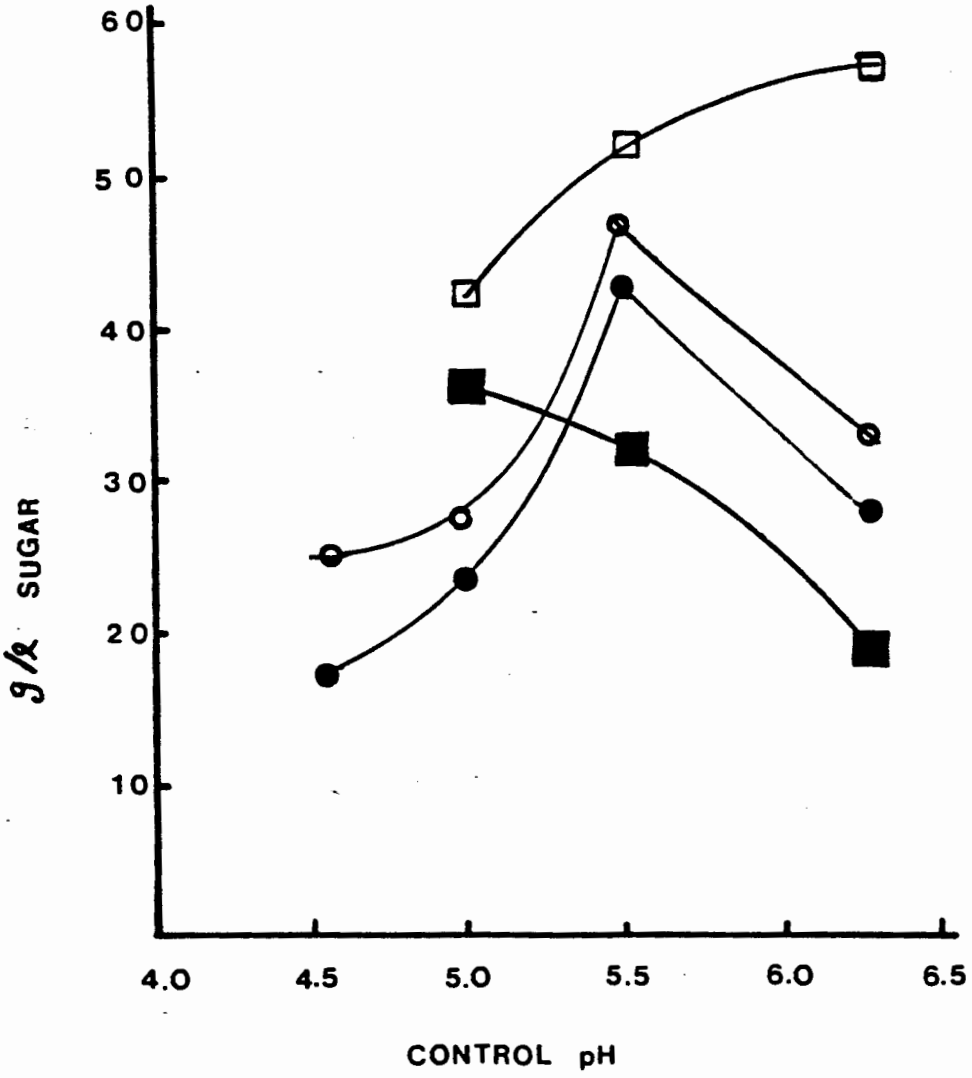

Figure 6. Experimental sugar consumption and Theoretical sugar consumed to form products as a function of the control pH (Initial pH 6.1-6.5)

Pure Culture	Mixed culture
o Experimental	□ Experimental
● Theoretical	■ Theoretical

References

(1) Lacy, W. J. and G. Rey. 1970. Federal Water Quality Administration, Washington, D.C. Presented at the Whey Utilization Conference, College Park, MD. June.

(2) Personal Communication. 1983. Mid-America Dairy - Kirksville, MO.

(3) Personal Communication. 1983. Mid-America Dairy - Emma, MO.

(4) Maddox, I. S. 1980. Production of n-butanol from whey ultrafiltrate. Biotechnol. Lett., Vol. 2, No. 11, pp. 493-498.

(5) Lindberg, S. 1983. M.S. thesis submitted to the Colorado State University, Fort Collins, CO.

(6) Nelson, N. 1944. A Photometric Adaption of the Somogi Method for Determination of Glucose. J. Biol. Chem. 153(2): pp. 375-380.

(7) Aiba, S., A. E. Humphrey and N. F. Millis. 1973. Biochemical Engineering. Academic Press, New York. 2nd Edition, p. 27.

(8) Atkinson, B. and F. Marituna. 1983. Biochemical Engineering and Biotechnology Handbook. MacMillian, Surrey, England. p. 396.

(9) Stevens. D. 1984. M.S. thesis submitted to the University of Missouri-Columbia, Columbia, MO.

PRELIMINARY PROCESS DESIGN FOR ETHANOL FROM SWEET SORGHUM ENSILAGE FEEDSTOCK

Keith D. Lange
Department of Agricultural and Chemical Engineering
Colorado State University
Fort Collins, Colorado 80523

Introduction

The preliminary process design for ethanol from sweet sorghum ensilage feedstock was undertaken as part of a more comprehensive study into the use of ensiling as a preservation method for sweet sorghum for storage periods of up to 155 days. For use of sweet sorghum as a fermentation feedstock, it was determined that ensiling not only was a viable means of preservation, but in fact enhanced the enzymatic hydrolysis of the combined hemicellulose and cellulose factions (1). Utilizing the data from the experimentation on these matters, the preliminary process design was undertaken to determine the economic attractiveness of producing ethanol from sweet sorghum.

Simplified Flow Diagram

The laboratory procedure for obtaining fermentable sugars from sweet sorghum involves two basic schemes as shown in Figure 1. The sorghum can be pressed and the juice stream could be utilized directly as it contains around 9 percent fermentable sugar, or the high cellulosic content of the sorghum can be converted to fermentable sugars by enzymatic hydrolysis. In this study, a combination of both methods was employed in order to utilize both sources of sugar. The enzymatic hydrolysis route involves field chopping the stock sorghum and ensiling. After a period of time, the silage is pasteurized and then hydrolyzed by cellulase enzymes. Finally, the hydrolysis residue is dewatered to produce an animal feed and the hydrolysate is concentrated for fermentation. The simplified flow diagram becomes considerably more complex when designing the actual process.

Process Flow Diagram

Figure 2 depicts the actual process flow diagram for a 50 million gallons/year ethanol production facility using sweet sorghum as a feedstock. The process was analyzed for an operating time of 330 days per year, allowing for 10 percent down time per year.

Sweet sorghum from a 12.5 mile radius to be a central production facility is field chopped and ensiled at the farm. Ensiling is a well-recognized practice in which forage crops are stored and preserved in silos or open pits. A layer of sorghum is put down,

packed and an inoculum is spread across the top, more sorghum is then added, packed and treated. This process continues until the pit is full. In the laboratory studies, 500 mg of *Lactobacillus* was added per kilogram of dry sorghum.

The silage is transported an average of 7.5 miles to the plant where the solid and liquid factions are separated by means of a screw press. The juice goes to an evaporator and the silage is pasteurized so that the *Lactobacillus* will not utilize the hydrolyzed sugars produced in a later step.

After pasteurization, the silage is delignified by the addition of sodium hydroxide. This step was added after laboratory extractions revealed that increased enzymatic hydrolysis of cellulose was realized by addition of sodium hydroxide. This proved to be quite substantial as two to three times greater sugar yields resulted. Following delignification, pH is adjusted to approximately 5 by adding concentrated sulfuric acid.

After pH adjustment, the silage enters a series of eight absorption-filtration units from which 65 percent of the enzyme is recovered from the hydrolysate stream. Silage enters absorption I, the solution is filtered, the liquid is sent to the evaporator, and the solids go to absorption II where is comes in contact with the liquid from absorption III. This scheme allows for counter-current flow of liquids and solids so that absorption of the enzyme can be maximized on the unhydrolyzed cellulose in the solids stream. This pattern continues until absorption VIII.

The solids stream from filtration VIII is split into two streams each of which enters a series of six hydrolysis units to which water and make-up enzyme are added. The hydrolysis product is filtered, residual solids are recovered, and the liquid enters absorption VIII eventually finding its way to the liquid stream leaving filtration I. The combined pressed juice and hydrolysate streams then enter a five-effect, feed backward evaporator removing water and volatile acids and producing a 16-weight percent sugar solution for fermentation.

The concentrated sugar stream is split into two streams and enters a series of eight staggered reactors each having a residence time of 48 hours. The fermentation broth is then distilled to 95-weight percent ethanol in a 39 stage column.

With the flow rates determined, the equipment was then sized and the economic attractiveness of the process determined.

Economics

The economics of producing ethanol from sweet sorghum ensilage feedstock were determined by methods outlined in Peters and

Timmerhaus (2) and involve the calculation of capital costs based on equipment costs and production costs based on raw materials cost.

Equipment Costs

Equipment costs were determined on the basis of available cost data (2) and updated by using a Marshall and Swift index of 771 corresponding to the first quarter of 1984.

The total equipment costs amount to $37,158,000 of which 47 percent can be attributed to enzyme recovery and hydrolysis. The fermentation units also account for a large portion of the equipment costs making up 31 percent of the total. The equipment costs for each step of the process are given in Table 1.

Capital Costs

For a large capacity fluids-solids facility, the total capital investment is estimated based upon applicable percentages of the total equipment costs. The individual capital costs and percentages are detailed in Table 2. This analysis gives a fixed capital investment of $115,804,000 and a total capital investment of $136,240,000.

Raw Materials Costs

Raw materials costs were found from data in *Chemical Marketing Reporter* and by conversations with distributors. The cellulase enzyme is a combination of 2 percent cellulase complex and 0.2 percent cellobiase selling at $6 and $3 per treated kilogram, respectively, from Novo Corporation (Welton, Connecticut). This gives an annual cellulase cost of $15,126,000 or 39 percent of the total raw materials cost. The other raw material costs and their unit prices are given in Table 3.

Production Costs

The production costs involve the direct costs associated with the processing of the sorghum, the fixed charges due to capital investment and the general expenses of operation. The direct costs are based primarily on percentages of the total capital costs, the fixed charges are based on various percentages of the capital costs and the general expenses are based on the total product cost. The total yearly product cost is $95,989,000 of which 72 percent is related to the direct costs. Table 4 details the costs associated with production.

Product Value

In addition to the ethanol produced, the residual solids following hydrolysis and the distillation bottoms both have some value. The total product value is $110,310,000. Table 5 gives the unit and total product values.

Discussion

The break-even point for the process is determined by subtracting the by-product value from the total production costs and dividing by the quantity of ethanol produced. This turns out to be $1.55/gal compared to the current selling price for 95 percent ethanol of $1.84/gal. The return on investment for the process is 7 percent.

As the nature of this analysis involves around 30 percent uncertainty, the range of ethanol costs that can be expected are from $1.08 to $2.02 per gallon. If production costs could be reduced to correspond with $1.08/gal, the return on investment that could then be realized is nearly 18 percent.

As the sweet sorghum and enzyme costs constitute a majority of the raw materials costs, an analysis of their effect on ethanol price was considered. Figure 3 shows this relationship with the dashed lines indicating the base case of $30/MT sweet sorghum costs and 65 percent recovery of cellulase. This graph shows that any combination of sweet sorghum costs and enzyme recover that falls below an ethanol price of $1.84/gal will result in a net profit.

References

1. Linden, J. C., L. L. Henk and V. G. Murphy (1984). Storage of potential fermentables in sweet sorghum by ensiling. Presented at the 6th Symposium on Biotechnology, Gatlinburg, TN. May 17-19.

2. Peters, M. S. and K. D. Timmerhaus (1980). Plant Design and Economics for Chemical Engineers. McGraw Hill Book Co., New York.

3. Dale, B. E. (1983). Biomass refining: protein and ethanol from alfalfa. I.&E.C. Prod. Res. Dev. 22:446.

Table 1. Equipment costs.

Unit	Dollars (thousands)
Screw press	648
Pasteurization	383
Delignification	391
pH adjustment	240
Enzyme recovery	3,314
Hydrolysis	14,137
Evaporation	4,674
Fermentation	11,351
Distillation	2,202

Table 2. Capital costs.

	Dollars (thousands)
Direct costs	
Equipment	37,158
Installation (10% E)	3,716
Instrumentation and controls (8% E)	2,973
Piping (20% E)	7,432
Electrical (9% E)	2,973
Buildings (15% E)	5,574
Yard improvements (5% E)	1,858
Service facilities (35% E)	13,005
Land (4% E)	1,486
	76,175
Indirect costs	
Engineering and supervision (32% E)	11,890
Construction expenses (34% E)	12,634
	24,524
Total direct and indirect costs	100,699
Contractors fee (5% D+I)	5,035
Contingency (10% D+I)	10,070
Fixed capital investment	115,804
Working capital (15% TCI)	20,436
Total capital investment	136,240

Table 3. Raw materials costs.

Item	Dollars (thousands/yr)
Sweet sorghum ($30/dry ton)	19,974
Sodium hydroxide ($0.37/lb)	1,623
Lactobacillus ($0.95/treated wet ton)	2,107
Sulfuric acid ($0.034/lb)	150
Cellulase	15,126
	38,980

Table 4. Production costs

	Dollars (thousands/yr)
Direct costs	
Raw materials	38,980
Operating labor (10% TPC)	9,599
Supervising labor (10% op. lab.)	960
Utilities (15% TPC)	14,398
Maintenance and repairs (2% FCI)	2,316
Operating supplies (10% M&R)	232
Laboratory (20% op. lab.)	1,920
	68,405
Fixed charges	
Depreciation (10% E + 2% buildings)	3,827
Local taxes (4% FCI)	4,632
Insurance (1% FCI)	1,158
Plant overhead (50% op. lab., sup. lab., M&R)	6,438
	16,055
General expenses	
Administration (15% op. lab., sup. lab., M&R)	1,931
Distribution and selling (5% TPC)	4,799
Research and development (5% TPC)	4,799
	11,529
Total product cost	95,989

Table 5. Product value.

Item	Dollars (thousands/yr)
Residual solids (3) ($220/MT protein)[1]	12,610
Distillation bottoms (3) ($150/MT protein)[2]	5,700
Ethanol (95-wt. %) ($1.84/gal)[3]	92,000
	110,310

[1]Based on 8 percent protein content of sweet sorghum plus enzyme protein lost in combined form with hydrolysis residue.

[2]Based on yeast biomass yield of 0.12 on fermentable sugars.

[3]Chemical Marketing Reporter, April 1984.

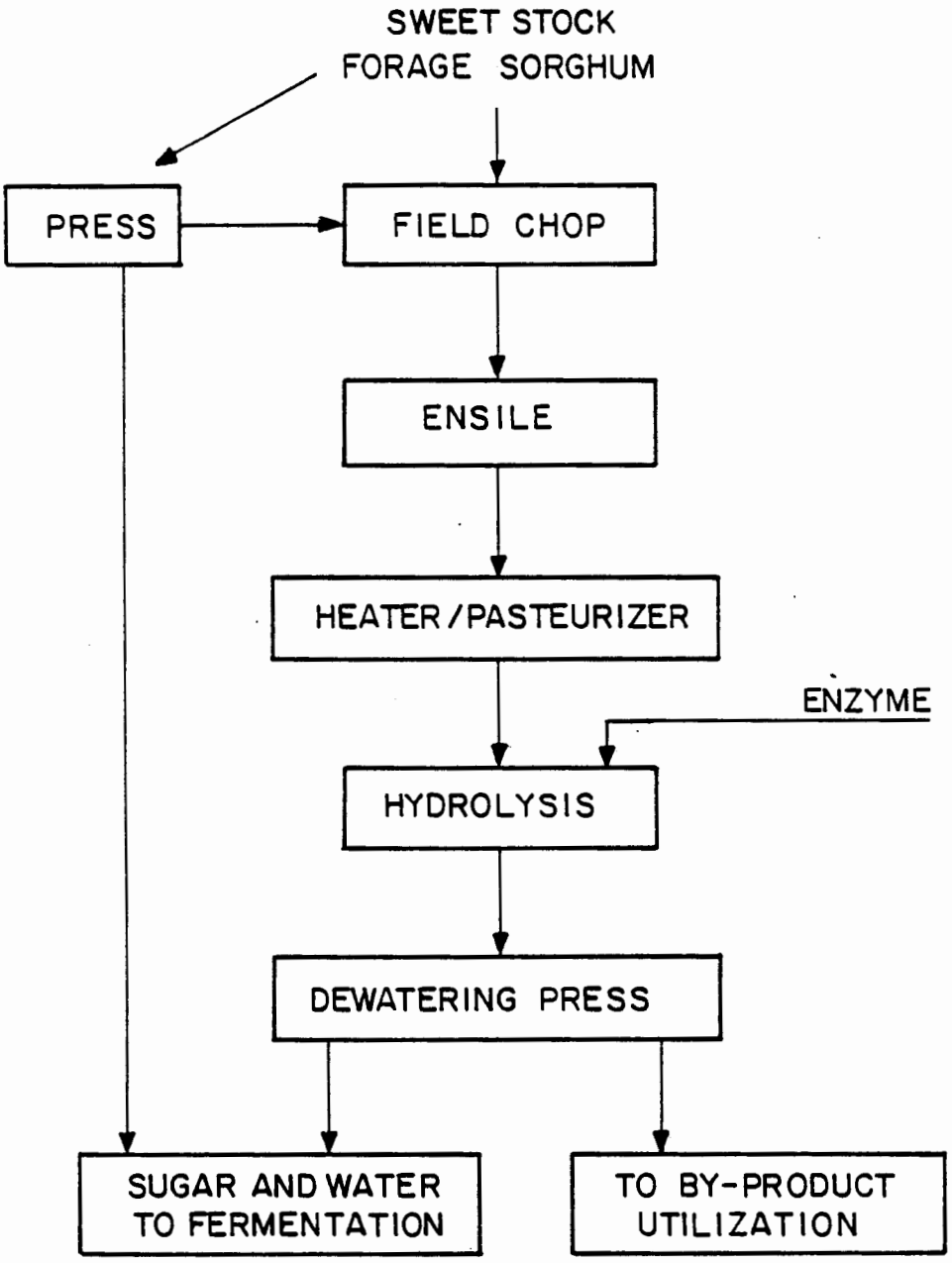

Figure 1. Simplified flow diagram for producing fermentable sugars from sweet sorghum.

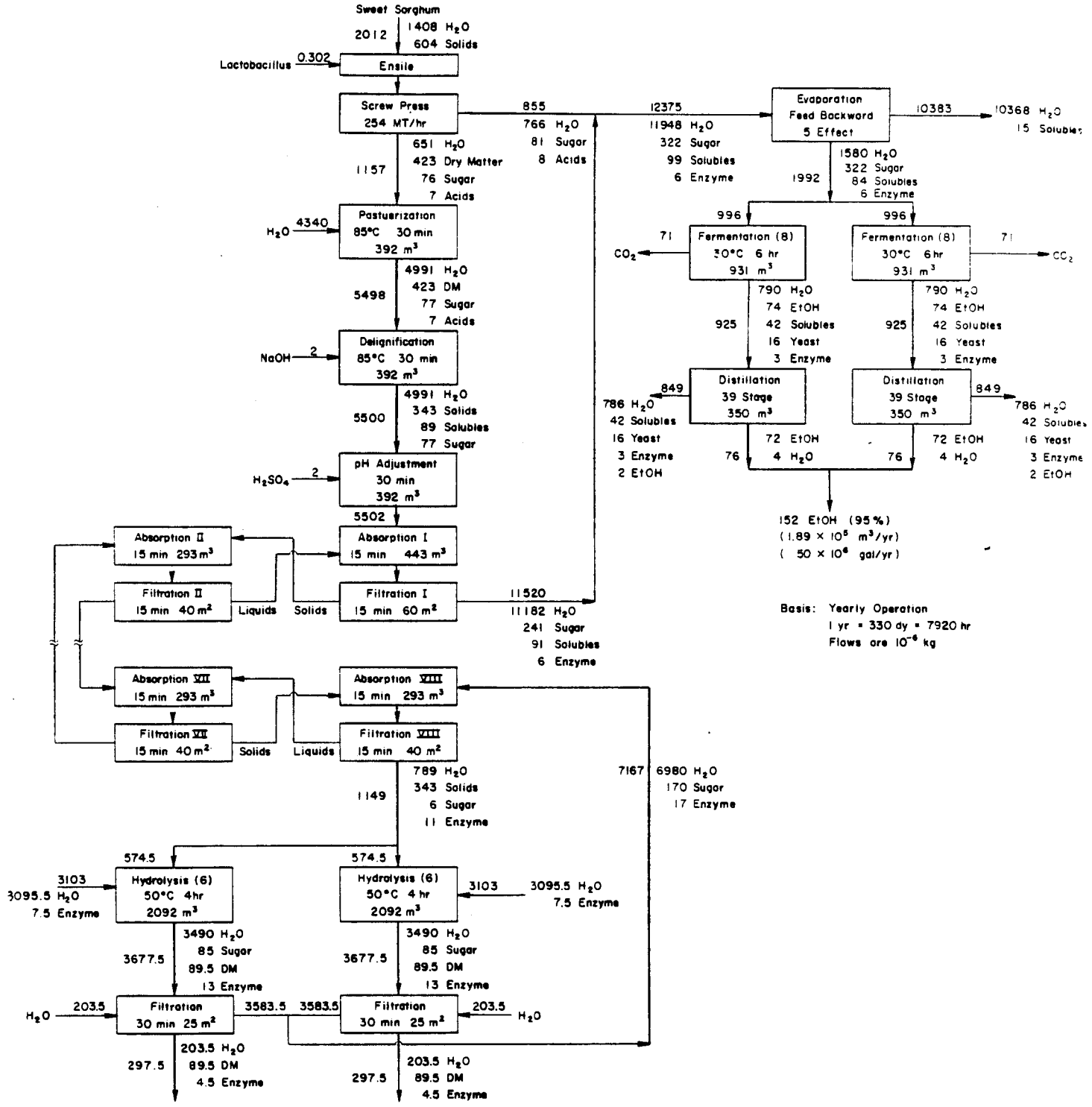

Figure 2. Process flow diagram for a 50 million gal/yr ethanol production facility.

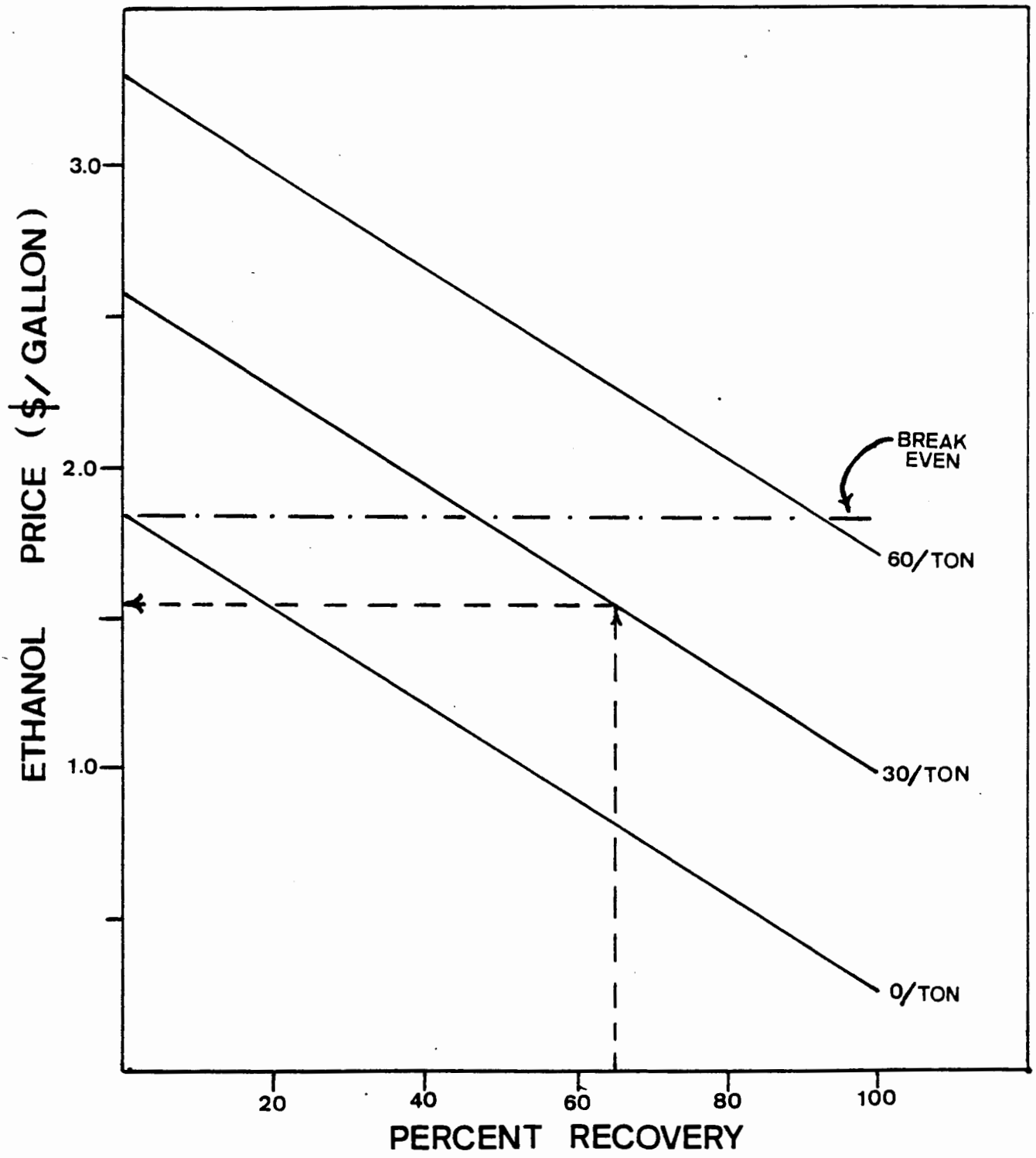

Figure 3. Effect of feedstock price and cellulase recovery on ethanol price.

LAMELLA SETTLER FOR ETHANOL FERMENTATION

* Y. Jayanata, M. Grote, M. Reuss

Technische Universitaet Berlin
Fachbereich Fermentation and Brauwesen
Seestr. 13
1 Berlin 65
W. Germany

INTRODUCTION

One of the possibilities in increasing the productivity of ethanol fermentation is the continuous process with biomass recycling. It is obvious that the efficiency of the separation devices plays an important role for the total productivity, that is the productivity based upon total process volume (fermentor and settler). Advances towards optimal design and operation of the whole system, fermentor and settler, will not be obtainable without a deeper understanding and mathematical modelling of the settling devices itself. This work is aimed to present a comprehensive mathematical model for the settler in developing a mathematical framework, in which settling characteristics and fermentation operations can be treated as an integrated system. The analysis is, however, restricted to a special type of settler, namely, lamella settler in the form of inclined tube.

Lamella settler are high-rate sedimentation devices consisting of inclined parallel plates, tubes, or structures with honeycombed and wavelike cross sections, stacked to form channels into which a slurry is fed for gravitational separation (fig.1). According to the directions of the liquid flow and the flow of sedimented solid, three different operation methods can be distinguished: cocurrent, counter-current and cross-current (fig. 2). The beneficial effects of inclined surfaces in a vessel designed for sedimentation operation has been known for a considerable period of time /1/. In consideration with ethanol fermentation following advantages of lamella settler can be observed:

1. Additional separation area results in a higher separation efficiency per unit volume.
2. Reduction of liquid height for rising bubbles results in less back-mixing/disturbance under conditions of CO_2 - evolution.
3. Possibility of separation of bacterial infection from yeast suspension.

---

*Present address:
University of Missouri-Columbia
Department of Chemical Engineering
Columbia, MO 65211

THEORITICAL CONSIDERATIONS:

Two different approaches to the mathematical modelling of the sedimentation characteristic in tube settler have followed, namely:
1. Window-model (Binder et al. /2,3/).
2. Distributed parameter modelling.

Window-model:

The fundamental principle of the so called "Window-model" for sedimentation is the calculation of particle trajectories on the basis of hydrodynamic considerations. Fig. 3 visualizes the particle trajectories in a tube-settler for counter-current operation conditions. A particle will be separated if a trajectory ends at bottom area of the inclined tube. The limit for complete separation is approached under conditions in which the yeast cells from the upper inclined surface in the entering region are being captured on the lower inclined surface at the exit. Increasing the flow rate beyond this critical point leads to an "entrance-window" containing those yeast cells which cannot be separated.
From the calculation of the trajectories of single particle, Binder /2,3/ derived the following theoretical equation for clarification efficiency

$$\beta = 1 - \frac{8}{\pi}\left[Y_F\sqrt{\frac{1}{4} - Y_F^2}\,(1-W_S \sin\alpha) + \frac{8}{3}\,Y_F\left(\frac{1}{4} - Y_F^2\right)^{3/2} - \frac{1}{4}\arcsin(2Y_F) - Y_F\,W_S\,L^*\cos\alpha\right] \quad (1)$$

for inclined tube settler in counter-current operation condition. The dimensionless velocity W_S is

$$W_S = \frac{W_{XO}}{W_F} \quad (2)$$

and

$$W_F = \frac{V}{n_R \frac{\pi}{4} d_R^2} \quad (3)$$

where as n_R = number of the tube

d_R = tube diameter

W_{XO} = sedimentation velocity of single yeast cell

W_F = average fluid velocity in tube

α = angle of inclination

The characteristic width of the entrance-window Y_F of a limiting trajectory can be calculated iterativly from

$$\sqrt{\frac{1}{4} - Y_F^2}\cdot\left(-1 + 4Y_F^2 + \frac{3}{4}\,W_S \sin\alpha\right) + \frac{3}{8}\,L^*\,W_S\cos\alpha = 0 \quad (4)$$

(L^* = ratio of tube length to diameter L/d_R)

The clarification efficiency, β, is defined by (see fig. 4):

$$\beta = \frac{X_{sed} \quad \dot{V}_{sed}}{X^{\alpha} \quad \dot{V}} \tag{5}$$

Distributed parameter modelling:

Applying the general assumption in plug flow reactor and additional neglection of the sediment layer in inclined tube, the mass balance of biomass in volume element (Fig. 5) for sedimentation condition without fluidization is:

$$\frac{\partial}{\partial t} (X(z)\, dV) = \dot{V}\ \dot{X}(z) - \dot{V}\ X(z) - \frac{\partial}{\partial z} (\dot{V}\ X(z))\, dz\ \dot{m}_{Sed} \tag{6}$$

with the sedimented biomass flow, m_{Sed},

$$\dot{m}_{Sed} = X(z)\ W_X\, dA_F \tag{7}$$

where W_X is the concentration depending settling velocity of the yeasts and the effective sedimentation area,

$$A_F = \frac{\pi}{4}\ d_R\ (d_R \sin\alpha + L \cos\alpha)$$

or

$$dA_F = A_F\ \frac{dz}{L} = \frac{\pi}{4}\ d_R\ \left(\frac{d_R}{L} \sin\alpha\right)\ dz \tag{8}$$

Introducing eq. (7) and eq. (8) in eq. (6) it follows

$$\frac{\partial}{\partial t} \left(\frac{\pi}{4}\ d_R^2\ X(z)\ dz\right) = \dot{V}\ X(z) - \dot{V}\ X(z) - \frac{\partial}{\partial z} (\dot{V}\ X(z))\, dz - W_X\ \frac{\pi}{4}\ d_R \left(\frac{d_R}{L} \sin\alpha + \cos\alpha\right) X(z)\, dz \tag{9}$$

In steady-state condition ($\partial X(z) / \partial t = 0$), eq. (6) becomes

$$\frac{dX(z)}{dz} = -\frac{W_X}{W_F} \left(\frac{\sin\alpha}{L} + \frac{\cos\alpha}{d_R}\right) X(\ ) \tag{10}$$

With the initial condition $X(z=0) = X^{\alpha}$, differential eq. (10) can be integrated numerically if an appropriate equation for the hindered settling velocity of yeast cells W_X is available. From sedimentation experiments in settling cylinder following correlation

$$W_X = k_W\ W_{Xo} \left(1 - \frac{X(z)}{X_{max}}\right)^n \tag{11}$$

where k_W, n = empirical constant

W_{Xo} = settling velocity of single yeast cell

X_{max} = maximal yeast concentration

can be verified. In principle, eq. (11) is similar to the known correlation of Richardson and Zaki /4/.
The maximal yeast concentration, X_{max}, can be calculated by using the viscosity function of baker's yeast according to Josić et al./5,6/:

$$X_{max} = \left[(0{,}0487\ P_{osm} + 1{,}59)\ \ 3{,}05\ 10^{-3} \exp(-3\ 10^{-2} P_{osm}) \right]^{-1} \qquad (12)$$

with the osmotic pressure

$$P_{osm} = \frac{1}{46}\ P\ R\ T \qquad (13)$$

where P = ethanol concentration g/ℓ
R = gas constant bar ℓ/mol k
T = temperature K

The yeast concentration in outlet $X^{\omega} = X(z=L)$ can be obtained by intergrating eq. (10) with eq. (11) and eq. (12) along the tube. From the mass balance in settler, the yeast concentration in the sediment can be calculated by

$$X_{Sed} = \frac{X^{\alpha}\ \dot{V} - X^{\omega}\ \dot{V}^{\omega}}{\dot{V}_{Sed}} \qquad (14)$$

This sediment concentration, X_{Sed}, is actually the controlling parameter in the fermentation process with biomass recycling, so that by knowing this concentration the whole process - fermentation and separation - can be simulated and predicted as an integrated system.

MATERIAL AND METHODS

The systems under study are single and multi-tube settlers (fig.6-7) in countercurrent operation conditions. The angle of inclination is varied between 30° to 60°. Fig. 8 shows the schematic flow sheet for sedimentation experiments of yeast suspension in isotonic saline solution (=1.15% NaCl, /5,6/). The connection with a fermentor for continuous fermentation with cell recycle is schematically shown in Fig. 9. The continuous fermentations were studied in a 1 liter fermentor (LH-Engineering, London, England) with a working volume of 0,75 liter.
For all the experiments, commercial baker's yeast Saccharomyces cervisiae (Uniferm, Monheim/Werne, W. Germany) was employed. This yeast strain is non-flocculent.

Fermentation media:

I. Glucose Go [g/ℓ] or Fructose Fo [g/ℓ] (variable), yeast extract = Go/10, NH_4Cl = Go/75.9, $MgSO_4.7H_2O$ = Go/862.1, $CaCl_2\ 2H_2O$ = Go/1190.5.

II. Best molasses (clarified and membrane filtered sterilized) M [g/ℓ] (variable), NH_4HPO_4 = M/200, $MgSO_4.7H_2O$ = M/800.

Fermentation conditions:

pH = 4.5; temperature = 30^{o} C; agitation = 500 rpm.

Analytical methods:

Biomass: gravimetric; glucose, fructose and sucrose: enzymatic

RESULTS AND DISCUSSION

Fig. 10 shows an example of the comparison between predicted clarification efficiency by window-model (eq.(1) with eq. (4)) and experimental observation as a function of the dimensionless velocity W_S for different inlet yeast concentration in isotonic saline solution. The effects of the angle of inclination can be observed from fig. 11.
We see from that figures that only a qualitative agreement between the model and experiment can be achieved. Although better separation can be obtained with angle of 30^{o}, long term experiments indicated that with 45^{o} angle of inclination continuous and effective sliding of the settled biomass can be guaranteed. The model, however, does not take into account the influence of inlet yeast concentration. On the other hand, the flow rate of sediment, V_{Sed}, affects the sedimentation efficiency drastically in some cases (fig. 12). It indicates that consideration of yeast inlet concentration in hindered settling velocity of the yeast alone is not able to quantify this phenomenon. Systematic analysis of this problem /7/ resulted in a possibility of applying the window-model for quantitative prediction by introducing an effective settling velocity of the yeast cells as an empirical function of characteristic yeast concentration in inlet as well as in the sediment. From the view point of integrated modelling of ethanol fermentation with biomass recycling (fermentation + separation), this expansion of the window-model, however, complicates the mathematical treatment of the system, particularly in connection with the objective of incorporating possible effects of CO_2 bubbles/disturbance in settler, which is important for optimal operation during the starting period and control of disturbances. It was decided, therefore, to apply the well known concept of the distributed parameter modelling instead.

Fig. 13 shows a comparison of the calculated biomass concentration in the sediment (eq. (10) - eq. (14)) with the experimentally observed data for single and multi-tube settlers and different inlet biomass concentrations. The relatively good agreement between the model prediction and the experimental observations allows one to expand the applicability of the concept of distributed parameter modelling in connected condition with CO_2 evolution in the settler.

Effects of CO_2 - evolution on settler characteristics:

In the ethanol fermentation process with cell recycle, incomplete substrate utilization in fermentor reduces the settler efficiency due to CO_2 - disturbance. The biomass concentration in the sediment that is recycled to the fermentor will moreover decrease which causes further reduction of cell concentration in fermentor so that the expected steady-state condition can not be obtained. The interaction of sedimentation, reaction and disturbance in a fluid element is shown in fig. 14. It is assumed that the effects of CO_2 -disturbance can be

quantified by an induced fluid velocity W_{CO_2} due to the rising bubbles. The effective sedimentation velocity is then

$$W_{eff} = W_X - W_{CO_2} \tag{15}$$

W_{CO_2} can be estimated from the dissipated energy due to rising bubbles N_B. According to Delente et al./8/, the specific dissipated energy is given by

$$\frac{N_B}{V_F} = q_{CO_2} \frac{1}{\rho_{CO_2}} P_B \left(\frac{P_B + P_H}{P_H} \ln \frac{P_B + P_H}{P_B} - 1\right) \tag{16}$$

where: q_{CO_2} = spec. CO_2 - production rate based upon working volume.

ρ_{CO_2} = spec. gravity of CO_2.

P_H = hydrostatic pressure = $\rho\ g\ d_R \cos\alpha$.

P_B = environment pressure.

Based upon the conception

$$\frac{N_B}{V_F} = \tau \frac{dw}{dx}, \tag{17}$$

with Newton's shear rate low

$$\tau = \eta_s \frac{dw}{dx}, \tag{18}$$

it follows for gradient of shear rate

$$\frac{dw}{dx} = \sqrt{\frac{N_B}{V_F} \frac{1}{\eta_s}} \tag{19}$$

One could assume that on the bottom side of the tube, dW/dx is zero. Integration of eq. (19) for a given rising distance results

$$W_{CO_2} \sim \sqrt{\frac{N_B}{V_F}} \quad \text{or} \quad W_{CO_2} = k_{CO_2} \sqrt{\frac{N_B}{V_F}} \tag{20}$$

Introducing eq. (20) with

$$N_B(z) = \frac{44}{46} \nu(z) \tag{21}$$

in eq. (16), it follows

$$W_{CO_2} = k_{CO_2} \sqrt{\frac{44}{46} \nu(z) \frac{X(z)}{\rho_{CO_2}} P_B \left[\frac{P_B + P_H}{P_H} \ln \frac{P_B + P_H}{P_B} - 1\right]} \tag{22}$$

where $\nu(z)$ is specific ethanol production rate at distance z from entrance and k_{CO_2} empirical fluidization factor. This derived correlation eq. (20) represent, of course, a simplification of the more complicated real conditions. However, the intensification of the disturbance due to increased ethanol production, thus, CO_2 - evolution, in settler can be well quantified from that equation. To characterize the clarification efficiency it is necessary to expand the differential balance equation for biomass, substrate and ethanol regarding growth and ethanol production.

In steady-state condition

$$\frac{\partial X(z)}{\partial t} = \frac{\partial G(z)}{\partial t} = \frac{\partial F(z)}{\partial t} = \frac{\partial Sc(z)}{\partial t} = \frac{\partial P(z)}{\partial t} = 0 ,$$

following balance equations for sucrose/molasses as substrate can be derived:

Biomass:

$$\frac{dX(z)}{dz} = \mu(z) \frac{X(z)}{W_F} - \frac{(W_X - W_{CO_2})}{W_F} \left(\frac{\sin\alpha}{L} + \frac{\cos\alpha}{d_R} \right) X(z) \qquad (23)$$

Ethanol:

$$\frac{dP(z)}{dz} = \frac{\nu(z)\, X(z)}{W_F} \qquad (24)$$

Glucose:

$$\frac{dG(z)}{dz} = \frac{X(z)}{W_F} \left(- \frac{\mu_G(z)}{(Y_{X/S})_{th}} - \frac{\nu_G(z)}{(Y_{P/S})_{th}} + 0{,}525\, r_{inv}(z) - m_G \right) \qquad (25)$$

Fructose:

$$\frac{dF(z)}{dz} = \frac{X(z)}{W_F} \left(- \frac{\mu_F(z)}{(Y_{X/S})_{th}} - \frac{\nu_F(z)}{(Y_{P/S})_{th}} + 0{,}525\, r_{inv}(z) - m_F \right) \qquad (26)$$

Sucrose:

$$\frac{dSc(z)}{dz} = - r_{inv}(z) \frac{X(z)}{W_F} , \qquad (27)$$

where the specific growth rate $\mu(z)$

$$\mu(z) = \mu_F(z) + \mu_G(z) \qquad (28)$$

with

$$\mu_G(z) = \mu_m^G \frac{G(z)}{K_G(1+aF(z)) + G(z)} \quad \frac{1}{1+P(z)/K_{P1}+P(z)^2/K_{P2}} \tag{29}$$

$$\mu_F(z) = \mu_m^F \frac{G(z)}{K_F(1+G(z)/a) + F(z)} \quad \frac{1}{1+P(z)/K_{P1}+P(z)^2/K_{P2}} \tag{30}$$

and the specific production rate $\nu(z)$

$$\nu(z) = \nu_F(z) + \nu_G(z) \tag{31}$$

with

$$\nu_G(z) = \nu_m^G \frac{G(z)}{K_G'(1+bF(z))+G(z)} \quad \frac{1}{1+P(z)/K_P'} \tag{32}$$

$$\nu_F(z) = \nu_m^F \frac{F(z)}{K_F'(1+G(z)/b) + F(z)} \quad \frac{1}{1+P(z)/K_F'} \tag{33}$$

The specific hydrolysis rate, $r_{inv}(z)$, is

$$r_{inv}(z) = r_m E(z) \frac{1}{1+M/K_{I1}} \quad \frac{Sc(z)}{K_M(1+M/K_{I2})+Sc(z)} \quad \frac{1}{1+P(z)/K_a} \tag{34}$$

with the spec. invertase concentration

$$E(z) = E_{max} \frac{1 + k_1 (G(z) + F(z))^4}{1 + k_2(G(z) + F(z))^4} \tag{35}$$

Due to CO_2-evolution in the settler, thus, two-phase flow condition in the tube, the fluid velocity, W_F (eq. (3)) becomes

$$W_F = \Phi_F \frac{\dot{V}}{n_R \frac{\pi}{4} d_R^2} \tag{36}$$

where Φ is the correction factor of the two-phase flow condition.

The equations eq. (28) - (35) have been verified from previous systematic experiments of continuous ethanol fermentation and successfully applied for simulation and prediction of that fermentation for different process conditions/9/.
By intergrating eq. (23) - (27) along the tube for given different k_{CO_2} one can perceive the effects of this fluidization factor on the k_{CO_2} concentration profile in tube-settler. From fig. 15 we observe that the measured biomass outlet concentration lies logically between the two extreme plug flow conditions, complete fluidization and complete sedimentation. Table 1 shows an example of model calculations for different k_{CO_2} compared with experimental observations in settler of ethanol k_{CO_2} fermentation with cell recycle on molasses and glucose by non-complete sugar utilization in fermentor. We recognize here that with a fluidization factor of

$$k_{CO_2} = 2\ 10^{-7}\ \ m^2/N^{0.5}\ s^{0.5}$$

the effect of CO_2 disturbance can be tendentiell predicted.

Without difficulties the above settler model based upon distributed parameter modelling, with or without CO_2-disturbances, has been successfully intergrated with the fermentation kinetics in fermentor, so that process with cell recycle can be simulated and predicted as a whole system /9,10/.

REFERENCES:

1. Boycott, A. E., Nature 104, 532 (1920).
2. Binder, H., Dissertation Technical University Berlin, 1980, W. Germany.
3. Wiesman, U.; Binder, H., Advances in Biochemical Engineering, Edited by A. Fiechter, Vol. 24, 119 (1982).
4. Richardson, G. F.; Zaki, W.N., Chem. Eng. Sci., 3, 65 (1954).
5. Josić, D., Dissertation Technical University Berlin, 1981, W. Germany.
6. Reuss, M.; Josić, D.; Popović, M.; Bronn, W. K., European J. Appl. Microbiol. Biotechnol., 8,167 (1979).
7. Grote, M., Master Thesis Technical University Berlin, 1983, W. Germany.
8. Delente, J.; Akin, C.; Krabbe, E.; Ladenburg, K., Biotechnol. Bioeng., 11, 631 (1969).
9. Jayanata, Y., Dissertation Technical University Berlin, 1983, W. Germany.
10. Jayanata, Y.; Reuss, M., 7th International Biotechnology Symposium, New Delhi, India, 1984.

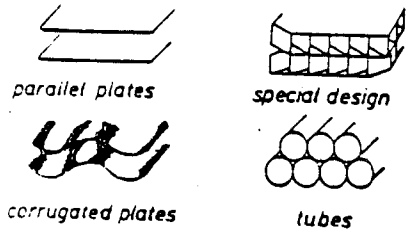

Fig. 1 Lamella type of settler.

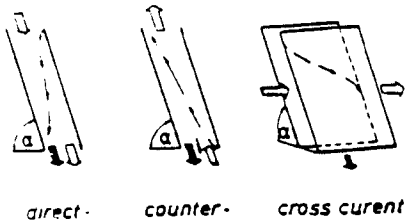

Fig. 2 Operation conditions of lamella settler.

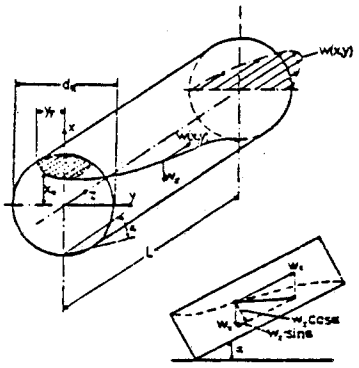

Fig. 3 Particle trajectories in counter-current sedimentation in a tube.

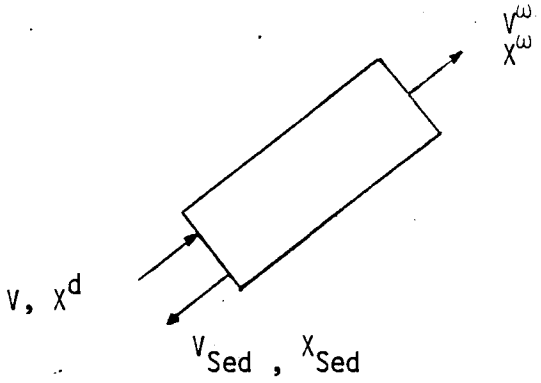

Fig. 4 Counter-current sedimentation in an inclined tube.

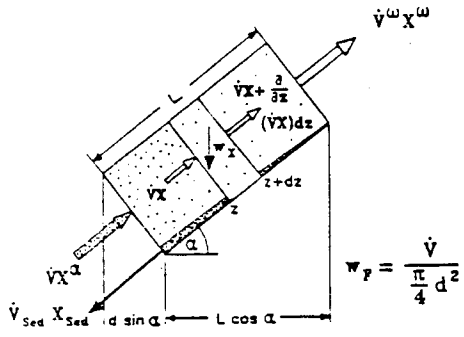

Fig. 5 Settling in an inclined tube.

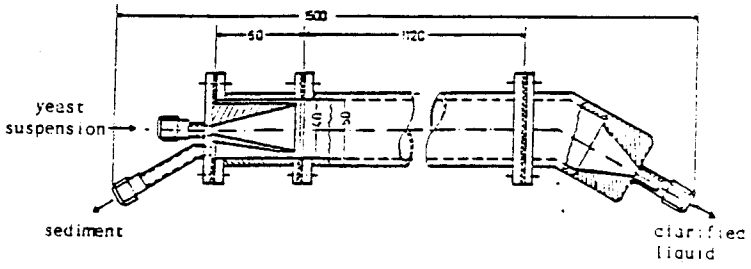

Fig. 6 Principle construction of single tube settler.

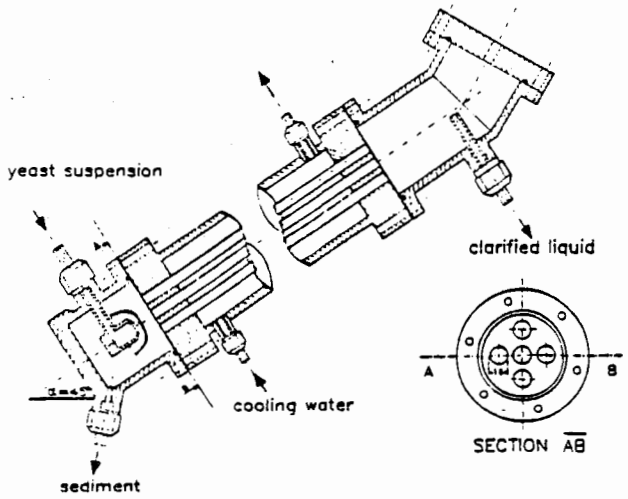

Fig. 7 Multi-tube settler.

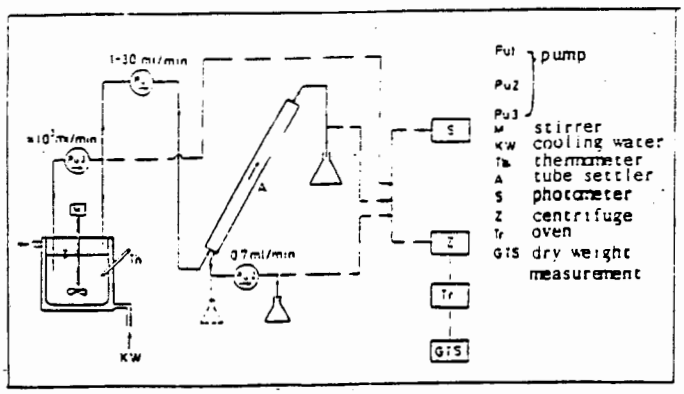

Fig. 8 Schematical flow shees of sedimentation experiments in tube settler.

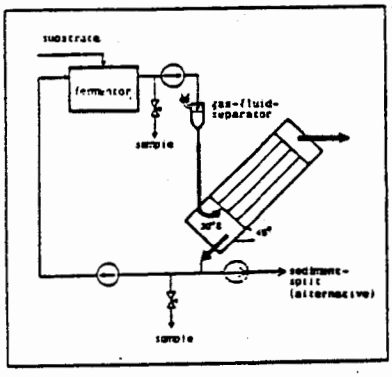

Fig. 9 Operation of multi-tube settler in a fermentation with cell recycling.

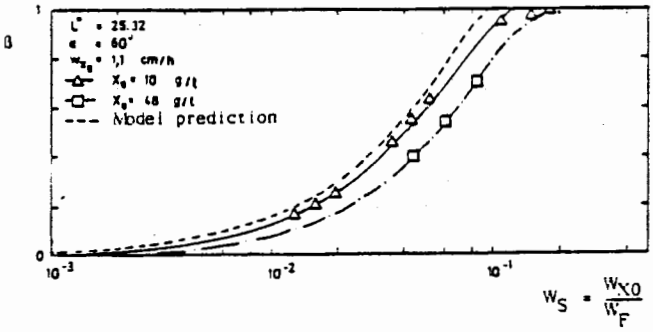

Fig. 10 Comparison between predicted separation efficiency by window-model and experimental results.

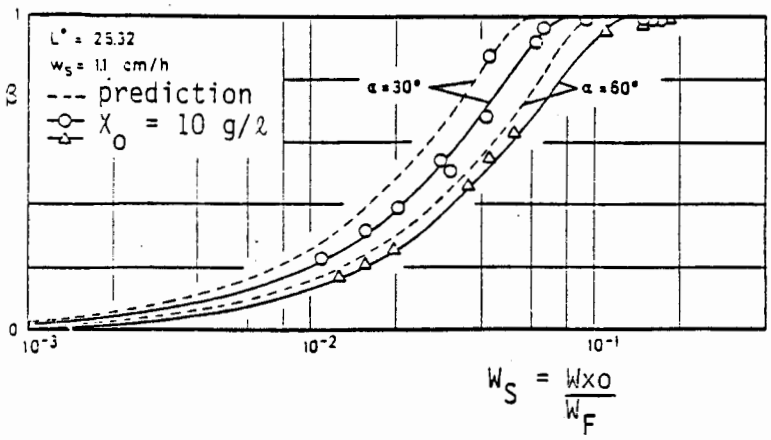

Fig. 11 Comparison between predicted clarification efficiency by window-model and experimental results.

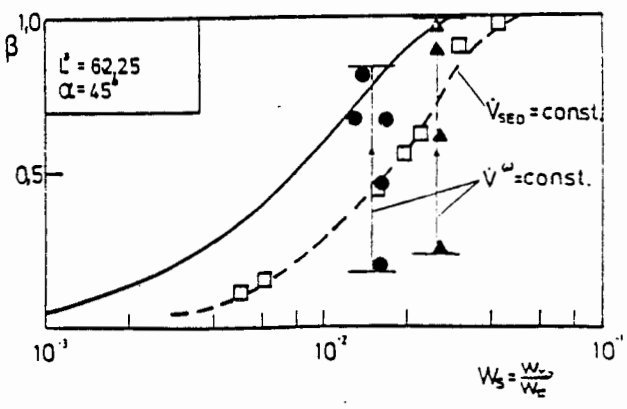

Fig. 12 Effects of the sediment flow rate on the clarification efficiency.

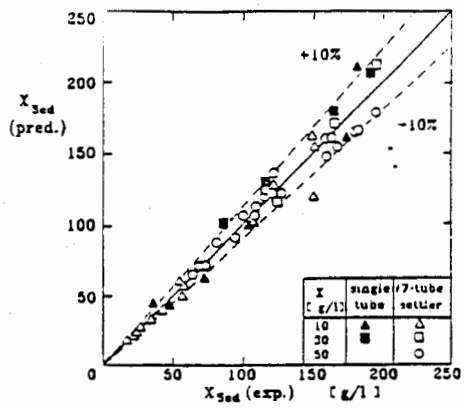

Fig. 13 Comparison between predicted yeast concentration in the sediment X_{Sed} by distributed parameter modelling and experimental observed datas.

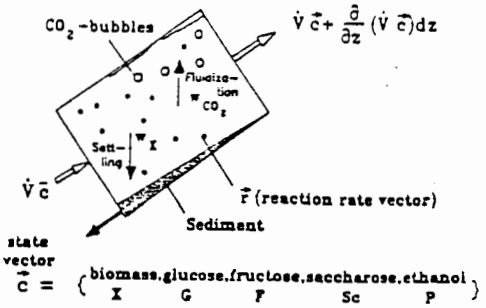

Fig. 14 Reaction, sedimentation and fluidization due to CO_2-evolution in volume element.

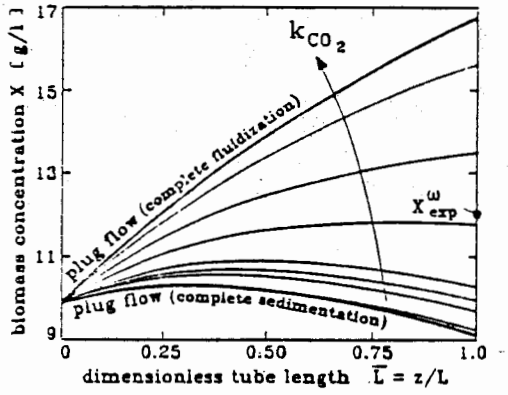

Fig. 15 Effects of fluidization factor on sedimentation characterics.

Table 1: Comparison between model prediction and experimental result under the condition further fermentation in settler

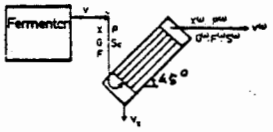

Medium: glucose G_o = 130 g/l
molasses M = 100 g/l
+ nutrient

Settler:
5 tubes, d_R = 1,8 cm, L = 50 cm
temperature = 30 °C

inlet conditions	X^{ω} [g/l]		G^{ω} [g/l]		F^{ω} [g/l]		P^{ω} [g/l]		k_{CO_2}
	exp.	pred.	exp.	pred.	exp.	pred.	exp.	pred.	[m²/(N/m²s)]
$\dot{V}$ = 4,21 ml/min	5,7	1,2	13,6	22,2	48,4	54,7	44,5	46,8	5 10^{-8}
$\dot{V}^{\omega}$ = 1,2 ml/min									
X = 15,2 g/l		1,8		20,6		52,9		48,5	1 10^{-7}
P = 35,5 g/l									
substrate from molasses fermentation									
G = 33,9 g/l		5,6		15,1		45,8		54,7	2 10^{-7}
F = 66,6 g/l									
Sc = 0									
$\dot{V}$ = 5,8 ml/min	15,5	1,7	6,2	13,0	22,1	38,8	56,7	52,3	5 10^{-8}
$\dot{V}^{\omega}$ = 1,2 ml/min									
X = 19,8 g/l		2,7		10,9		35,9		54,8	1 10^{-7}
P = 38,3 g/l									
substrate from molasses fermentation									
G = 26,7 g/l		11,7		3,9		22,6		64,8	2 10^{-7}
F = 54,7 g/l									
Sc = 0									
$\dot{V}$ = 3,6 ml/min	12,7	9,7	0	0	-	-	75,3	75,6	5 10^{-8}
$\dot{V}^{\omega}$ = 1,8 ml/min									
X = 46,3 g/l		10,5		0		-		75,6	1 10^{-7}
P = 71,1 g/l									
substrate from glucose fermentation									
G = 10,05 g/l		11,6		0		-		75,6	2 10^{-7}

BUBBLE SIZE DISTRIBUTION IN THE DOWN-FLOW SECTION OF AN AIR-LIFT COLUMN

Snehal A. Patel and C. H. Lee

Department of Chemical Engineering
Kansas State University
Manhattan, Kansas 66506

INTRODUCTION

The gas-liquid interfacial area in a fermentor is an important factor that affects the rate of mass transfer. It becomes the controlling factor for a well mixed system where liquid hydrodynamics plays a lesser role. In a split column fermentor mass transfer takes place in two separate sections, the upflow and downflow sides, respectively. Each of these sections has its own characteristics with respect to the bubble size distribution.

Earlier studies [1, 2] have shown that break-up is the major mechanism that controls bubble size distribution on the upflow side. The effects of liquid viscosity, electrolyte concentration and power input on bubble size distribution have also been studied for the upflow side.

The purpose of this paper is to present results from studies made on the downflow side of the column for air-water and air-salt water systems. These results have then been related to those obtained for the upflow side.

OBJECTIVES

The objectives for this study include the effect of gas flow rate (power input), electrolyte concentration, position along column length, and viscosity on bubble size distribution.

Gas flow rate is measured before it enters the upflow section of the column and therefore would not reflect the actual power input into the down flow section. However, it would directly affect the amount of power available on the downflow side, thus becoming an important parameter. The study of electrolyte concentration serves a two-fold purpose. Firstly it simulates, to a certain extent, the environment in a fermentation broth where electrolytes are always present and, secondly, it shows how the interfacial area would be affected when mass transfer studies are made by the sulfite method. Position along column length would help in completely characterizing the down flow side bubble size distribution. Studies made at higher viscosities are useful in duplicating the actual conditions during fermentation. However, these studies have not been included in this paper since results are not yet available.

MATERIAL AND METHODS

The fermentor used in these experiments is a 136 cm high, 15 cm in diameter plexi-glass column with a baffle separating it into the down-flow and up-flow compartments as shown in Figure 1. Air is sparged through 38 1.6 mm holes on the upflow side. The properties of the two different systems studied are presented in Table 1.

The procedure involved taking photographs of the dispersed phase through optical windows at four different locations along the column. The negatives were converted to tracings with the aid of an enlarger. This was to resolve overlapping bubbles. The tracings were then scanned and reduced to histographic data using a Bausch and Lomb image analysis system. Each of these data sets was then converted to a cumulative volume distribution after appropriate smoothing using a triangular digital filter.

RESULTS AND DISCUSSION

The effect of smoothing is shown on Figure 2, where the original data points are compared with the smoothed curve obtained after passing the data thrice through a triangular digital filter.

Figures 3 to 5 show cumulative volume distribution for the air-tap water system for air flow rates of 30, 60, and 90 SCFH (equivalent superficial gas velocities being 5.18, 7.77, and 10.36 cm/sec) respectively. At low air flowrates the dispersion appears only at the top two windows with the top most window having the largest bubbles. However, with increasing flowrate the distribution at this window (#4) moves to the left while the largest bubbles appear at a lower position along the column (at #3 as in Figures 4 and 5). Figure 6 summarizes the information for the air-tap water system. While the sauter mean diameter at window 4 decreases with air flowrate (power input on upflow side), the diameter for window 3 peaks at 90 SCFH (7.77 cm/sec) and then drops at 120 SCFH (10.36 cm/sec). The distribution first appears at window 2 at 90 SCFH, however, the sauter mean diameter decreases as flowrate is increased to 120 SCFH.

Figures 7 through 10 show cumulative bubble size distributions for the air-salt water system at air flowrates of 30, 60, 90, and 120 SCFH (i.e., 2.59, 5.18, 7.77, and 10.36 cm/sec) respectively. The trend here is similar to that observed for the air-tap water system. The largest bubbles are at window 4 at lower flow rates, however, as air flowrate is increased to 120 SCFH (10.36 cm/sec) the largest bubbles appear to be at windows 2 and 3. Figure 11 summarizes the observations for the air-salt water system. The sauter mean diameter for both windows 3 and 4 peak at an air flow rate of 60 SCFH, while that for windows 1 and 2 increases with power input.

The results presented above show that the downflow section of the fermentor is divided into two zones. In the upper zone breakage is prevalent while coalescence becomes dominant further down the column. In the upper zone there is enough energy left over from the upflow side to cause break up at high flow rates. This results in smaller bubbles at window 4 for both the systems at higher air flow rates. However, coalescence causes the sauter mean diameter to increase when dissipation rate becomes negligible. Further down the column the diameter once again decreases due to buoyancy effect which prevents larger bubbles from being carried further down the column.

Earlier studies had shown that bubble size decreases with air flowrate on the upflow side unlike the two zones present on the downflow side. While break-up was the dominating mechanism on the upflow side, the downflow side shows coalescence at lower flow rates followed by breakup at higher flow rates. However, studies on both sections show that coalescence decreases

for high electrolyte concentrations. That might explain the peak in sauter mean diameters at a lower flowrate for the air-salt water system as compared to the air water system.

CONCLUSIONS

This study characterizes the bubble size distribution in a split column fermentor and the effects power input and electrolyte concentration have on it. It has been seen that addition of an electrolyte significantly decreases the sauter mean diameter as was the case for the upflow side. This might be advantageous for mass transfer as a result of increased interfacial area. However, it is possible that at high viscosities, the assumption of perfect mixing may not be valid and mass transfer rates may decrease even though interfacial area increases. This might happen as a result of the bubbles being carried along with the liquid with no slip velocity and hence no surface renewal. Mass transfer studies would be necessary to verify this. It would be possible to model the bubble size distribution for the fermentor using a stochastic model. However, this would require energy dissipation rate data along the entire column length. These studies are being conducted at present and an effort will be made to make a model to simulate the data presented here.

REFERENCES

1. Lee, C. H. and Snehal A. Patel, Proceedings of the 13th Annual Biochemical Engineering Symposium, April 23, 1983 at Ames, Iowa; p. 81-90.

2. Glasgow, L. A., L. E. Erickson, C. H. Lee, and Snehal A. Patel, "Wall Pressure Fluctuations and Bubble Size Distributions at Several Positions in an Airlift Fermentor", Chemical Engineering Communications (In Press).

ACKNOWLEDGMENT

This work was partially supported by the National Science Foundation, Grant CPE-8108-799.

Table 1. Physical properties of systems studied.

SYSTEM	DENSITY (g/cm^3)	VISCOSITY (cp)	SURFACE TENSION (dyne/cm)
Air-tap water	0.989	0.890	64.889
Air-salt water (0 6% NaCl)	0.991	0.902	55.380

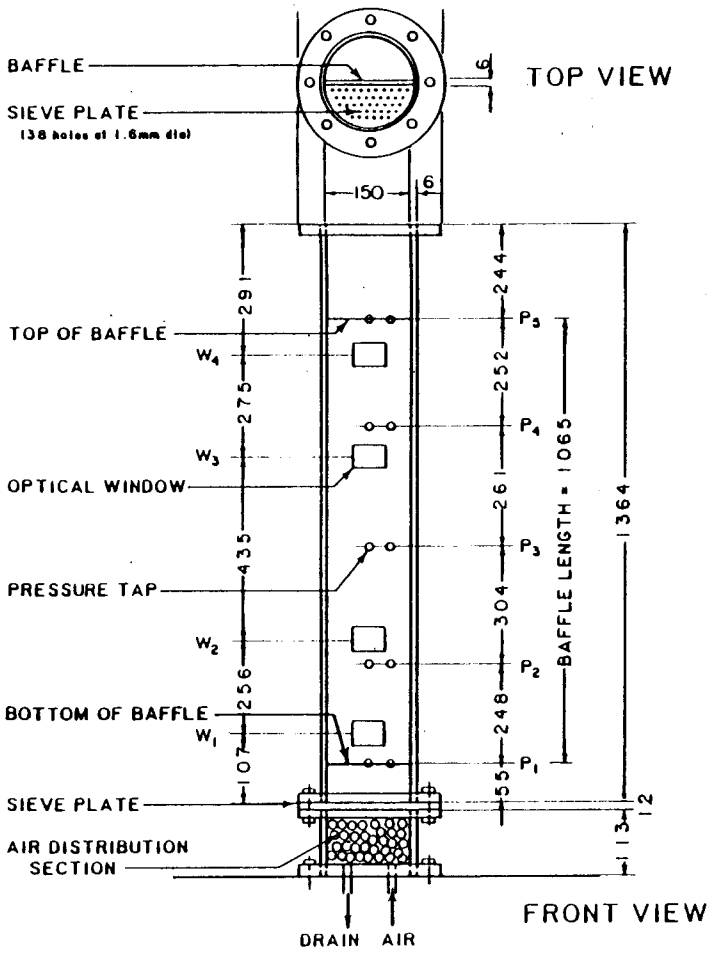

Figure 1. Plexi-glass airlift column used in the experiment (all dimensions are in millimeters)

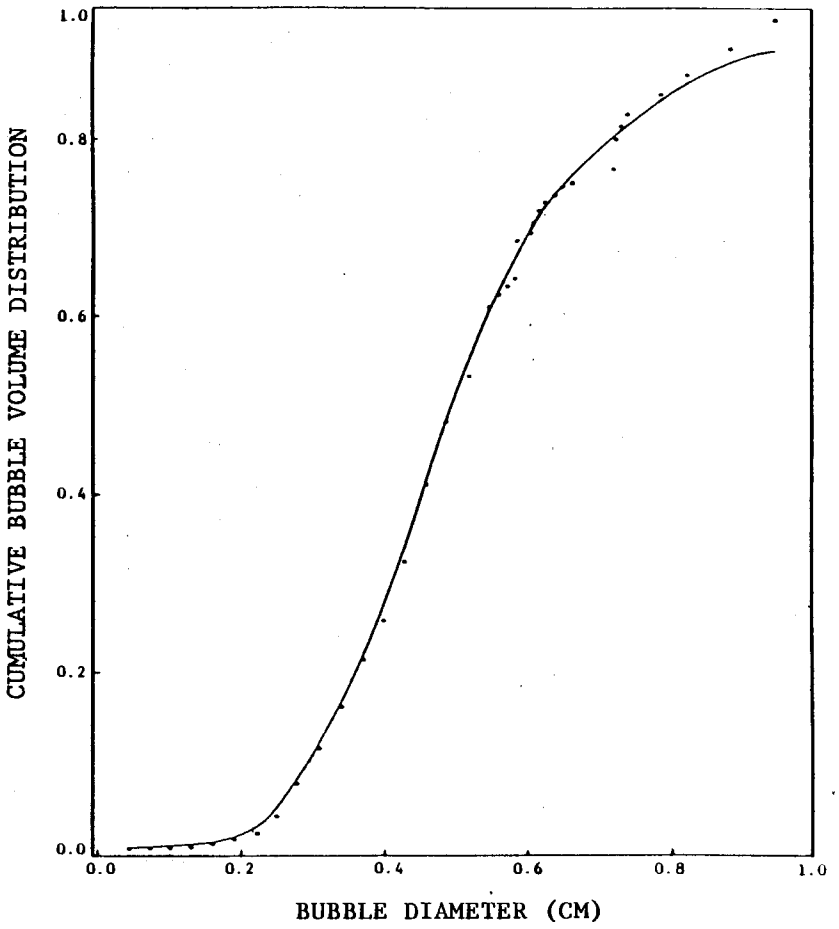

Figure 2. Comparison of original data with smoothed curve (after three passes through a triangular digital filter)

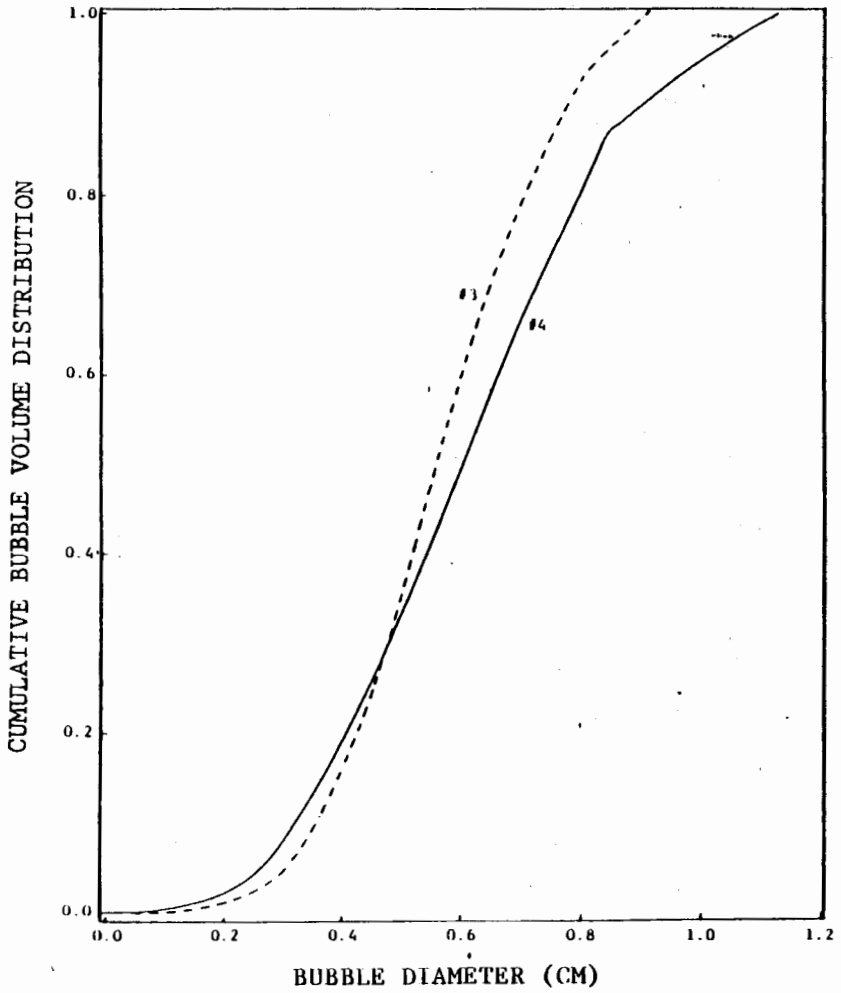

Figure 3. Distributions at 60 SCFH (5.18 cm/sec) for air-tap water system (see Fig. 1 for window locations)

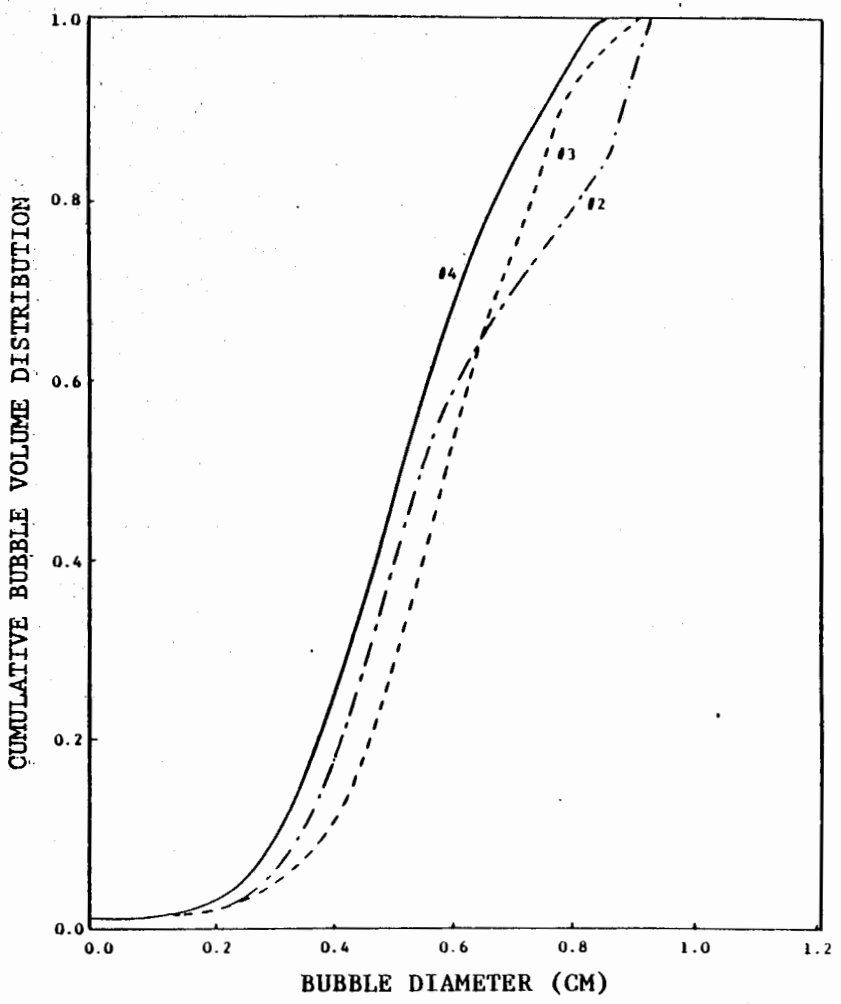

Figure 4. Distributions at 90 SCFH (7.77 cm/sec) for air-tap water system (see Fig. 1 for window locations)

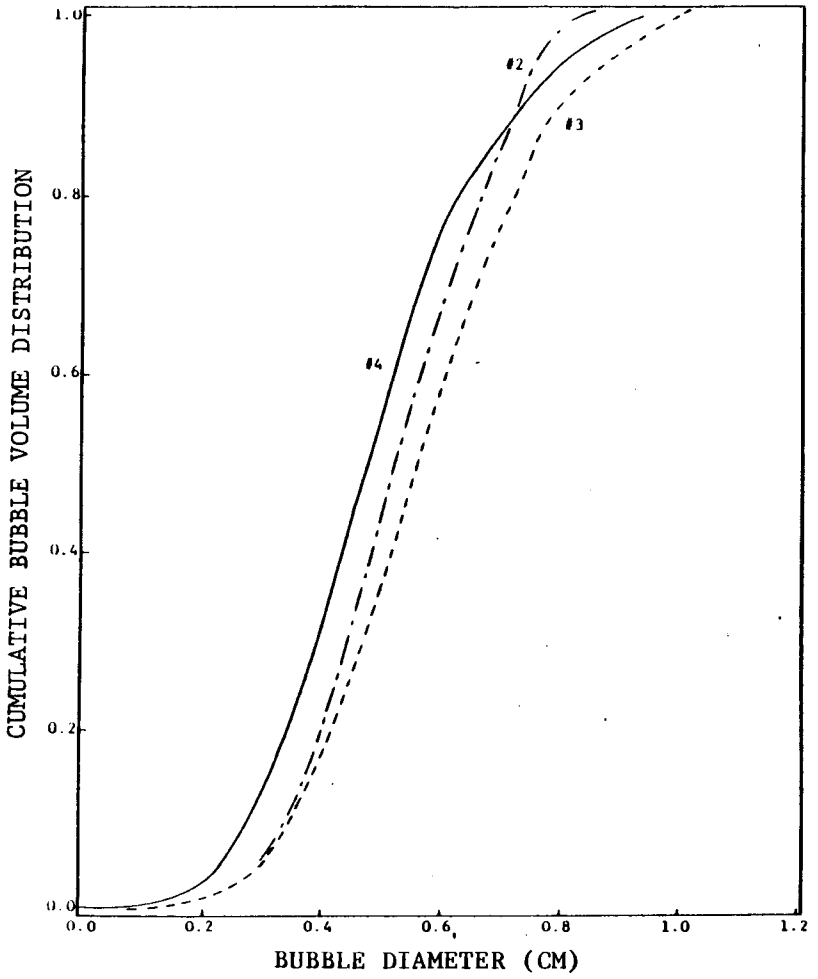

Figure 5. Distributions at 120 SCFH (10.36 cm/sec) for air-tap water system (see Fig. 1 for window locations)

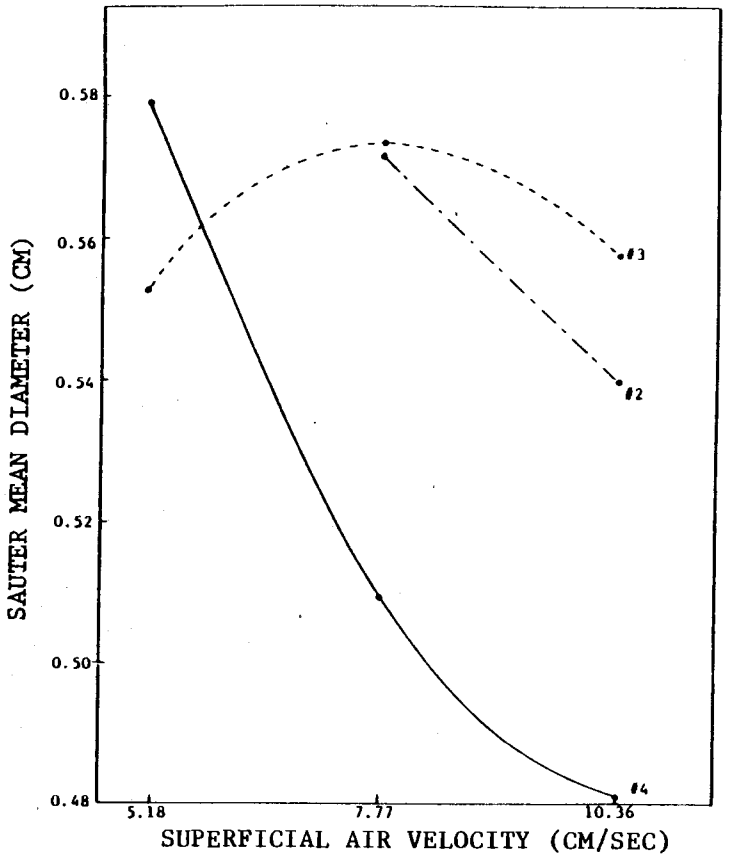

Figure 6. Effect of air flowrate on sauter mean diameter for air-tap water system (see Fig. 1 for window locations)

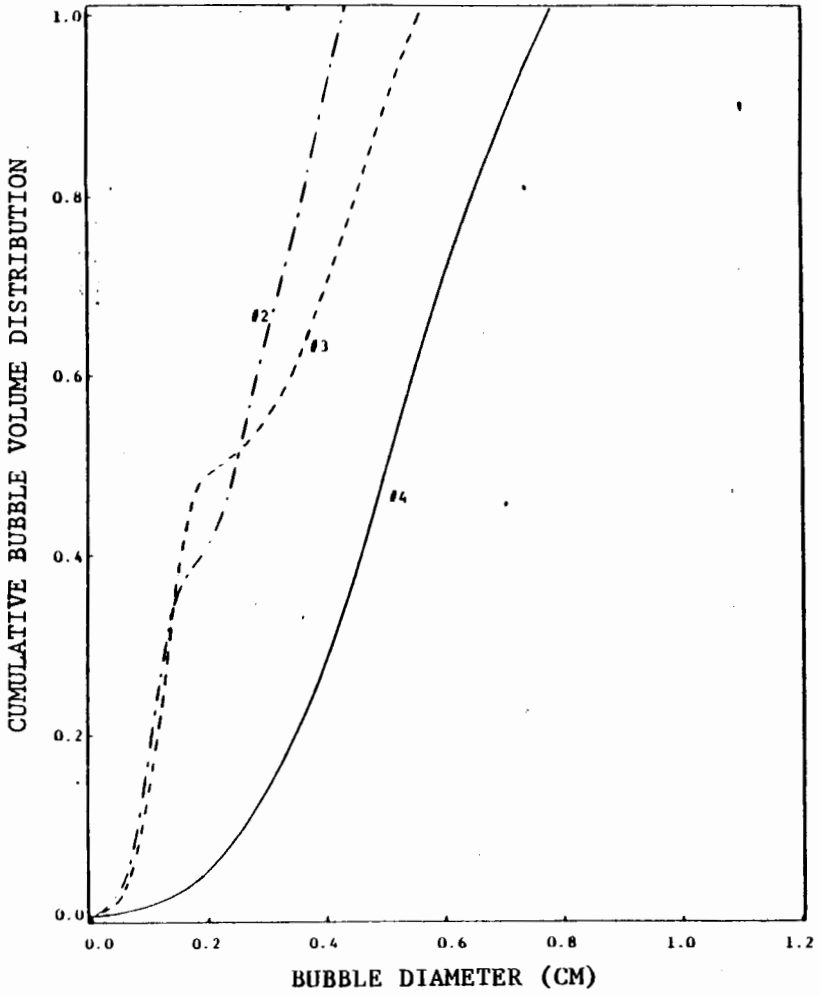

Figure 7. Distributions at 30 SCFH (2.59 cm/sec) for air salt-water system (see Fig. 1 for window locations)

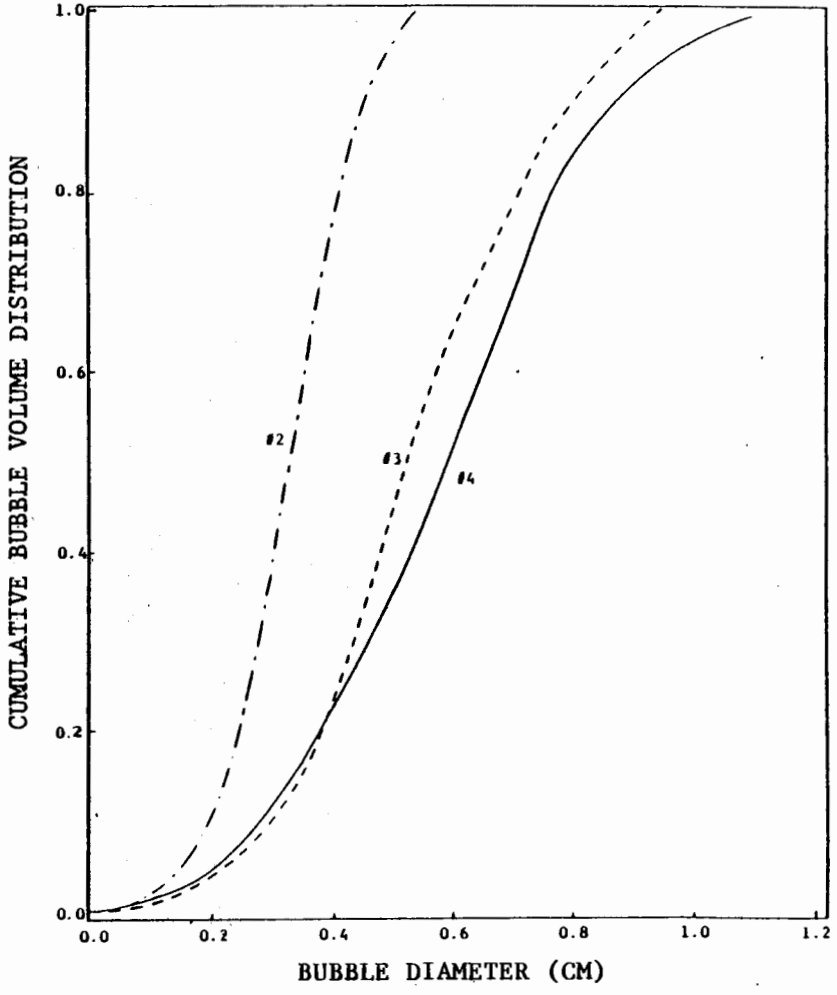

Figure 8. Distributions at 60 SCFH (5.18 cm/sec) for air salt-water system (see Fig. 1 for window locations)

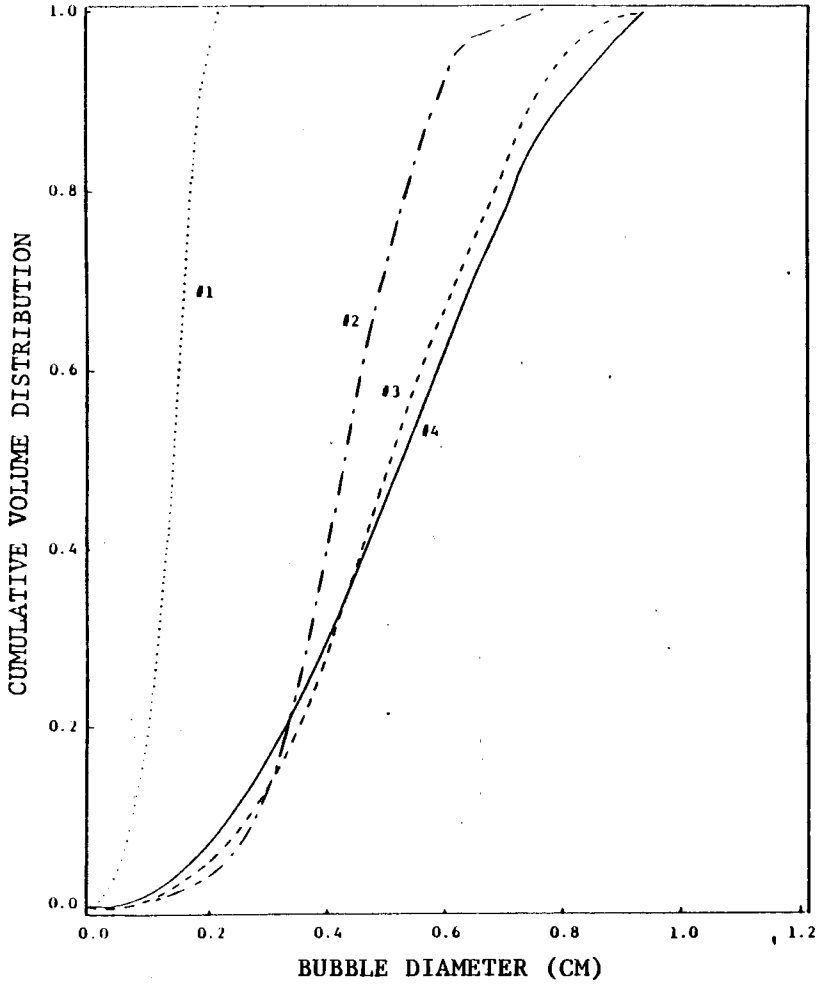

Figure 9. Distributions at 90 SCFH (7.77 cm/sec) for air salt-water system (see Fig. 1 for window locations)

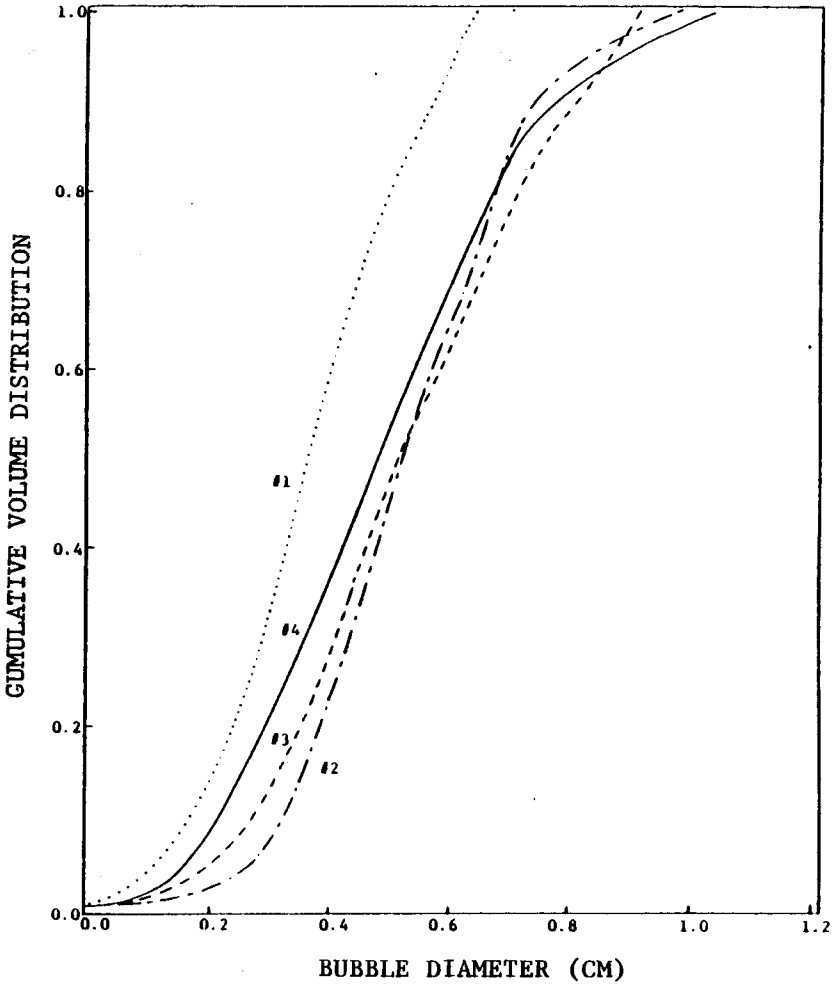

Figure 10. Distributions at 120 SCFH (10.36 cm/sec) for air salt-water system (see Fig. 1 for window locations)

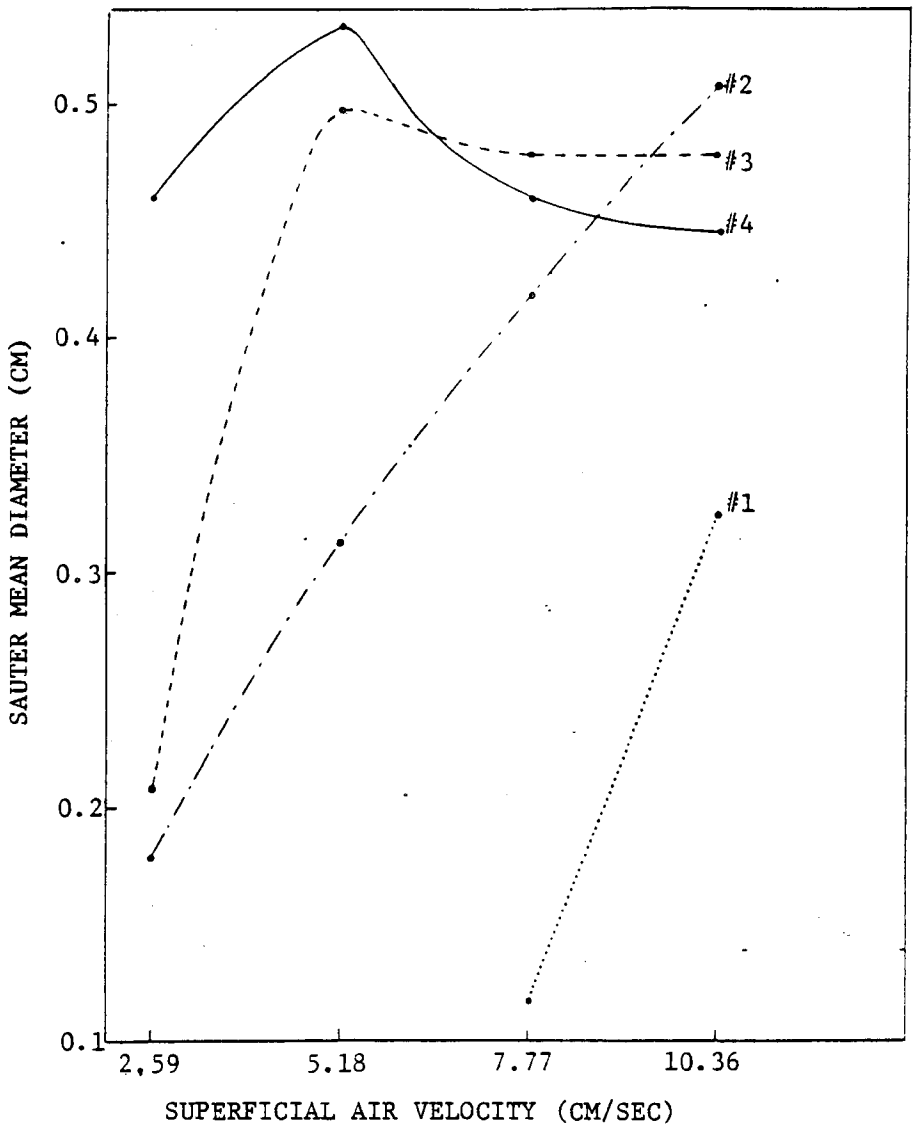

Figure 11. Effect of air flowrate on sauter mean diameter for air-salt water system (see Fig. 1 for window locations).

THE SENSITIVITY OF PLANT CELLS TO SHEAR STRESS

Morris Z. Rosenberg & Eric H. Dunlop

Biochemical Engineering Lab
Department of Chemical Engineering
Washington University
St. Louis, Missouri 63130

INTRODUCTION

There is currently a great deal of interest in the scale up of plant tissue culture from the shake flask to the large scale bioreactor. Two potential uses of large scale plant tissue culture frequently mentioned are the production of secondary metabolites for specific specialty chemicals and pharmaceutical uses and the rapid selection of mutant plants bearing useful traits such as herbicide resistance.[1,2]

Scale up is currently limited by the following factors: plant cells have very slow growth and metabolic rates with doubling times on the order of 50 to 100 hours; plant cells in suspension culture are reported to be extremely sensitive to hydrodynamic shear stress; aggregation of plant cells which creates mixing problems; plant cells can exist in several different states of differentiation and the state of differentiation influences the amount of product produced; most secondary metabolites are stored in the plant vacuole rather than secreted; the slow growth rate imposes stringent requirements for sterility.[3]

Some of the above mentioned problems are appropriately tackled by plant biologists while others are more amenable to an engineering approach. We believe that the key issue in scaling up plant cell culture is the hydrodynamic sensitivity of plant cells. Although the literature is filled with observations of plant cell sensitivity to shear stress there have been no reasonable attempts to quantify this observation.[4,5] To determine the sensitivity of various plant cell lines to shear stress we placed a suspension culture in a couette viscometer and subjected the cells to a known shear rate for a given length of time. To access sensitivity we looked at three responses to shear stress, the disruption of plant cell aggregates, the decrease in viability, and the lysis of plant cells.

Ideally one would like to apply the information learned in a couette viscometer directly to a fermenter. Carrot cell fermentations have been carried out in both 1 liter shake flasks (low shear regime) and a 2 liter Braun Biostat M fermenter (high shear regime). Growth rate, anthocyanin production, and cell viability are compared.

MATERIALS AND METHODS

Daucus carota (carrot) was grown in Murishige and Skoog's media supplemented with .1 mg./lit. 2,4-dichlorophenoxyacetic acid (2,4-D).[6] *Petunia Mitchell* was grown in Murishige and Skoog's media supplemented with 2 mg./lit. p-chlorophenoxyacetic acid and .05 mg./lit. kinetin. Both plant cell lines were grown in 500 ml. baffled shake flasks containing 200 ml. of cell suspension. The shake flasks were kept on an orbital shaker at 100 rpm at 25 C. The cells were grown under Gro & Sho plant lights on a 12 hour cycle.

Plant cells were subjected to known shear rates in a Haake RVII Rotoviscometer. Shearing was done in a nonsterile environment at a constant temperature of 27 C using either an MVII, MVIIP, or MV paddle system.

The size of plant cell aggregates before and after shearing in the viscometer were measured with an electronic micrometer attached to a Leitz light microscope. Using a pointer wired to a potentiometer the longest chord across a roughly spherical aggregate was measured to the nearest tenth of a micron.

The viability of plant cells was measured by a tetrazolium salt reduction assay based on the method of Towill and Mazur.[7] Carrot or petunia cells in suspension were collected either before or after being subjected to shear and a 1.0 ml. sample was mixed with 2.0 ml. of 0.8% triphenyltetrazolium chloride (TTC) in 0.5 M phosphate buffer (pH= 6.90). The mixture was kept in the dark at 25 C for 18 hours after which the cells were collected by centrifugation. 5 ml. of 95% ethanol was used to extract the formazan product of TTC reduction. The amount of product was determined by reading the absorbance of the extract at 485 nm. Controls were run on unsheared plant cells of the same age and culture conditions and percent viability was calculated as the ratio of absorbance of sheared cells to unsheared cells.

To measure the percent lysis of carrot or petunia cells the absorbance of nucleic acids released into the supernatant was measured at 260 nm. The percent lysis was determined by referring absorbance values to a standard curve prepared by lysing a known quantity of carrot or petunia cells.

Fermentations of carrot cells were carried out in a Braun Biostat M fermenter. 1.4 liters of MS media with 0.1 mg./lit. 2,4-D was inoculated with 100 ml. of a carrot cell suspension (6 gm./lit.) in exponential growth phase. The temperature was kept constant at 25 C and the pH, dissolved oxygen and various metabolites were monitored on a daily basis. Dry weights were determined by collecting 10 ml. of suspension on pre-weighed filter paper and then washing with 3 volumes of water before drying the samples in a vacuum oven overnight. Anthocyanin was extracted from carrot cells by the method of Dougall et. al.[8] Anthocyanin levels were determined by measuring the absorbance of

the extract at 530 nm. Total protein was extracted from carrot cells by the method of Wilson et. al.[9] Protein levels were determined by the method of Lowry et. al..[10]

RESULTS AND DISCUSSION

When carrot tissue is suspended in a liquid media and then subcultured for several weeks the cells will form small aggregates. Figure 1 presents a frequency histogram of carrot cell aggregates. It is clear that the population of carrot cells exists in a wide size range. The typical carrot cells is approximately spherical, with an average diameter of 30 microns. Thus the aggregates represent conglomerations of 2-3 cells up to as many as 50 cells. Petunia cells also exhibit a similar distribution pattern (data not shown). To determine the effect of viscous shear forces on these aggregates plant cells were placed in a couette viscometer and sheared at a known shear rate in the range 10 s^{-1} to 1000 s^{-1}. Figure 2 illustrates the effects of shear rate and length of shearing time on the dimensionless mean aggregate size of carrot cells. To permit direct comparison of data the dimensionless mean aggregate size is used. It is defined as the mean aggregate size at a given shear rate and length of shearing time divided by the mean aggregate size of unsheared carrot cells of the same age and culture conditions. In each case the mean aggregate size increased initially and then either remained constant or decreased. An increase in the mean aggregate size could imply that shear stress was inducing aggregate formation as is seen in polymer solutions.[11] Why the aggregate size did not decrease at 100 s^{-1} as it did at 10 s^{-1} and 1000 s^{-1} is not clear. It could be that at some intermediate shear rate aggregation of plant cells is stabilized. This concept is currently being investigated.

The above experiment was performed with an MVPII system. In such a system we discovered that the larger plant cell aggregates settled out of solution rather quickly in the laminar flow field. Subsequent experiments were therefore performed with the MV paddle system which generates a turbulent flow regime that inhibits settling of large plant cell aggregates. Although a definitive shear rate can not be calculated in such a system an effective shear rate can be determined.

Figure 3 presents the effects of shear rate on the viability of petunia cells (similar results were achieved with carrot cells). Viability was assessed by measuring the ability of plant cells to reduce a tetrazolium salt to an extractable formazan dye utilizing the electrons from the mitochondrial electron transport chain.[7] The viability of a plant cell is directly proportional to the amount of formazan dye produced. In every case the viability of the petunia cells decreased with time. Although viability decreased more rapidly when the cells were subjected to a higher shear rate the correlation between shear rate and viability is not straight forward. For example, petunia cells were significantly less viable at a shear rate of 2250 s^{-1} than

at 3000 s^{-1}.

Finally the effects of shear rate on cell lysis were examined. Figure 4 shows the percent lysis as measured by the absorbance at 260 nm. of nucleic acids released into the supernatant after shearing in a couette viscometer. The degree of cell lysis was directly proportional to the shear rate and to the length of shearing time.

In order to apply what we have learned from the experiments done in the couette viscometer we performed fermentations of carrot cells in a 2 liter Braun Biostat M fermenter and compared the results with fermentations carried out in a one liter shake flask. Fermentations in the Braun fermenter were performed at 100 rpm, 500 rpm, and 750 rpm. Fermentations in shake flasks were done on an orbital shaker at 100 rpm. In each case the carrot cells failed to grow in the liquid phase but, instead, grew along the walls and on the surfaces of the various probes at the air-liquid interface. Figure 5 compares the growth rate of carrot cells in the liquid phase of the fermenter to that in the shake flask. Figure 6 shows the production of the secondary metabolite, anthocyanin, in the shake flask and in the fermenter. The carrot cells in the shake flask produced 6 micrograms of anthocyanin per milligram dry weight of cells after two weeks while the carrot cells in the fermenter could not produce a measurable amount secondary metabolite. It was possible to quantify the amount of anthocyanin in the carrot cells growing on the walls of the fermenter and it was found to be 2 micrograms of anthocyanin per milligram dry weight of cells. This is significantly more than the level of anthocyanin in the cells in the liquid phase. This data implies that shear may be affecting the ability of the carrot cells to produce secondary metabolites. Finally we looked at cell viability over time in the shake flask and in the fermentor. Figure 7 shows that cell viability decreases significantly after a period of 72 hours in the fermenter while it remains high throughout the fermentation in the shake flask.

CONCLUSION

These experiments illustrate that shear rate and the length of shearing time have a marked influence on the behavior of plant cells in suspension culture. Experiments performed in the well defined shear environment of a couette viscometer have shown that increasing shear and length of shearing time can decrease the mean aggregate size and viability of plant cells. Experiments in which plant cells were grown in the relatively high shear environment of a fermenter were compared with plant cells grown in the low shear environment of the shake flask. Growth rate, secondary metabolism, and viability were all found to be much lower in the high shear environment of the Braun fermenter. Further experiments are planned in order to further define the influence of shear on growth and secondary metabolism of plant cells in suspension culture.

REFERENCES

1. Fowler, M.W., Progress in Industrial Microbiology,Vol. 17, Ed. M. J. Ball, Elsevier Scientific Publ. Co., New York,pp. 207-229, 1982.

2. Zenk, M.H., Frontiers of Plant Tissue Culture, Ed. T.A. Thorpe, International Assoctiation for Plant Tissue Culture, pp. 1-13, 1981.

3. Shuler, M.L., Ann. New York Acad. Sci., Vol. 12, pp. 65-79, 1981.

4. Tanaka, H., Biotech. & Bioeng., Vol. 23, pp. 1203-1218, 1981.

5. Matsumoto, T., Okanishi, K., Nahida, K., Agric. Biol. Chem., Vol. 36, pp. 2177-2186, 1972.

6. Murashige, T., Skoog, F., Physiol. Plant, Vol. 15, pp. 473-497, 1962.

7. Towill, L.E., Mazur, P., Can. J. Bot., Vol. 53, pp. 1097-1102, 1975.

8. Dougall, D.K., Weyrauch, K.W., Biotech. & Bioeng., Vol. 22, pp. 337-352, 1980.

9. Wilson, G., Marron, P., J. Exp. Bot., Vol. 29, No. 111, pp. 837-851, 1978.

10. Lowry, O.H., Rosebrough, N.J., Farr, A.L., Randall, R.J., J. Biol. Chem., Vol. 193, pp. 245-251, 1951.

11. Dunlop, E.H., Cox, L.R., Physics of Fluids, Vol. 20, No. 10, pp. 203-213, 1977.

ACKNOWLEDGEMENTS

Support for this work was provided by a fellowship grant from the Monsanto Company. Eric Dunlop is a Shell Faculty Fellow.

Figure 1. Frequency Histogram

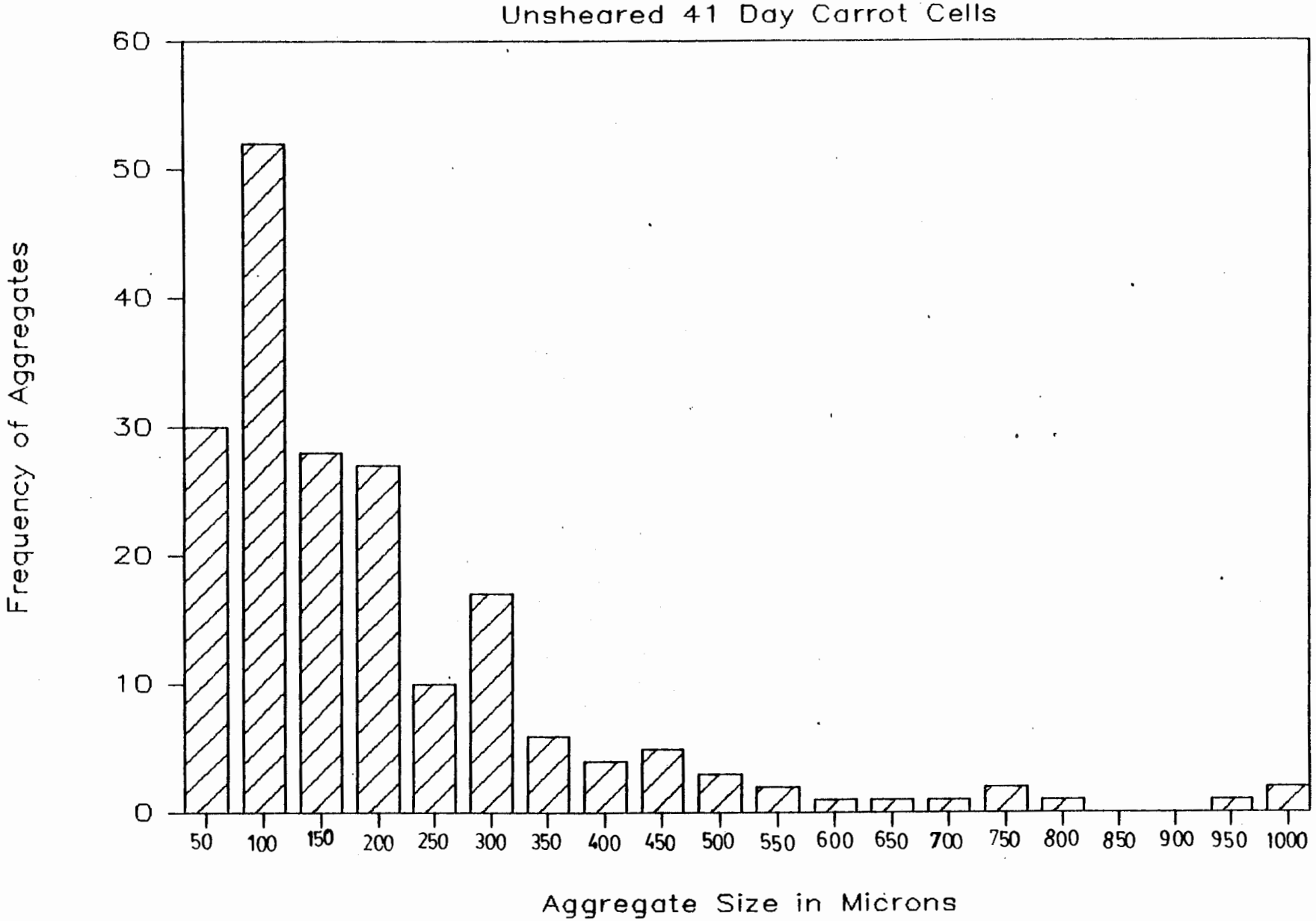

Figure 2. Carrot Cells Sheared

in Couette Viscometer

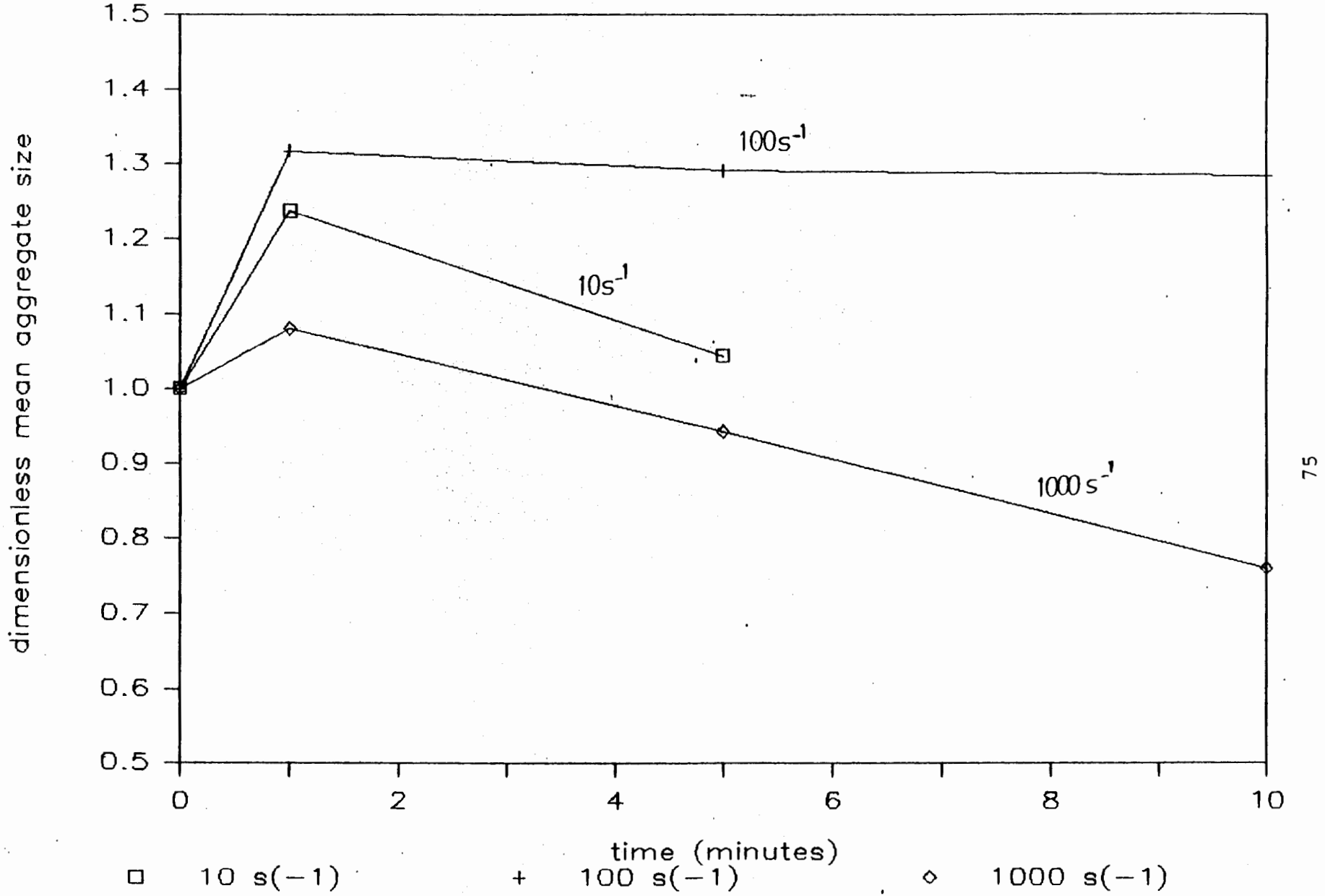

Figure 3. Relative Viability

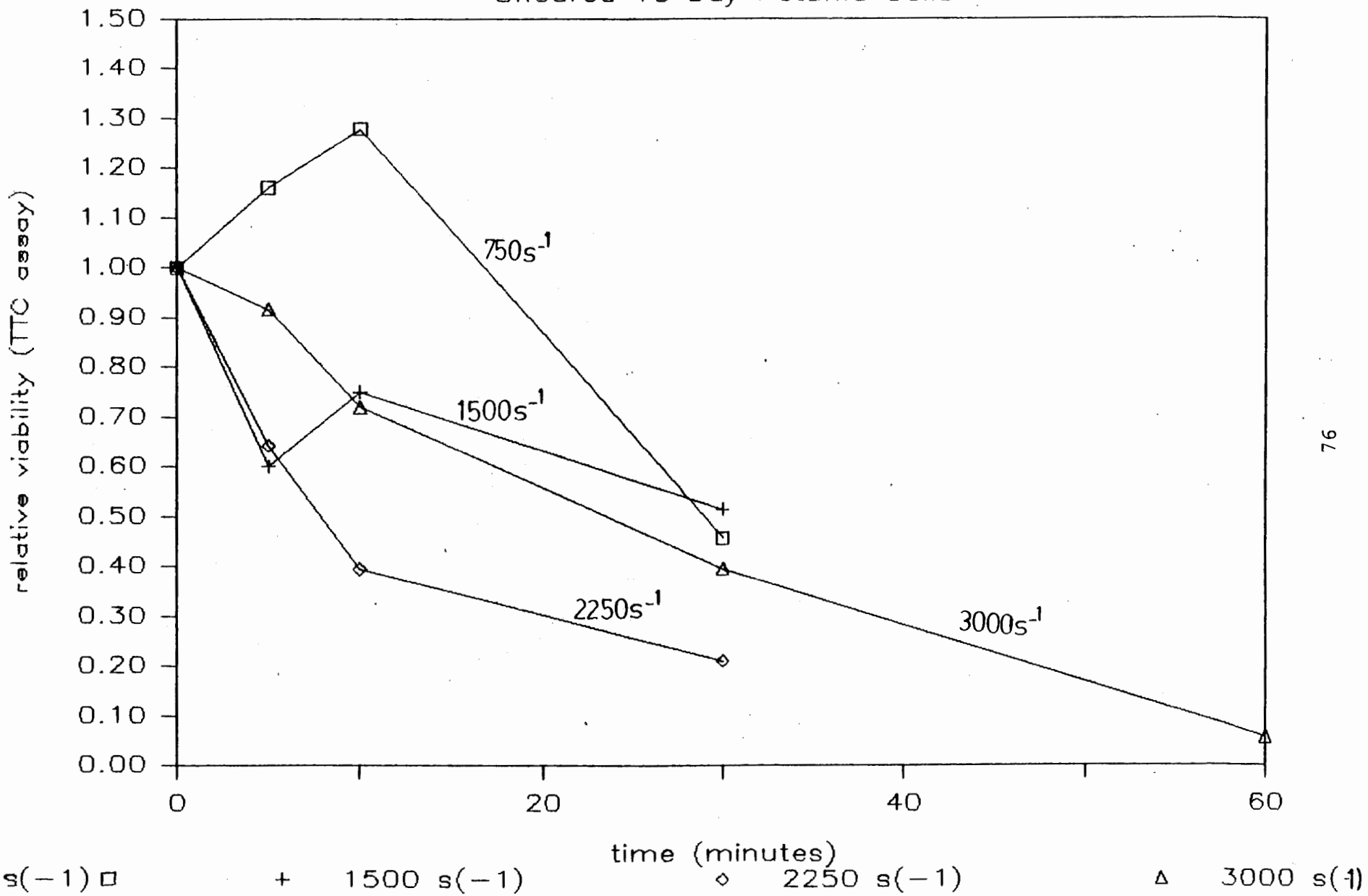

Figure 4. Petunia Lysis

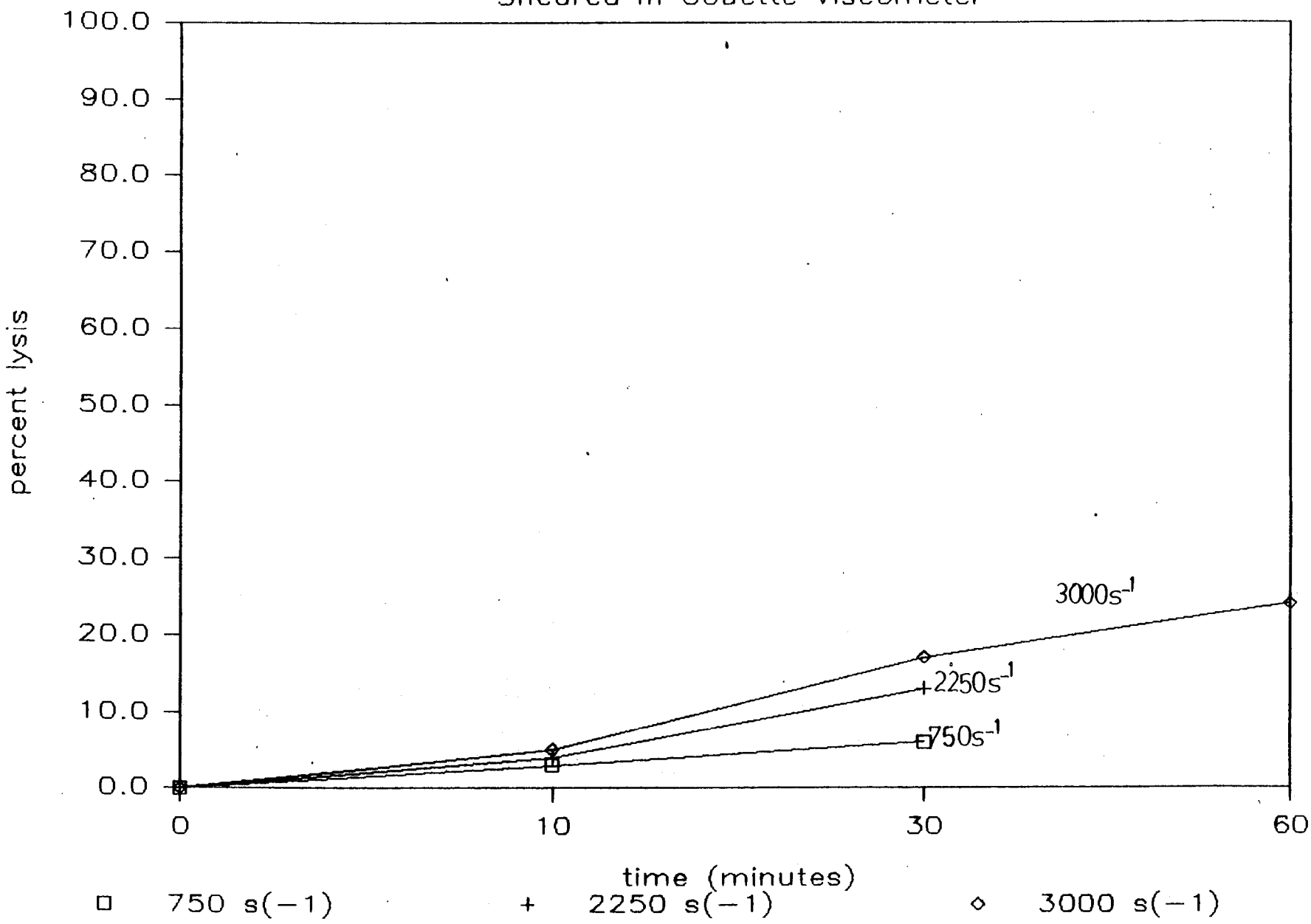

Figure 5. Growth Rate of Carrot Cells

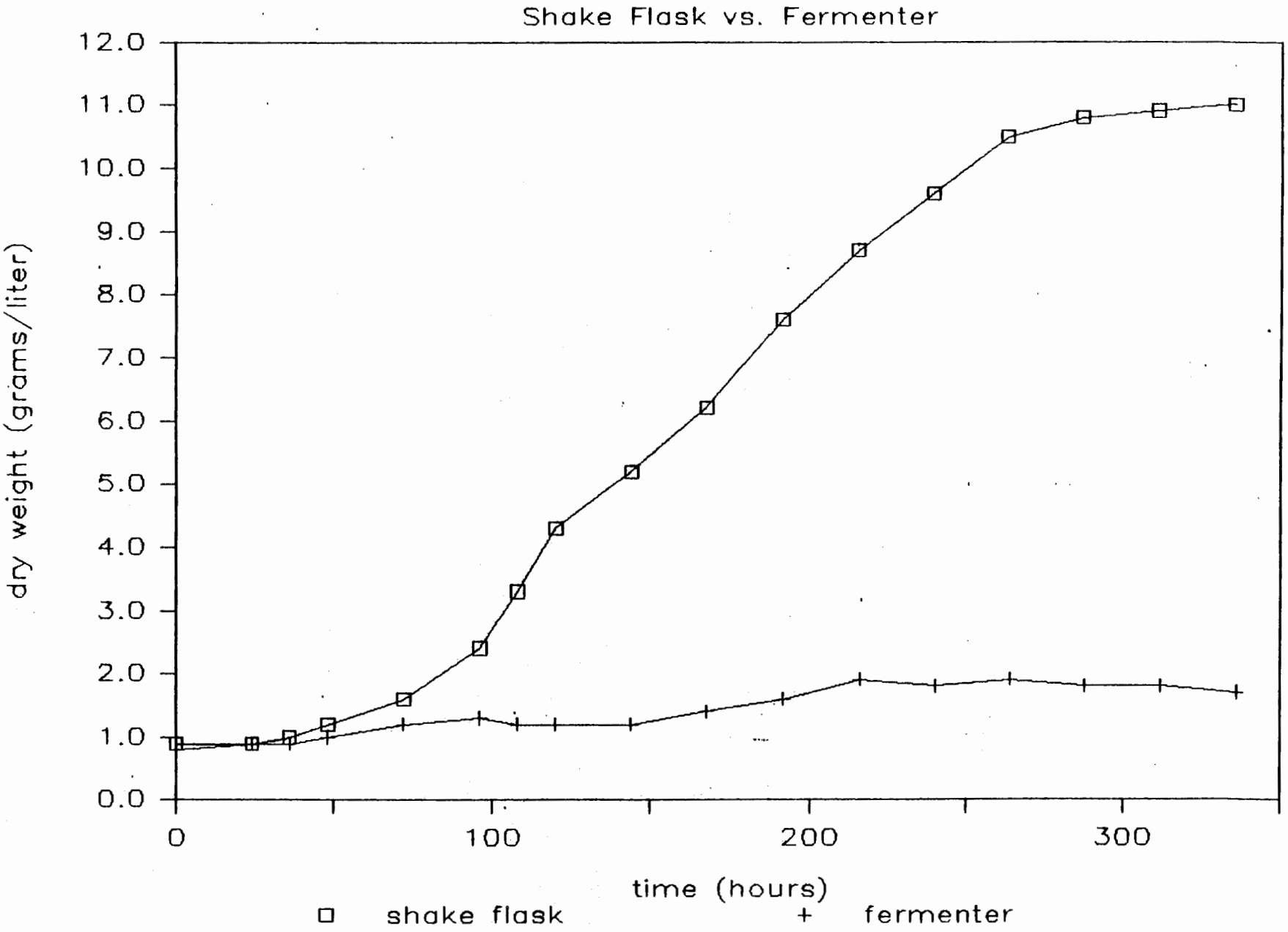

Figure 6. Anthocyanin Production

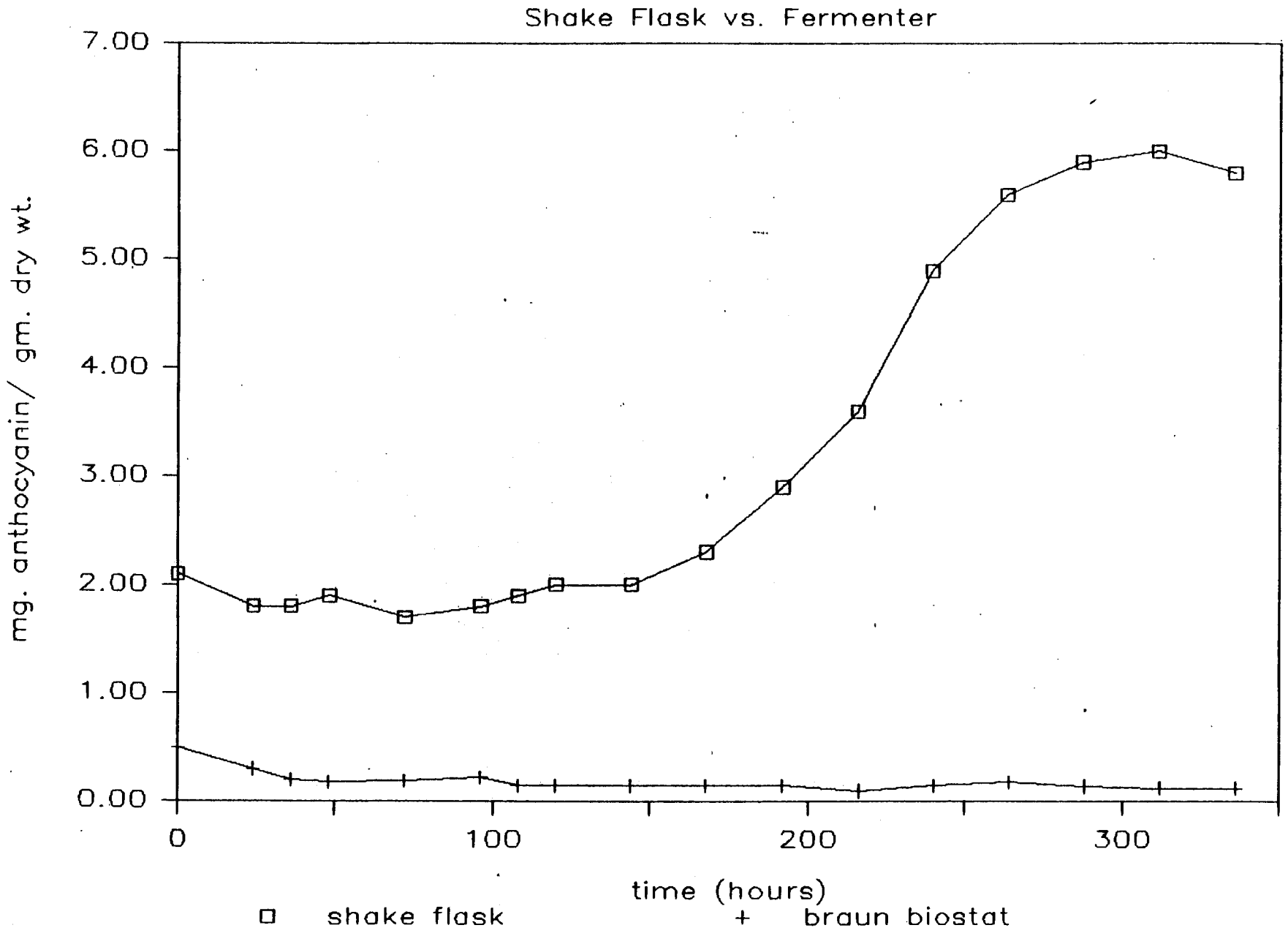

Figure 7. Viability of Carrot Cells

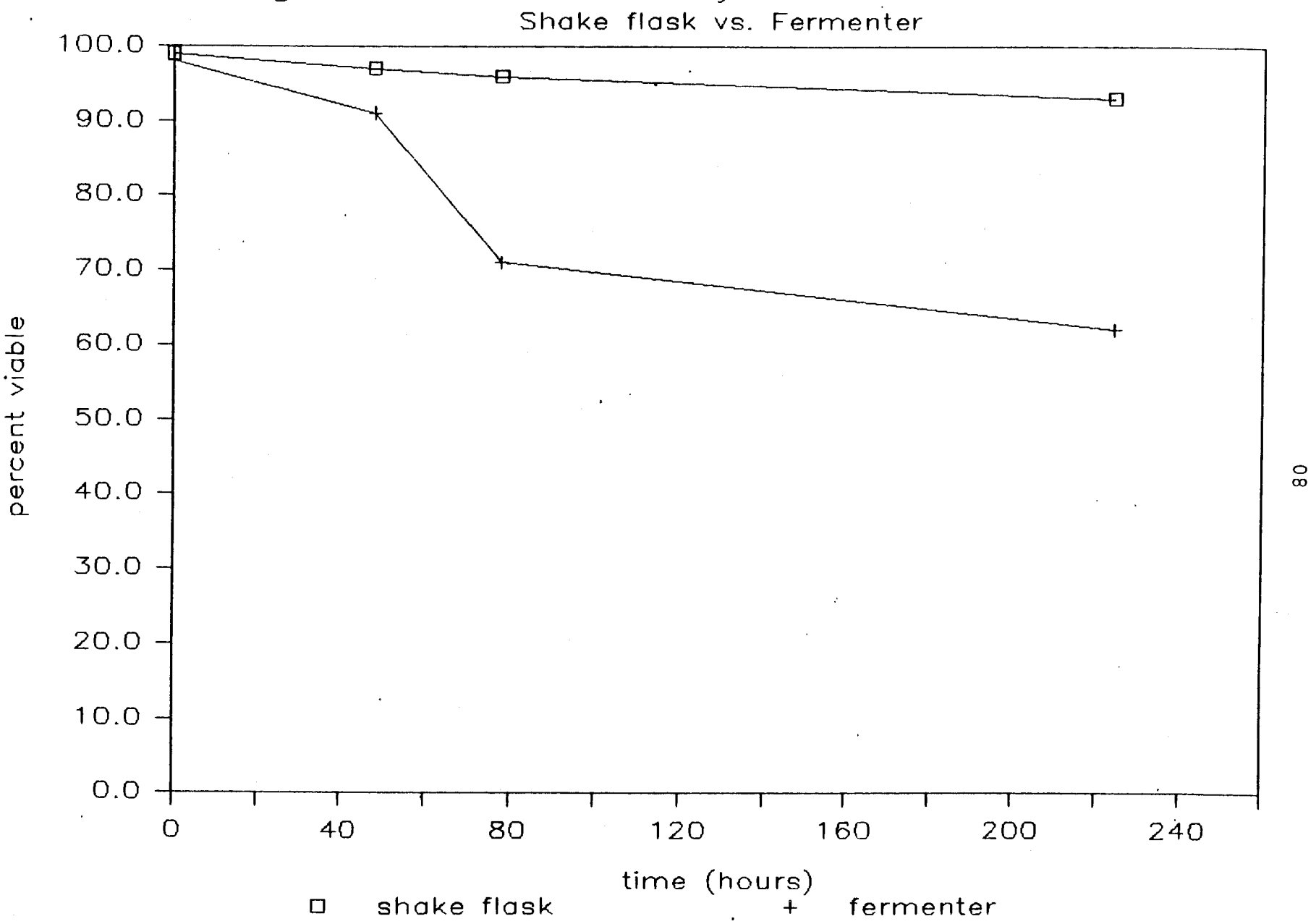

ESTIMATION OF GROWTH YIELD PARAMETERS ASSOCIATED WITH MIXOTROPHIC GROWTH

HYEON Y. LEE

Department of Chemical Engineering
Kansas State University
Manhattan, Kansas 66506

INTRODUCTION

Mixotrophic growth involves microbial growth with an organic substrate and light as sources of energy for growth. When the primary source of energy is the organic substrate, the mixotrophic process is similar to heterotrophic growth with net CO_2 production except that part of the energy is provided by light energy. For mixotrophic growth with algae, there may be either a net consumption or a net production of oxygen. For purple and green bacteria, which do not produce oxygen, oxygen is only involved if there is a net consumption of oxygen. Mixotrophic growth may be advantageous for producing useful chemicals and foods (1-18).

Expressions for bioenergetic yield in terms of growth yield and maintenance parameters are developed and used with available experimental data to estimate these parameters.

THEORY

The efficiency of mixotrophic growth can be expressed in terms of the ratio of the energy incorporated into biomass to the summation of energy in substrate and light. When photosynthetic bacteria grow mixotrophically on organic substrates of known chemical formula, such as glucose or acetate, under anaerobic conditions, the chemical balance is written as follows, assuming no oxygen is produced:

$$CH_mO_l + aNH_3 \xrightarrow{\text{light}} y_c\, C\, H_pO_nN_q + d\, CO_2 \qquad (1)$$

where CH_mO_l denotes the organic substrate, ammonia is the nitrogen source, y_c is the ratio of carbon in biomass from organic substrate, and $CH_pO_nN_q$ is the chemical composition of the photosynthetic bacteria. Minkevich and Erosnin (9) found regularities for heterotrophic microorganisms. The values of weight fraction carbon, σ_b, reductance degree, γ_b, and the energy content per equivalent of available electrons, Q_o, have recently been reported for photosynthetic organisms by Lee and Erickson (10).

The carbon balance is derived from Equation (1); it is

$$y_c + d = 1 \qquad (2)$$

where

$$y_c = \frac{X\sigma_b}{(S_o - S)\sigma_s} \quad \text{and} \quad d = \frac{12\, Q_{CO_2} X}{(S_o - S)\sigma_s D}$$

where S_o is the initial concentration of organic substrate, Q_{CO_2} is the specific evolution rate of carbon dioxide, and D is the dilution rate.

The available electron balance for photosynthetic bacteria under anaerobic conditions can be written in terms of the available electron biomass yield, H, as

$$H = \frac{DVX\sigma_b\gamma_b}{DV(S_o-S)\sigma_s\gamma_s} = y_c \frac{\gamma_b}{\gamma_s} = 1 \qquad (3)$$

that is, all available electrons in the substrate are transferred to biomass without any loss, assuming there is no product formation and that there is no oxygen production or consumption in the system.

The valences, C = 4, H = 1, O = -2, and N = -3 are used to calculate reductance degree of biomass, γ_b, when the nitrogen source is NH_3.

The energetic yield for mixotrophic growth in continuous culture is

$$\eta_{kcal} = \frac{DXV\sigma_b\gamma_bQ_o/12}{I_aA + D(S_o-S)V\sigma_s\gamma_sQ_o/12} = \frac{H}{f+1} \qquad (4)$$

where I_a is the light intensity, A is the area over which light enters and

$$f = \frac{I_aA}{D(S_o-S)V\sigma_s\gamma_sQ_o/12}$$

Three other indirect methods of estimating the energetic yield, η, are possible. The available electron balance, Equation (3), reduces to H=1. Thus,

$$\eta_E = \frac{1}{f+1} \qquad (5)$$

and

$$\eta_{A.E.} = \frac{H}{f+H} \qquad (6)$$

may be obtained by using the available electron balance with Equation (4). Equation (5) involves light and organic substrate consumption measurements. Equation (6) involves light and biomass measurements.

When the carbon balance is used with Equation (4), one obtains

$$\eta_c = \frac{H}{f+y_c+d} \qquad (7)$$

in which biomass, carbon dioxide and light measurements are required. Equations (4)-(7) provide four different measurements of the biomass energetic yield, η.

When yeast extract is used together with another organic substrate, Equations (6) and (7) may be used to obtain values of η even though yeast extract consumption is not measured because substrate data are not required. For equation (7) an average value of γ_s for the substrate and yeast extract is required.

The true biomass energetic yield, η_{max}, and the maintenance coefficient,

m_e, in Pirt's model (7,11) may be estimated using covariate adjustment methods (8,12). Form I of Pirt's model is

$$\frac{1}{\eta} = \frac{1}{\eta_{max}} + \frac{m_e}{\mu} \qquad (8)$$

where μ is the specific growth rate. Form II is obtained by multiplying every term by μ.

RESULTS AND DISCUSSION

The results of estimating the biomass energetic yield from the data of Ogawa and Aiba (3) are shown in Table I for Chlorella vulgaris grown on glucose and light under anaerobic conditions. Since this organism is capable of producing oxygen, only Equation (4) is used to estimate the biomass energetic yield. The true growth energetic yield, η_{max}, and maintenance parameter, m_e, are estimated in Table II using the data in Table I and Forms I and II of Equation (8). The results show that a relatively high value of the confidence interval is large because only five observations were used.

Table III contains the results of checking carbon and available electron balances and estimating four different energetic yields from Equations (4)-(7) for photosynthetic bacteria (1). Based on the carbon and available electron balances, the results are relatively consistent. The luminosity of light is converted to radiant intensity of light using the conversion factor of 283 lumens/watt based on the fluorescent lamp (14). The light intensity is also considered as the amount of light energy adsorbed by the microorganisms, based on the Lambert-Beer law as applied by Iehana (15). The relationship of Iehana is as follows:

$$F = \exp(-0.0141-1.32X)Z \qquad (9)$$

where F is the fraction of light transmitted at distance Z, and X is the cell concentration in g/l. Further analysis is reported by Erickson and Lee elsewhere (16). In this work, Z is taken to be 16 cm from the front to the back of the fermenter.

The results of estimating growth parameters are shown in Table IV. Only point estimates are reported here because of the wide range of confidence intervals due to the small number of data points. The application of covariate adjustment is not recommended for the same reason. The true growth yield of R. sphaeroides S is lower than that of Chlorella in Table II.

The results of Sasaki et al. (1) for propionate and yeast extract as substrates are presented in Tables V and VI for microaerobic growth. Since yeast extract consumption was not measured, data consistency can not be checked using the carbon and available electron balances. The biomass energetic yields are obtained using Equations (6) and (7). Equation (6), which is derived for anaerobic conditions, is valid here if Q_O is assumed to be zero. The good agreement for the two estimates of biomass energetic yield suggests that Equation (6) is approximately correct for this data.

Values of γ_s in Table V for propionate and yeast extract as substrate were obtained by weighting the relative consumption of propionate and yeast extract based on the measured values of consumed propionate and the calculated values of consumed yeast extract based on the carbon balance. The value of 4.29 was used for γ for yeast extract.

Estimates of the true biomass energetic yield and maintenance coefficient are presented in Table VI. The energetic yields in Tables V and VI are considerably better than those in Tables III and IV for R. sphaeroides S. The estimates obtained using all the data with no covariates have much shorter confidence intervals than the results obtained with one covariate because of the

small number of data points.

Tables VII and VIII compare the true growth yields and maintenance parameters for the blue-green algae, Chlorella vulgaris and the bacteria R. sphaeroides S. under heterotrophic and mixotrophic growth conditions. The results in Table VII indicate that the highest true energetic growth yields can be obtained under mixotrophic conditions for Chlorella vulgaris; however, the actual observed values of η in Table 1 are considerably smaller than the true growth yield. The very high maintenance coefficient values for mixotrophic growth should be investigated further.

In Table VIII, the true growth yield is larger for heterotrophic growth of R sphaeroides S. than for mixotrophic growth. Since the efficiency with which light energy is converted to biomass via photosynthesis is less than the efficiency of heterotrophic aerobic growth, this result appears to be reasonable. Further research is needed to identify when mixotrophic growth is advantageous.

REFERENCES

1. Sasaki, K., Y. Nishizawa, and S. Nagai, Biotech. and Bioeng., 22, 2529, (1980).
2. Aiba, S., J. Koizumi, and Y. Nishizawa, J. Chem. Tech. Biotech., 29, 311, (1979).
3. Ogawa, T., and S. Aiba, Biotech. and Bioeng., 23, 1121, (1981).
4. Endo, H., H. Sansawa, and K. Nakajima, Plant and Cell Physiol., 18, 199, (1977).
5. Aiba, S., Adv. Biochem. Eng., 23, 85, (1982).
6. Lee, H.Y., L.E. Erickson, and S.S. Yang, The Estimation of Growth Yield and Maintenance Parameters for Photoautotrophic Growth; Biotech. and Bioeng., In Press, (1984).
7. Pirt, S.J., Principles of Microbe and Cell Cultivation, Blackwell Scientific, London, (1975).
8. Solomon, B.O., S.S. Yang, and L.E. Erickson, Biotech. and Bioeng., 25, 2683 (1983).
9. Minkevich, I.G., and V.K. Eroshin, Folia Microbiol., 18, 376, (1973).
10. Lee, H.Y., L.E. Erickson, Characterization of Algae Using Regularites; Biotech. and Bioeng., In Press. (1984).
11. Pirt, S.J., Y.K. Lee, R. Amos, and M.W. Pirt, J. Chem. Tech. Biotech., 30, 25, (1980).
12. Yang, S.S., B.O. Solomon, M.D. Oner, and L.E. Erickson, Technometrics, In Press (1984).
13. Stewart, W.D.P., Algal Physiology and Biochemistry, pp. 392, Univ. of California Press, Berkley, (1974).
14. Amick, L.L., Flourescent Lighting Manual, 2nd ed., pp. 318, McGraw-Hill Book Co., N.Y. (1947).
15. Iehana, M., J. Fermt. Tech., 61, 457, (1983).
16. Erickson, L.E., and H.Y. Lee, Process Analysis and System Design for Photoautotrophic Growth; A Workshop on the Present Status and Future Directions for Biotechnologies Based on Algal Biomass Production (April, 1984); University of Colorado, Boulder.
17. Kreuzberg, K., Energy from Biomass, 2nd ed., Strub. A. (ed.), pp. 303, Applied Science Pub. (1982).
18. Lee, H.Y., Estimation of Yield and Maintenance Parameters Associated with Single Cell Protein Production on C-1 Compounds; M.S. Thesis (1984).

ACKNOWLEDGMENT

This work was partly supported by NSF Grant - CPE-8120039.

Table I. Energetic Yields and Data Consistency Check in Mixotrophic Growth of Chlorella vulgaris Grown on Glucose Media under Anaerobic-Light (0.104 kcal/cm^{2}hr) conditions.†

D (1/hr)	X (g/l)	S_0 (mM)	S (mM)	Energetic Yield η_{kcal}
0.085	0.276	2.78	0	0.3590
0.116	0.274	2.78	0	0.3561
0.140	0.269	2.78	0	0.4362
0.170	0.282	2.78	0	0.4903
0.190	0.253	2.78	0.106	0.4683

*Reductance degree and weight carbon fraction of biomass are γ_b = 4.402, and σ_b = 0.4766, respectively.

†Data from Ogawa and Aiba (3).

Table II. Estimation of Growth Yield Parameters for Chlorella vulgaris Grown on Glucose Media under Anaerobic-Light Conditions in Table I.

Data Used	Form	η_{max}		m_e (hr^{-1})	
		Point Estimate	95% Confidence Interval	Point Estimate	95% Confidence Interval
η_{kcal}	I	0.6822	0.3558, 0.8529	0.1226	-0.0441, 0.2894
	II	0.7353	0.3808, 0.9632	0.1365	-0.0472, 0.3203

Table III. Data Consistency Check and Energetic Yields for Mixotrophic Growth of R. sphaeroides S Grown on Acetate Medium under Anaerobic-Light (2.5 klux**) Conditions.††

D (1/hr)	X (g/l)	Q_{CO_2} ($\frac{mmole}{g/hr}$)	Carbon Balance y_c	Carbon Balance d	Available Electron Balance	Energetic Yields† η_{kcal}	$\eta_{(E)}$	η_c	$\eta_{(A.E.)}$
0.009	0.12	0.07	0.831	0.156	0.908	0.1089	0.1200	0.1091	0.1102
0.010	0.06	0.06	0.831	0.180	0.908	0.0760	0.0837	0.0761	0.0766
0.017	0.05	0.13	0.890	0.164	0.973	0.1115	0.1146	0.1107	0.1118
0.022	0.02	0.17	0.831	0.155	0.908	0.0889	0.0980	0.0891	0.0897

*Reductance degree and weight carbon fraction of biomass are $\gamma_b = 4.37$ and $\sigma_b = 0.4986$, respectively.

**Light intensity is converted with 283 lumens/watt.

†Yields are corrected by using fraction of light transmitted through the vessel, $F = \exp(-0.0141 - 1.3X)Z$.

††Data from Sasaki et al (1).

Table IV. Estimation of Growth Yield Parameters for R. sphaeroides S. Grown in Acetate Medium under Anaerobic-Light Conditions in Table III.

Data Used	Form	η_{max}	m_e (hr^{-1})
Average	I	0.1010	0.0051
	II	0.0979	0.0005
η_{kcal}	I	0.0987	0.0065
	II	0.0949	0.0008
$\eta_{(E)}$	I	0.1037	0.0020
	II	0.1023	0:0001
$\eta_{(A.E.)}$	I	0.0995	0.0058
	II	0.0995	0.0006
η_c	I	0.0983	0.0060
	II	0.0949	0.0008

Table V. Data and Energetic Yields for Mixotrophic Growth of R. sphaeroides S. Grown on Propionate-Yeast Extract Media under Microaerobic-Light (4.5 klux**) Condition.†

D (hr^{-1})	X (g/l)	Q_{CO_2} ($\frac{mmole}{g/hr}$)	Q_{O_2} ($\frac{mmole}{g/hr}$)	Propionate Concentration†† S_{op} (g/ℓ)	Propionate Concentration†† S_p (g/ℓ)	Substrate Reductance Degree, γ_s	Energetic Yields η_C	Energetic Yields η (A.E.)
0.028	2.17	0.03	≈ 0	1.30	0.26	4.467	0.2671	0.2721
0.040	1.76	0.04	≈ 0	1.21	0.33	4.476	0.2961	0.3023
0.053	1.48	0.05	≈ 0	1.40	0.81	4.487	0.3101	0.3172
0.064	1.37	0.10	≈ 0	1.40	0.46	4.542	0.3386	0.3504
0.071	1.27	0.10	≈ 0	1.29	0.48	4.525	0.3455	0.3568
0.082	0.84	0.10	≈ 0	1.40	0.83	4.542	0.2898	0.2977
0.096	0.90	0.29	≈ 0	1.32	0.75	4.514	0.3320	0.3471

*Reductance degree, γ_b = 4.29, and weight carbon fraction σ_b = 0.4824, respectively.

**Light intensity is converted with 283 lumens/watt.

†Data from Sasaki et al (1).

††S_{0p}=Initial concentration of propionate; S_p=final concentration of propionate.

Table VI. Results of Estimation of True Growth Yield and Maintenance Coefficient for R. sphaeroides S. Grown on Propionate+Yeast Extract Media under Microaerobic-Light Conditions (4.5 klux*).

Data Used	Covariate Included	Form	η_{max}		m_e (hr^{-1})	
			Point Estimate	95% Confidence Interval	Point Estimate	95% Confidence Interval
All	z_1	I	0.3405	0.1735,8.9290	0.0233	-0.0314,0.0781
		II	0.2814	0.1460,3.9105	0.0043	-0.0869,0.0955
All	none	I	0.3739	0.2989,0.4991	0.0273	-0.0051,0.0598
		II	0.3574	0.2783,0.4994	0.0202	-0.0319,0.0724
η_c	none	I	0.3654	0.3013,0.4641	0.0264	-0.0018,0.0546
		II	0.3484	0.2735,0.4798	0.0187	-0.0328,0.0702
$\eta_{(A.E.)}$	none	I	0.3829	0.3124,0.4943	0.0283	-0.0033,0.0568
		II	0.3669	0.2832,0.5209	0.0218	-0.0310,0.0746

*Light intensity is converted with 283 lumens/watt.

Table VII. Comparison of Growth Yield Parameters under Different Culture Conditions for Blue-Green Algae, Chlorella vulgaris.

Culture Conditions	η_{max}		m_e (hr^{-1})	
	Point Estimate	95% Confidence Interval	Point Estimate	95% Confidence Interval
Heterotrophic Growth (with glucose)	0.5357	0.1745, infinite	-0.0175	-0.3888, 0.3037
Autotrophic Growth (with Light)	0.2670	0.2141, 0.3556	-0.0006	-0.0051, 0.0038
Mixotrophic Growth (on glucose and light)	0.7353	0.3808, 0.9632	0.1365	-0.0472, 0.3203

Table VIII. Comparison of Growth Yield Parameters under Two Different Culture Conditions for Photosynthetic Bacteria, R. sphaeroides S.

Culture Conditions	η_{max}		m_e (hr^{-1})	
	Point Estimate	95% Confidence Interval	Point Estimate	95% Confidence Interval
Aerobic Heterotrophic Growth (on Propionate + Yeast Extract)	0.5601	0.5077, 0.6266	0.0115	0.0011, 0.0219
Microaerobic Mixotrophic Growth (on Propionate + Y.E. + Light)	0.3739	0.2989, 0.4991	0.0273	-0.0051, 0.0598

CAPILLARY GAS CHROMATOGRAPHY OF TRIMETHYLSILYLATED TRISACCHARIDES

Etienne J. M. Selosse

Department of Chemical Engineering

Iowa State University

Ames, IA 50011

INTRODUCTION

Separation of trisaccharides by gas chromatography presents a number of problems. They have the same molecular weight, at least if they are composed of hexoses and their structures are very similar. In addition, they are thermolabile and need to be derivatized before they can be vaporized. Schwind et al. (1), Jouany (2), Bhatty et al. (3) have reported gas chromatographic data for trisaccharides. But these authors were mainly concerned with their identification in a mixture of carbohydrates of different lengths and not with their separation from each other. A more extensive study of the separation of trisaccharides was reported by Karkkainen (4,5). However, his method was a combination of gas chromatography and mass spectrometry. Our purpose was to design a simple method to analyze trisaccharide mixtures. For this purpose, TMS derivatives were used even though TFA derivatives give more volatile compounds, because this method allows some water to be present in the sample.

MATERIAL AND METHODS

Instrumentation

The gas chromatograph was a VARIAN 3700 with a flame ionization detector coupled to a Houston Omniscribe recorder. The column was a 30 m long, 0.26 mm i.d. fused silica capillary manufactured by J & W Scientific. It was coated with a 0.1 μm film of DB-5 bonded liquid phase.

Operating conditions

The analysis was conducted with a helium carrier gas velocity of 0.183 m/min and a splitting ratio of 1:100. For the flame ionization detector, hydrogen flow was 30 ml/min and air flow was 300 ml/min. The column temperature remained at 270° C for 8 min and then increased 5° C/min to 315° C. Injector and flame ionization detector temperatures were 340° C and 360° C respectively.

Sample preparation

The trisaccharides were derivatized using the method described by Brobst and Lott (6) with 1 mg of trisaccharide being dissolved in 1 ml of pyridine and equilibrated for 24 h at 50° C. Afterward, 0.9 ml of hexamethyldisilazane and 0.1 ml of trifluoroacetic acid were added and the mixture was shaken and allowed to stand for 15 min before injecting.

Trisaccharides standards

Raffinose (O-α-D-galactopyranosyl-(1-6)-O-α-D-glucopyranosyl-(1-2)-β D-fructofuranoside) was supplied by Pfanstiehl Laboratories (Waukegan, IL.). Melezitose (O-α-D-glucopyranosyl-(1-3)-O-β-D-fructofuranosyl-(2-1 -α-D-glucopyranoside), maltotriose (O-α-D-glucopyranosyl-(1-4)-O-α-D-gluco-pyranosyl-(1-4)-D-glucose), isomaltotriose (O-α-D-glucopyranosyl-(1-6)-D-α glucose) were purchased from Sigma (St. Louis, MO.). Cellotriose (O-β-D-glucopyranosyl-(1-4)-O-β-D-glucopyranosyl-(1-4)-D-glucose) was obtained from V-Labs (Covington, LA.). Panose (O-α-D-glucopyranosyl-(1-6)-O-α-D-glucopyranosyl-(1-4)-D-glucose) was purchased from BDH Chemicals (Poole, England). Xylotriose (O-β-D-xylopyranosyl-(1-4)-O-β-D-xylopyranosyl-(1-4) -D-xylose) was produced in this laboratory. The following compounds were gifts:Isopanose (O-α-D-glucopyranosyl-(1-4)-O-α-D-glucopyranosyl-(1-6)-D-glucose) from Dr. Bent Stig Enevoldsen of Carlsberg Research Center, O-α-D-glucopyranosyl-(1-6)-O-α-D-glucopyranosyl-(1-3)-D-glucose from Dr. John F. Robyt of Iowa State, and laminaritriose (O-β-D-glucopyranosyl-(1-3)-O-β-D-glucopyranosyl-(1-3)-D-glucose) from Dr. Elwin T. Reese of the U.S. Army Natick Laboratories.

RESULTS AND DISCUSSION

Figures 1-3 show chromatograms of trisaccharides using raffinose as internal standard. Significant differences in the peak shapes can be noticed. Raffinose and melezitose, which are nonreducing and in addition contain a fructose unit, give very sharp peaks. The peak corresponding to xylotriose, the only pentaoligosaccharide studied in this work, is very broad even though xylotriose is the first compound to elute. The glucooligosaccharide peaks vary in shape and width. Two of the compounds, maltotriose and cellotriose, give split peaks. To see if these could be due to partial separation of α- and β- anomers, proton NMR spectroscopy of maltotriose was performed using the method of Kamerling *et al.* (7). The spectrum is shown in figure 4. A rough estimation of the anomeric ratio based on the height of the Hα and Hβ doublets gives: 47% α-form and 53% β-form, suggesting that the two approximately equal GC peaks may correspond to the two anomers.

Several factors could explain the large differences in peak widths. The fructo-, xylo-, and gluco-compounds could have different diffusivity coefficients in the liquid phase, even though their similarity in size and conformation make this hypothesis unlikely. A more likely explanation would be that the reducing ends of the carbohydrates play an important role, since the non-reducing compounds (raffinose and melezitose) give sharp peaks while the reducing compounds elute in broad peaks. It can also be noticed that for the two trisaccharides presenting the beginning of an anomeric separation (maltotriose and cellotriose), the outer edges of the peaks are sharp. The large widths of the reducing sugar peaks could therefore be due to an interaction between anomers.

The retention times, relative retention times (with raffinose as reference), and resolutions appear in Table 1. The resolution between two neighbouring peaks was calculated using the formula

$$R_s = \frac{2\,(t_2 - t_1)}{w_1 + w_2}$$

where t_1 and t_2 are the retention times and w_1 and w_2 the baseline widths

of the two peaks. For maltotriose and cellotriose the peak width was estimated for each anomer by considering the peaks as gaussian and attributing to the inner edges the same slopes as the outer edges. These widths, however, were not used to calculate the resolution between anomers. Considering that a resolution of 1 means an almost complete separation, while a resolution of 1.5 gives baseline separation, this table indicates that only xylotriose, raffinose, melezitose, and maltotriose are well-separated from neighboring peaks. However, it may be noted that the order of elution here is very similar to that reported earlier for disaccharides of similar structure (8), compounds containing xylose eluting first, followed by those with fructose in the furanose form, then by compounds containing all glucose, with those possessing (1-6)-bonds being last.

CONCLUSIONS

Even though this method can help in the analysis of a trisaccharide mixture, it cannot provide a complete qualitative and quantitative determination. However if an even more temperature stable liquid phase could be designed the use of a thicker film could improve the separation, and then higher column temperatures could prevent excessive broadening of the peaks.

ACKNOWLEDGMENT

This project was supported by an NSF Grant and by the Engineering Research Institute, Iowa State University. (NSF Grant #420-20-27-00).

REFERENCES

1. H. Schwind, F. Sharbert, R. Schmidt and R. Kattermann, Jr. Clin. Chem. Clin. Biochem., 16 (1978) 145.

2. J. P. Jouany, Ann. Biol. anim. Bioch. Biophys., 12 (1972) 493.

3. T. Bhatti, R. E. Chambers, and J. R. Clamp, Biochim. Biophys. Acta, 222 (1970) 339.

4. J. Karkkainen, Carbohyd. Res., 17 (1971) 1.

5. J. Karkkainen, Carbohyd. Res., 17 (1971) 11.

6. K. M. Brobst and C. E. Lott, Jr., Cereal Chem., 43 (1966) 35.

7. J. P. Kamerling, M. J. A. de Bie, and J. F. B. Vliegenthart, Tetrahedron, 28 (1972) 3037.

8. Z. L. Nikolov and P. J. Reilly, J. Chromatogr., 254 (1983) 157.

Table 1 - Relative Retention Times and Resolutions of the TMS Ethers of Trisaccharides

Compound	Retention Time (Min)	Relative Retention Time (Min)	Peak Width (Min)	Resolution
Xylotriose	15.03	0.91	1.5	
				1.92
Raffinose	16.53	1.00	0.063	
				20.5
Melezitose	17.81	1.08	0.063	
				1.25
α-Maltotriose	18.02	1.09	0.275	
				-
β-Maltotriose	18.39	1.11	0.313	
				0.32
α-Cellotriose	18.47	1.12	0.188	
				-
Panose	19.32	1.17	1.06	
				-
β-Cellotriose	19.39	1.17	0.188	
				0.07
Glc-α-1,6α-Glc--1,3-Glc	19.56	1.18	0.474	
				0.05
Isopanose	19.61	1.19	1.5	
				0.29
Laminaritriose	19.85	1.20	0.15	
				1.79
Isomaltotriose	21.53	1.30	1.725	

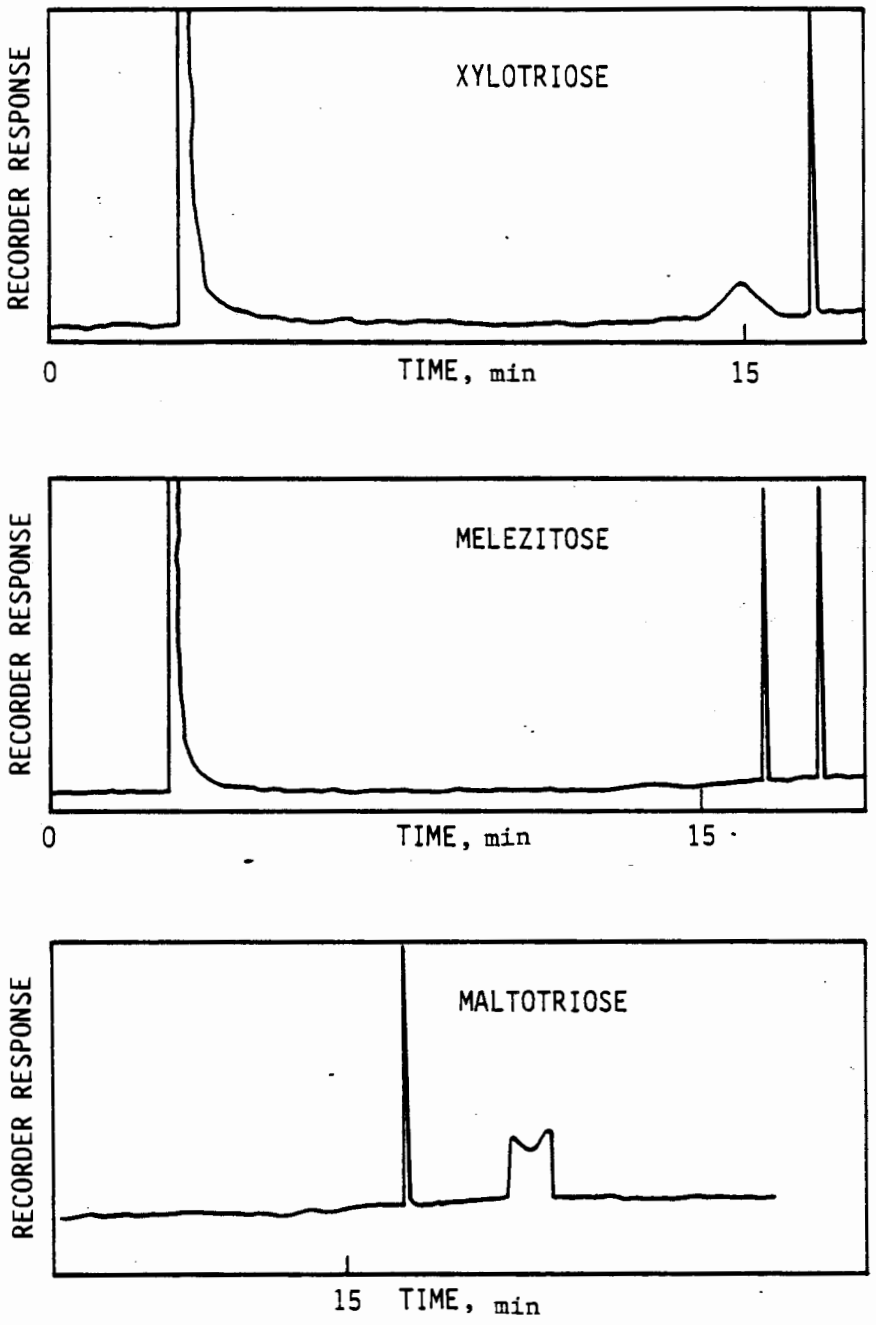

Fig. 1. Gas chromatograms of the TMS derivatives of xylotriose melezitose and maltotriose

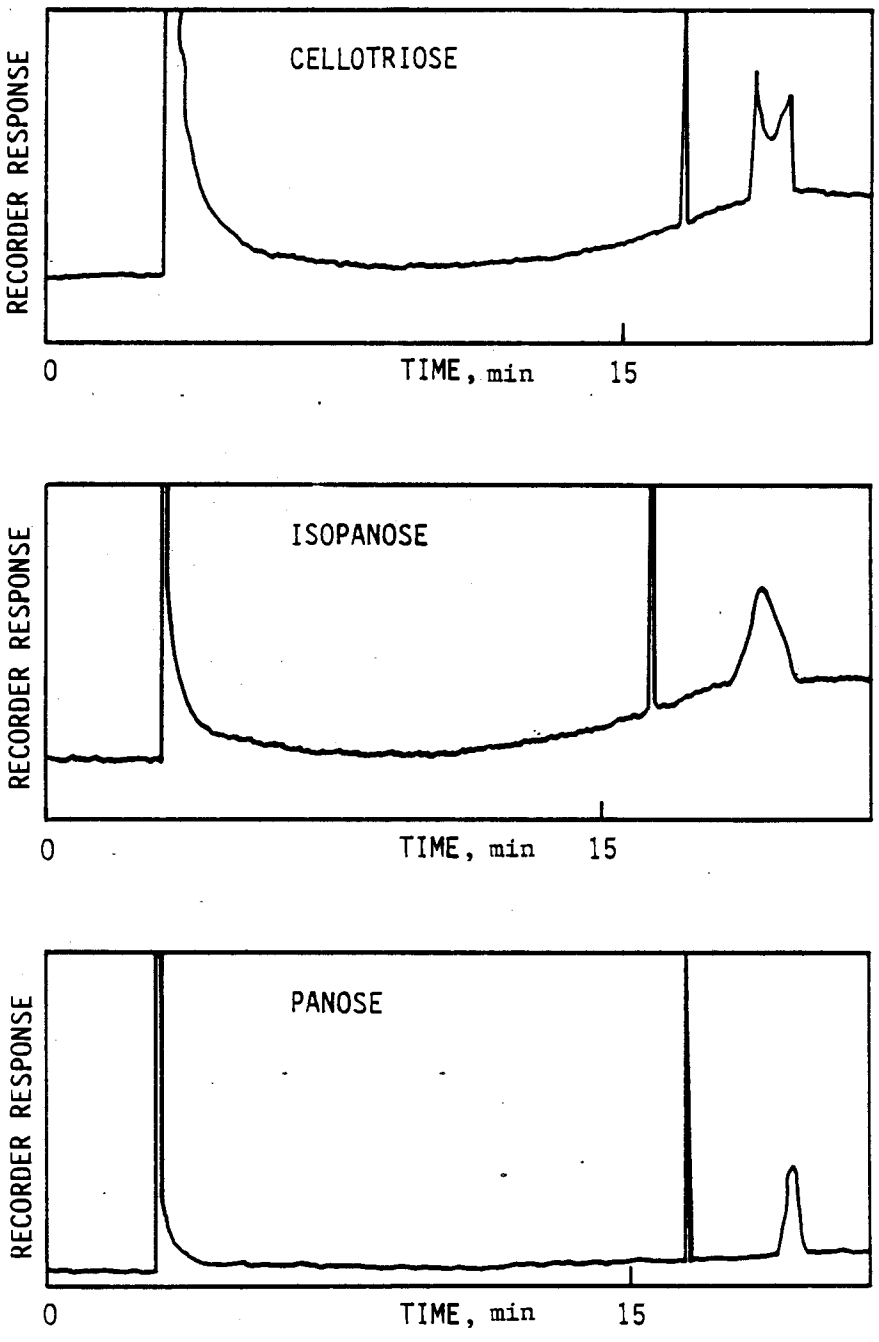

Fig. 2. Gas chromatograms of the TMS derivatives of cellotriose isopanose and panose

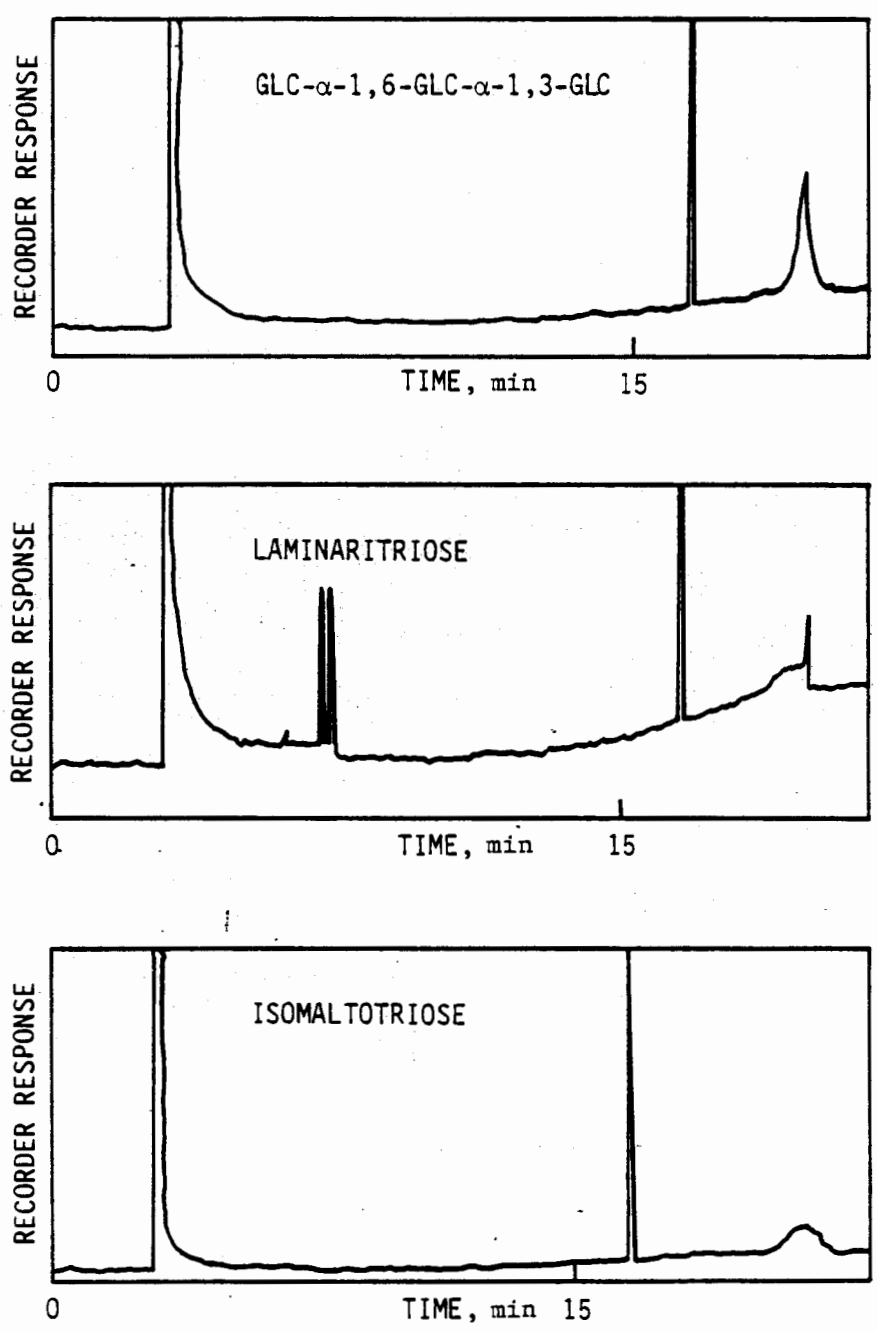

Fig. 3. Gas chromatograms of the TMS derivatives of GLC-α-1, 6-GLC-α-1, 3-GLC, laminaritriose and isomaltotriose

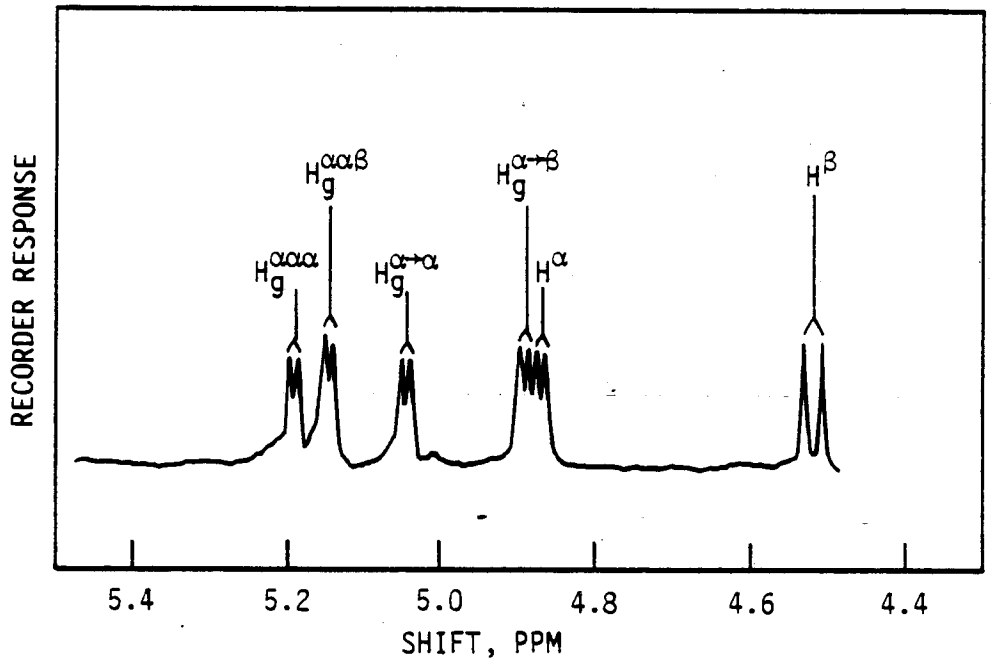

Fig. 4. Proton NMR spectrum in acetone-d_6 of TMS Maltotriose.

SUBSITE MAPPING OF AN ENDO-XYLANASE USING LABELED XYLOOLIGOSACCHARIDES

-BERNARD Y. TAO-

DEPARTMENT OF CHEMICAL ENGINEERING

IOWA STATE UNIVERSITY

AMES, IOWA 50010

INTRODUCTION

Xylan, a polysaccharide of xylose, is a major constituent of most plant cell walls. With roughly 4×10^{11} tons of xylan and other polysaccharides produced renewably every year, it is a potential major raw material source of fuels and chemicals. In order to utilize xylan efficiently, in most cases it must first be broken down into xylose residues. This may be done by acid or enzymatically.

An A. niger endo-xylanase which produces mainly xylose and xylobiose from soluble xylan is characterized in this work. Previous workers have determined the size, amino acid composition, and general kinetics parameters for this enzyme (1,2). The present work quantifies the hydrolytic kinetics of this enzyme using molecular subsite affinity structural models.

DERIVATION OF SUBSITE MODEL

The structure of depolymerase enzyme active sites has been proposed to consist of multiple subsites, each binding a single monomer residue (3,4). If the active center is internal to the subsite structure, i.e. an endo-depolymerase, a distribution of products may occur from a single substrate. This product distribution is dependent upon the binding specificity of the substrate with the enzyme. Accordingly, the product distribution may change with substrates of different length. This model attempts to quantitatively explain changes in the product distributions based on monomer subsite binding affinities.

Figure 1 depicts the general idea of different binding modes for a single substrate within an endo-depolymerase site. Note that both productive and nonproductive binding modes are possible.

The kinetic scheme for substrate binding and hydrolysis is given below:

$$E + S_n \underset{k_{-1,n,j}}{\overset{k_{1,n,i}}{\rightleftharpoons}} ES_{n,i} \xrightarrow{k_2} E + P_{r,i}$$

$$\underset{k_{-1,n,j}}{\overset{k_{1,n,j}}{\rightleftharpoons}} ES_{n,j}$$

Here, i represents the ith productive mode of binding, and j represents the jth nonproductive binding mode. n and r refer to substrate and product polymer length, respectively. Note that it is assumed that k_2 is independent of substrate length and binding mode.

Individual rates of product formation, $v_{n,i}$, can be calculated, assuming the conservation of enzyme and steady state concentration of enzyme-substrate intermediates:

$$v_{n,i} = k_2 * K_{n,i} * \frac{[E]_o * [S_n]}{1 + (\sum_q K_{n,q}) * [S_n]}$$

Here o refers to the total concentration and $K_{n,i}$, $K_{n,j}$, and $K_{n,q}$ are defined below:

$$K_{n,i} = \frac{k_{1,n,i}}{k_{-1,n,i} + k_2} \qquad \text{(productive)}$$

$$K_{n,j} = \frac{k_{1,n,j}}{k_{-1,n,j}} \qquad \text{(nonproductive)}$$

$K_{n,q}$ = either binding mode

The rate of substrate depletion, V_n, can be derived by summing overall productive binding modes. Rearranging this into the standard Michaelis-Menten format, we can define the maximum rate and Michaelis parameters, V_{mn} and K_{mn}, as follows:

$$V_{mn} = \frac{k_2 * (\sum_i K_{n,i})}{(\sum_q K_{n,q})} * [E]_o$$

$$= k_{on} * [E]_o$$

$$K_{mn} = \frac{1}{(\sum_q K_{n,q})}$$

Assuming that $[S_n] \ll K_{mn}$, the overall rate equation can be written as a first order system:

$$V_{mn} = \frac{k_{on}}{K_{mn}} * [E]_o * [S_n]$$

Since the terminal monomer residue is labeled, we can measure the specific labeled product distribution. The first order rate constant for a specific product, k_n^i, can be calculated using the specific product distributions:

$$k_n^i = \frac{k_{on}}{K_{mn}} * [E]_o * \frac{P'_{r,i}}{\sum_i P'_{r,i}}$$

where P′ denotes labeled product.

The enzyme site affinity for binding a substrate of length n in the ith binding mode, $\Delta G_{n,i}$, is then

$$\Delta G_{n,i} = -RT \ln k_n^i$$

Comparing the binding affinities for the S_n and S_{n-1} substrates in the ith binding mode (Fig. 2), the relative affinity for a single subsite can be determined (e.g. subsite a in Fig. 2):

$$\Delta G(a^{th} \text{ subsite}) = \Delta G_{n-1,\, i} - \Delta G_{n,i} = RT \ln \frac{k_n^i}{k_{n-1}^i}$$

Finally, by using a series of oligosaccharides of different lengths, the relative affinities of each subsite, within the enzymatic site, can be determined.

MATERIALS AND METHODS

THIN LAYER CHROMATOGRAPHIC ANALYSIS

Materials:

Preparative TLC Plates: Macherey-Nagel preparative silica gel TLC plates, 2 mm layer thickness (Brinkman, Westbury, N.Y.)

Preparative prewash solvent: acetonitrile:water, 50:50 (v/v).

Qualitative TLC plates: Whatman K5 silica gel TLC plates, 250 μm layer thickness (Whatman, Clifton, N.J.).

Quantitative TLC plates: Merck silica gel 60 plastic-backed TLC plates (MCB Reagents, Gibbstown, N.J.).

Elution solvent: acetonitrile:water:n-propanol, 70:20:10 (v/v).

Procedure:

Oligosaccharides were analyzed by separation on TLC silica gel plates.

Preparative TLC was performed by pretreating the TLC plates with a triple ascent of prewash solvent. Separation used a single ascent of elution solvent.

Qualitative identification used a single ascent of elution solvent.

Quantitative analysis was done using plastic backed TLC silica gel plates, with a single ascent of elution solvent.

Spotting volumes ranged from 1 µL to 5 µL, depending on concentration.

AUTORADIOGRAPHIC ANALYSIS

Materials:

X-ray film: Kodak SB5.

Surface autoradiographic enhancer: EnHance, New England Nuclear (Boston, Mass.).

Procedure:

TLC-separated, tritium-labeled oligosaccharides were imaged using autoradiography. This was done by spraying the developed TLC plates with surface autoradiographic enhancer, followed by contact exposure with X-ray film for 48 h. Preparative TLC did not use surface enhancer and plates were exposed for 7 days.

LIQUID SCINTILLATION ANALYSIS

Materials:

Heterogeneous scintillation cocktail: 4 g POP (2,5-diphenyl oxazole), 0.1 g POPOP (1,4-bis-2-(5-phenyloxazolyl) benzene), 1 L toluene.

Homogeneous scintillation cocktail: Ria-Solve II, Research Products International Corp. (Mt. Prospect, Ill.).

Liquid scintillation spectrophotometer: Packard TriCarb Model C2425.

Procedures:

Homogeneous liquid scintillation counting was used to quantify labeled oligosaccharide solution concentrations. 1 µL of oligosaccharide solution was added to 20 mL of cocktail and counted for one min. No significant quenching was detected.

XYLOOLIGOSACCHARIDES

A linear series of xylooligosaccharides, xylotriose to xylooctaose, was labeled at the reducing end with tritium(3). After labeling, the triose, tetraose, and hexaose were purified using preparative TLC. Using autoradiographic imaging, the areas corresponding to the isolated oligosaccharides were excised. The oligosaccharides were eluted from the chromatographic media with three 20 mL water washes. Each wash was centrifuged and the supernatant retained. The three supernatants were

filtered, combined, and concentrated to roughly 0.5 mL using freeze drying.

Concentrations of labeled oligosaccharides were calculated using homogeneous liquid scintillation.

HYDROLYSIS

All reactions were run at 40°C in closed, agitated reaction vials. pH was maintained at 4.8 using 0.05M sodium citrate buffer. Initial substrate concentration was 0.01mM for all reactions. Total reaction volume was 200 µL.

The buffer/substrate solution and the enzyme were pre-warmed separately for 20 min. prior to mixing. After adding the enzyme to the substrate solution, 20 µL samples were withdrawn at various time intervals. These samples were injected into 20 µL of sodium carbonate solution, pH 11.8, to stop the reaction.

HYDROLYSIS PRODUCTS ANALYSIS

After hydrolysis, 5 µL of each sample were spotted onto a plastic backed TLC plate and developed. After autoradiographic imaging, the separated hydrolysis products spots were excised and counted, using toluene cocktail. Background was less than 100 cpm in all cases.

RESULTS AND DISCUSSION

Bond cleavage frequencies are presented in Fig. 3. It was not possible to obtain all bond cleavage frequencies of xyloheptaose and xylooctaose because, at this point, the TLC resolution of the longer products has been insufficient.

First order rate constants were calculated from extent of reaction vs. time data, using linear regression (Fig. 4). All correlation coefficients were greater than 0.99. Note that the heptaose rate constant is intermediate between the hexaose and pentaose rate constants.

Subsite affinities were calculated using the model presented earlier. Ten subsites were modeled, including imaginary subsites (Fig 5). Taking subsites 1-3 and 9-10 to be imaginary, the proposed subsite affinity map is presented in Fig. 6.

It appears that there are five subsites which compose the enzymatic site, with the active center located two subsites to the left of the furthest reducing-end binding subsite. The very large affinity of subsite 5 appears to dominate the binding behavior of this enzyme, producing mainly xylose and xylobiose as eventual hydrolysis products.

It is not known why the rate constant for xyloheptaose is lower than that of xylohexaose. ^{13}C Fourier transform NMR indicates that the non-labeled source xyloheptaose is a linear chain of xylose residues. Acid hydrolysis of the nonlabeled source xyloheptaose shows only xylose residues. It may be that some type of inhibitor is in the labeled sugar or the labeling process has somehow modified the oligosaccharide. Current work is underway to resolve this mystery.

ACKNOWLEDGMENTS

This project was supported by the National Science Foundation, grant CPE-8022895, and the Engineering Research Institute, Iowa State University. The unlabeled xylo-oligosaccharides were supplied by Michael Meagher. Dr. John Robyt of the Dept. of Biochemistry, Iowa State University, is gratefully acknowledged for the use of the liquid scintillation spectrophotometer and the photographic laboratory. Helpful discussions with Thomas Binder, Steven Eklund and Dr. John Robyt are also gratefully recognized.

Binding mode	
1	O-O-O-X ¦
2	O-O-O-X¦
3	O-O-O¦X
4	O-O¦O-X
5	O¦O-O-X
6	¦O-O-O-X
	U-U^U-U-U
	1 2 3 4 5

O - monomer residue
X - labeled terminal residue
U - subsite
^ - active center
¦ - hydrolysis position

Figure 1. Modes of Enzyme-Substrate Binding

```
O-O-O¦X
  O-O¦X
U-U-U^U
a    i
```

Both substrates in the ith binding mode

Figure 2. Substrate binding to determine the ath subsite affinity

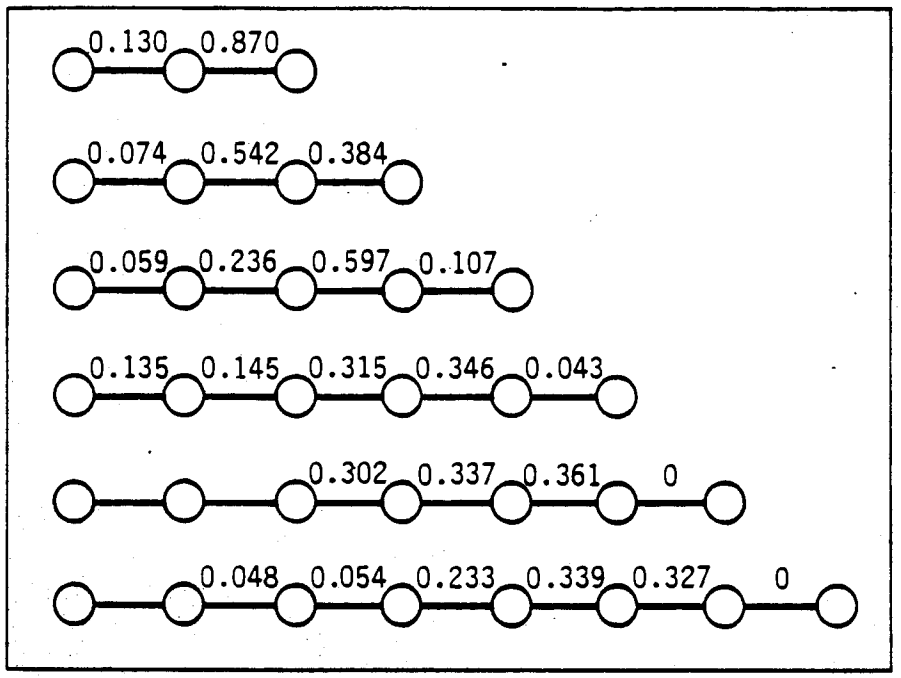

Fig. 3. Xylo-oligosaccharide bond cleavage frequencies.

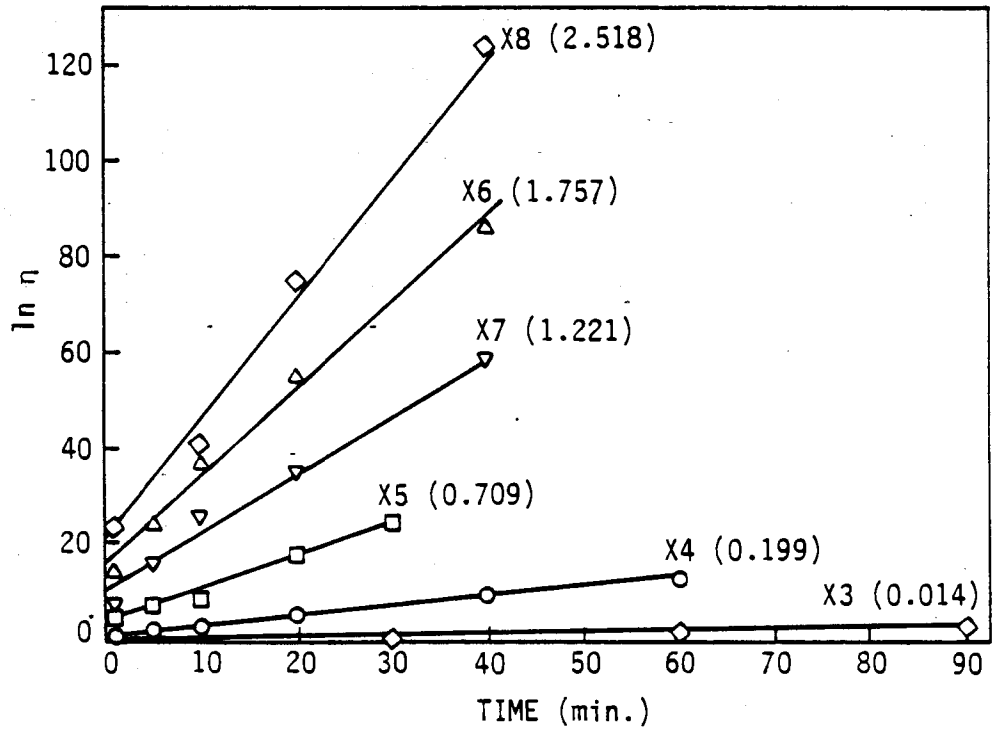

Fig. 4. Hydrolytic rate data (min^{-1} per IU).

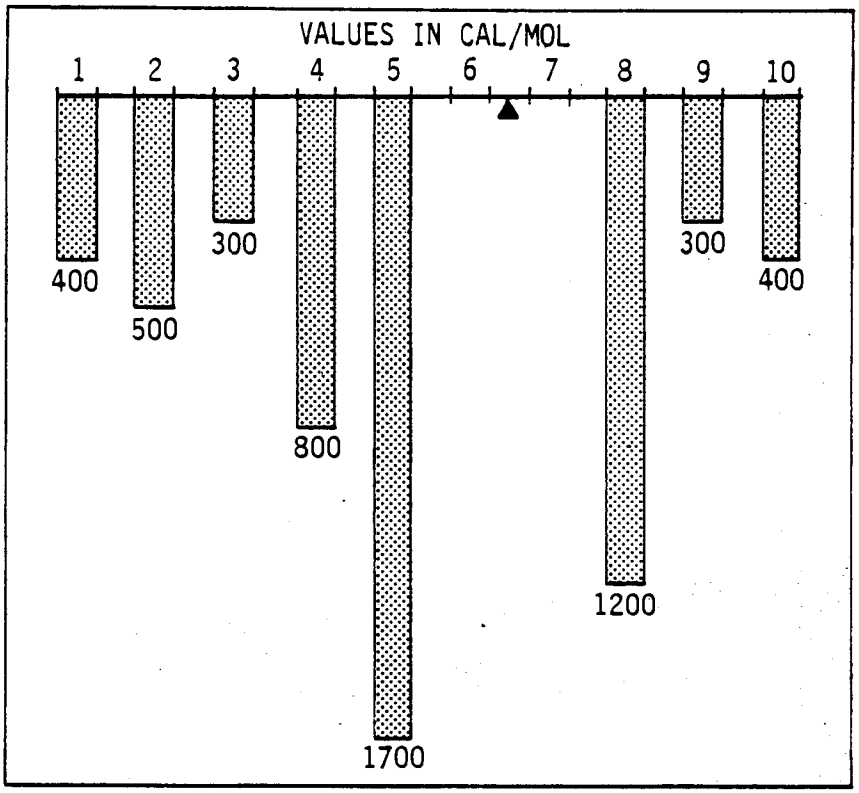

Fig. 5. Subsite affinity map including imaginary subsites.

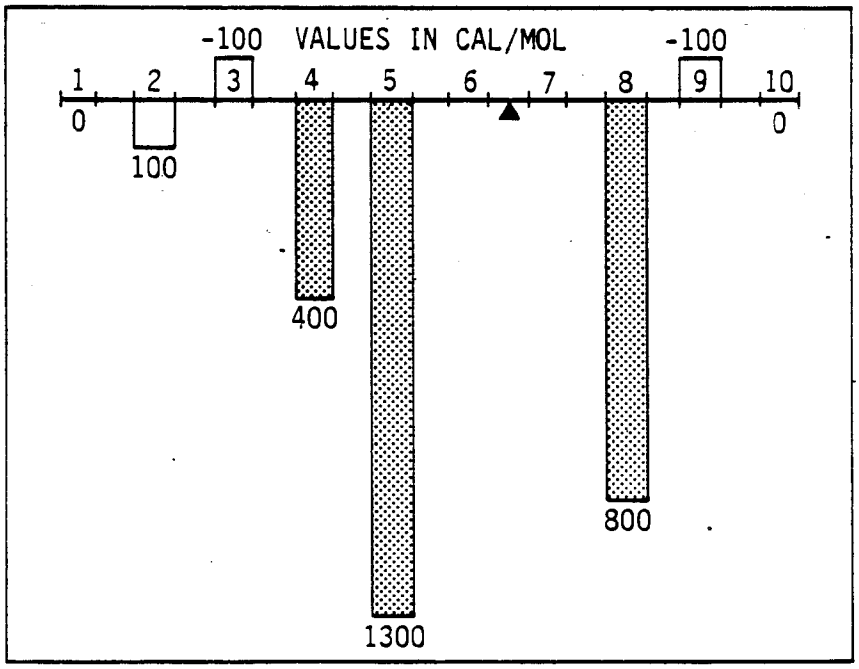

Fig. 6. Proposed subsite affinity map (shaded areas).

REFERENCES

1. Frederick, M. M., Frederick, J. R., Fratzke, A. R., and Reilly, P. J., Carbohydr. Res., 97 (1981) 87.

2. Meagher, M. M., M.S. Thesis (1984), Dept. of Chemical Engineering, Iowa State University, Ames, Iowa.

3. Thoma, J. A., Rao G. V. K., Brothers, C., and Spradlin, J., J. Biol. Chem., 18 (1971) 5621.

4. Suganuma, T., Matsuno, R., Ohnishi, M., and Hiromi, K., J. Biochem., 84 (1978) 293

CELLULASE ENZYME RECYCLE

Kate M. V. Baptie

Department of Agricultural and Chemical Engineering
Colorado State University
Fort Collins, Colorado 80523

Introduction

The use of cellulosic materials as a renewable resource for the production of liquid fuels is greatly hindered by the cost of the cellulase enzymes. Some recent assessments show that the production of the cellulase enzymes represents 40 to 60 percent of the overall expense involved with the biomass to fuel conversion process (1,3). To aid the economics of glucose production, much research is focused on increasing the activity and productivity of the cellulase enzymes by fungal mutants and genetic engineering approaches (4,5). Considerable research is also concentrated on the reuse of cellulase enzymes following hydrolysis (2,6,7).

In the cellulose-cellulase system, enzyme adsorption is a necessary condition for hydrolysis (8). As hydrolysis proceeds, enzyme is released into solution and can be reused in subsequent hydrolyses. Ryu and Mandels recently reported that the adsorbed enzymes do not completely desorb from the insoluble substrate, even upon repeated washings with buffer (9). The enzymes remain on the substrate and continue digestion. Consequently, means for enhancing the desorption of cellulase from cellulose are necessary for maximum enzyme recovery.

Cellulose strongly adsorbs to cellulase at pH 4-5 and 40-50°C, the conditions which are optimum for enzymatic activity. As the pH's increase to 7 at 40-50°C, enzyme activity decreases to less than 10 percent of maximum (10). At least some of this decrease in activity is believed to be due to enzyme desorption.

This paper reports on the recycle of cellulases from *Trichoderma reesei* supplemented with cellobiase from *Aspergillus niger*. The desorption of cellulases on cellulose was studied as a function of pH. Desorption of enzymes by changing the pH of the enzyme-substrate mixture after a standard hydrolysis procedure was followed by reuse of the soluble enzymes in another standard hydrolysis procedure. These results were compared with recycling of the soluble enzymes without a post-hydrolysis pH change.

Materials and Methods

Enzymes. The cellulase enzymes used were Celluclast™ (200-L) and Novozym™ 188) obtained from Novo Enzyme Corporation (Danbury, CT). Celluclast™ is a cellulase preparation made by submerged

fermentation of a strain of *Trichoderma reesei*. Novozym™ is a cellobiase prepared by submerged fermentation of a strain of *Aspergillus niger*. The enzymes were prepared in the ratio of 2 percent (w/v) Celluclast™ and 0.2 percent (w/v) Novozyme™ in 0.05 M acetate buffer and assayed according to Mandels (12).

Cellulose. The substrate for these studies was ammonia freeze exploded (AFEX) treated wheat straw (11). The cellulose content was 40.1 percent and the hemicellulose content was 12.3 percent. The average moisture content was 5 percent. Sample mesh size was 2 mm.

Enzymatic Hydrolysis of Cellulose. Appropriate dilutions of the enzyme solutions were made to yield an initial activity of 80 IU/g dry AFEX treated wheat straw in a solid:liquid ration of 1:20. Optimal conditions for the standard 24-hour hydrolysis of 50°C, pH 4.8, and 125 rpm in a rotary shaker were the same for each of the following procedures:

Control: The first hydrolysis mixture was made with 50 ml of 80 IU/g enzyme solution and 2.5 g of fiber. The second hydrolysis mixture had 25 ml of the enzyme solution from the first hydrolysis and 1.25 g of fresh (unhydrolyzed) fiber. The third hydrolysis mixture had 10 ml of enzyme from the second hydrolysis and 0.5 g of fresh (unhydrolyzed) fiber.

pH Change: The same enzyme to fiber ratio as above was employed in this series. After the first hydrolysis, the enzyme-substrate mixture was equilibrated to pH 6.8 with 1 M NaOH. The fibers were removed by filtering and the pH of the remaining enzyme liquor was returned to 4.8 with 1 percent H_2SO_4. The second and third hydrolyses were identically handled.

All hydrolysis samples were duplicated.

Dialysis. A 24-hour dialysis followed each hydrolysis to reduce the concentration of inhibitory sugars. The cellulose membranes (Spectrapor, MWCO 6-8000), after being filled with hydrolysate, were submerged in 0.05 M acetate buffer at 5°C with constant stirring. The dialysis loading was 0.5 ℓ buffer for every 0.5 g sugar to be dial zed.

Sugar and Enzyme Activity Determination. Reducing sugar was determined by the dinitrosalicylic acid method (DNSA) with glucose as a standard (12). Enzyme activity was determined by the filter paper assay (FPA) reported by Mandels (12). Residual enzyme activity after each hydrolysis was determined by two methods. In both cases, the sugar produced during the filter paper assay was determined by subtracting measurements from DNSA and FPA. This reports residual activity after a hydrolysis. The first method yields percent recovery based on the activity during the previous hydrolysis. The second is based on initial activity.

Results and Discussion

The results of dialysis of the reducing sugar are shown in Figure 1. The following dialysis results were obtained from hydrolysis samples after a 24-hour hydrolysis: 72 percent of the sugars were removed from the liquor after 5 hours of dialysis, 89 percent were removed after 12 hours, and 94 percent after 24 hours. Filter paper activity of the hydrolysis sample showed that 20 percent of the enzyme activity was lost during the first 5 hours of dialysis. No significant activity was lost at longer dialysis times. An enzyme sample which had not been subjected to hydrolysis lost 15 percent of its activity over 3 hours, 23 percent of its activity over 24 hours, and 40 percent of its activity over 70 hours. As a result of this study, a 24-hour dialysis was chosen to remove a maximum amount of reducing sugars and retain a large proportion of enzyme activity in the hydrolysis samples.

The preliminary results of cellulase recycle with intervening dialysis are given in Table 1 and Figure 2 in which the percent recovery of activity is based respectively on activity prior to the immediately preceeding hydrolysis and on original activity. Table 1 shows increasing activity recovery in the study incorporating pH change; 98 percent recovery was obtained between the second and third hydrolyses. Possibly a portion of the cellulase enzymes may be indefinitely reusable. The behavior of the control is less clear from the data presented.

Figure 2 shows percent initial enzyme activity recovery as a function of the number of hydrolyses. After the third hydrolysis, the control had retained 15 percent of the initial activity. The pH change study had 36 percent of the initial activity. From these preliminary results, a pH change would appear advantageous in enzyme recovery.

Conclusions

Dialysis proves to be a simple method for removing reducing sugars from an enzyme-sugar mixture. Enzyme activity is negligibly affected during this procedure.

The pH change study produced enzyme with more than twice the activity of the enzyme in the control based on results after three hydrolyses. More research is presently being conducted to determine enzyme recovery after "infinite" hydrolyses.

References

1. Ryu, D., R. Andreotti, M. Mandels, B. Gallo, and E. T. Reese. Biotechnology and Bioengineering. 21:1887 (1979).

2. Wilke, C. R., R. D. Yang, A. F. Sciamanna, and R. P. Freitas. Biotechnology and Bioengineering. 23:163 (1981).

3. Blanch, H. W., and C. R. Wilke. Proc. Ethanol from Biomass Symp., Winnipeg, Canada. pp. 451 (1981).

4. Mandels, M. *In* Annual Reports on Fermentation Processes, Vol. 5, G. T. Tsao, Ed., Academic Press, NY. pp. 35-78 (1977).

5. Montencourt, B. S. and D. E. Eveligh. *In* Hydrolysis of Cellulose: Mechanisms of Enzymatic and Acid Catalysis. R. B. Brown and L. Jurasek, Eds., American Chemical Society, Washington, D.C. pp. 289 (1979).

6. Mandels, J., J. Kosick and R. Parizek. J. Polymer Sci., Part C. 36:445 (1971).

7. Mitra, G. and C. R. Wilke. J. Fermentation Technology. 50(12):914 (1972).

8. Lee, S. B., H. S. Shin and D. Ryu. Biotechnology and Bioengineering. 24:2137 (1982).

9. Ryu, D., C. Kim and M. Mandels. Biotechnology and Bioengineering 26:488 (1984).

10. Posorske, L. H. A Long Term Stability Study of Dilute Solutions of Celluclast™ and Cellobiase. Novo Enzymes Report.

11. Dale, B. E. and M. J. Moreira. A freeze-explosion technique for increasing cellulose hydrolysis. Biotechnology and Bioengineering Symp. No. 12, Biotechnology in Energy Production and Conservation. pp. 31 (1983).

12. Mandels, M., R. Andreotti, and C. Roche, C. Biotechnology and Bioengineering Symp. No. 6. pp. 21 (1976).

Table 1. Cellulase recycle with and without pH change.

Sample	Hydrolysis number	Percent recovery (based on activity prior to immediate hydrolysis)	Percent recovery (based on initial enzyme activity)
Control	1	60	60
	2	36	22
	3	67	15
pH change	1	50	50
	2	74	37
	3	98	36

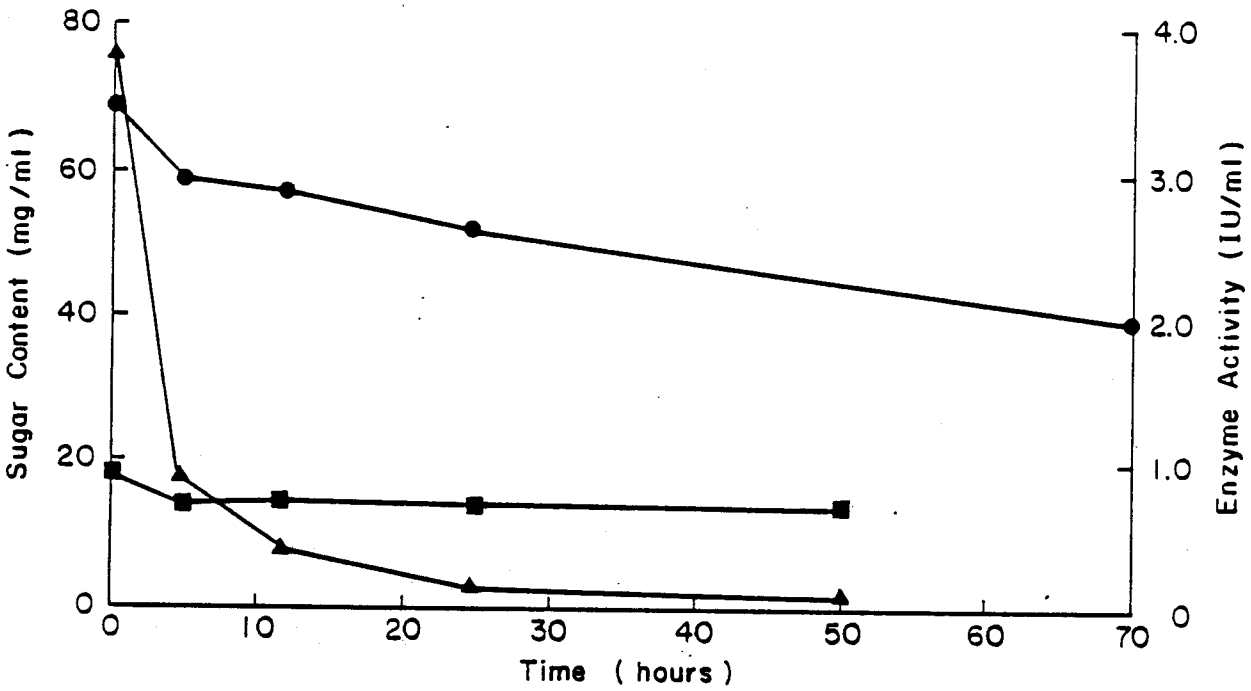

Figure 1. Dialysis results from a standard dialysis.

▲—▲ Glucose content inside membrane measured by the DNSA method.

●—● Residual activity of enzyme within membrane not subjected to a 24-hour hydrolysis.

■—■ Residual activity of enzyme which has undergone a 24-hour hydrolysis. Sugars produced during this hydrolysis are being dialyzed.

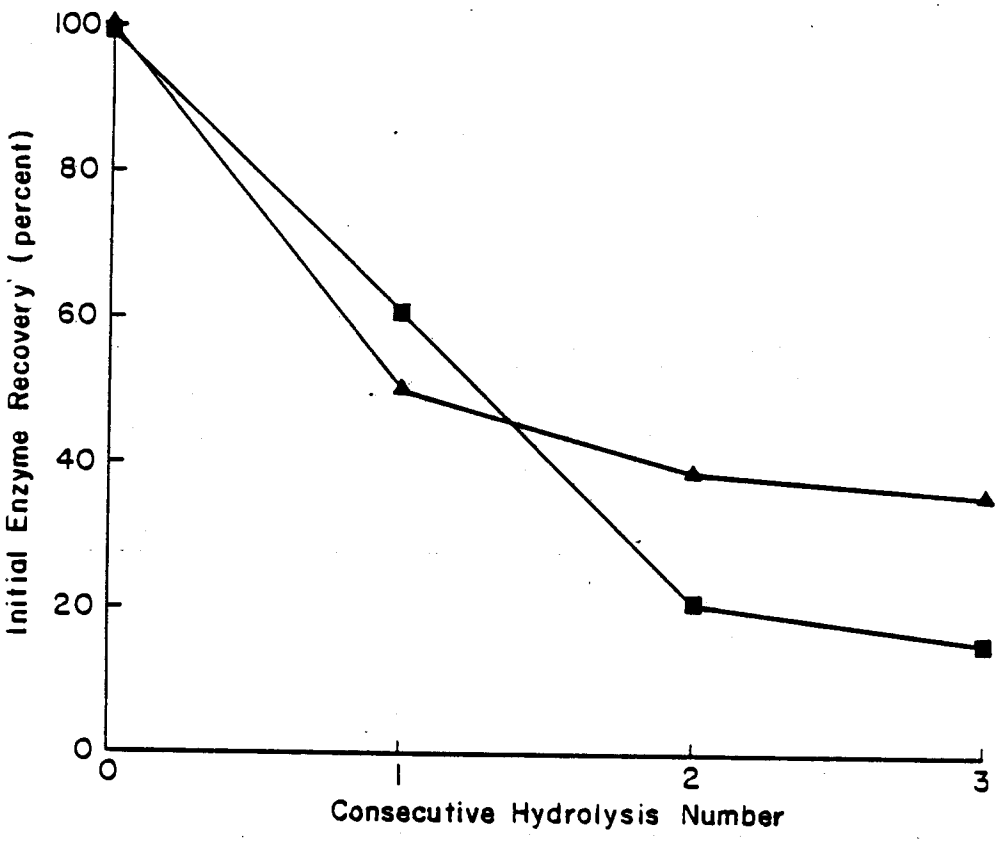

Figure 2. Recovery of initial enzyme activity. Activity calculations follow hydrolysis and proceed dialysis.

■——■ Control study of enzyme recycled without post-hydrolysis treatment.

▲——▲ pH change study of enzyme-substrate mixture treated with base to change pH from 4.8 to 7. Enzyme was changed back to pH 4.8 after substrate was filtered.

NON-HOMOGENEOUS POISSON RENEWAL REWARD PROCESS FOR MODELING ENZYMATIC HYDROLYSIS OF CELLULOSE

M. M. Gharpuray and L. T. Fan
Department of Chemical Engineering
Durland Hall
Kansas State University
Manhattan, Kansas 66506

April 28, 1984

INTRODUCTION

The conversion of cellulosic materials into fuel via hydrolysis has received increasing attention in recent years because of the high and unstable price of fossil fuel. Among a variety of cellulosic materials, wheat straw represents a relatively low cost feedstock for hydrolysis in select areas of this country, e.g., the state of Kansas.

In the enzymatic hydrolysis process, insoluble cellulose particles are contacted with enzyme macromolecules in an aqueous solution. This heterogeneous reaction has been modeled by visualizing a three step mechanism (Lee et al., 1980). In the first step, the enzyme molecules diffuse from the bulk phase of the solution to the surface of cellulose particles where they are adsorbed. In the second step, the physical contact between the enzyme and cellulose induces the hydrolysis of cellulose to sugar, mainly glucose. In the third step, the product sugar and enzyme molecules are desorpted from the surface of the cellulose particles and diffuse back into the bulk phase of the solution. One characteristic feature of this reaction is product inhibition, i.e., the sugar formed as a result of reaction deactivates the enzyme molecules, thereby, suppressing the rate of the reaction that would otherwise yield additional sugar (Lee et al., 1980; Lee, 1981). A typical curve representing the progress of enzymatic hydrolysis shown in Fig. 1 (Fan et al., 1981). The leveling off of the sugar concentration after an extended period of hydrolysis (> 16 hours) is a direct consequence of the product inhibition.

In the current work, the hydrolysis process is modeled as a non-homogeneous Poisson renewal reward process (see, e.g., Ross, 1980). The number of encounters (or collisions) between the cellulose particles and the enzyme molecules is considered to follow the non-homogeneous Poisson process. The formation of sugar upon such collision, or simply the reward, is assumed to follow Bernoulli distribution.

MODELING

The parameter $\lambda(t)$ of the non-homogeneous Poisson process, signifying the frequency at which the cellulose particles and enzyme molecules collide,

---

*For presentation at the 14th Annual Biochemical Engineering Symposium, Univ. of Missouri, Columbia, Mo., April 28, 1984.

is considered to decrease with the progress of time. This decreasing $\lambda(t)$ is a mathematical representation of the product inhibition. This decrease in $\lambda(t)$, or equivalently, in the frequency at which the cellulose particles and the enzyme molecules collide, is attributable firstly to the reduction in the number of cellulose particles due to their conversion to the product sugar and secondly to the reduction in the mobility of enzyme molecules in the solution due to the presence of an increasing amount of sugar. Furthermore, it is assumed that only a fraction of these encounters (collisions) between the cellulose particles and the enzyme molecules result in product (sugar) formation. The reward process, whether a collision yields sugar or not, is modeled as a Bernoulli process with time-invariant parameter p. This yields

$$X(t) = \sum_{i=1}^{N(t)} Y_i \tag{1}$$

where

$X(t)$ = number representative of sugar concentration in the solution at time t and corresponds to cumulative number of successful collisions starting at time zero until time t,

$N(t)$ = non-homogeneous Poisson process with parameter $\lambda(t)$ and is equal to the cumulative number of collisions starting at time zero until time t,

Y_i = an independent random variable having Bernoulli distribution with parameter p; naturally, p is the probability of sugar formation upon a collision.

A sample discrete data, read off Fig. 1, is shown in Table 1 (Fan et al., 1981). For simplicity, we resort only to the following functional forms for $\lambda(t)$;

$$\lambda(t) = \lambda\beta t^{\beta-1}, \tag{2}$$

i.e., the Weibull process, and

$$\lambda(t) = \eta e^{-\theta t}, \tag{3}$$

i.e., the exponential process.

The non-homogeneous Poisson process, N(t), representing the cumulative number of collisions, has a distribution given by (Ross, 1980)

$$P[N(t) = k] = \frac{e^{-m(t)}(m(t))^k}{k!}$$

where

$$m(t) = \int_0^t \lambda(t)\, dt$$

and has both the mean and variance equal to m(t). Similarly, the Bernoulli distribution with parameter, p, has

$$\text{mean } [Y_i] = p = E[Y_i] = \mu_{Y_i}$$

$$\text{variance } [Y_i] = p(1 - p) = \sigma^2_{Y_i}$$

For the function given in eq. (2)

$$m(t) = \lambda t^{\beta} \tag{4}$$

For the function given in eq. (3),

$$m(t) = \frac{\eta}{\theta} [1 - e^{-\theta t}] \tag{5}$$

It can be shown that the means and variances of the renewal reward process given in eq. (1) (Ross, 1980)

$$E[X(t)] = \mu_Y m(t) \tag{6}$$

$$\text{Var } [X(t)] = (\sigma^2_Y + \mu^2_Y)\, m(t) \tag{7}$$

Therefore, for the function given in eq. (2) or simply function 1, we obtain from eqs. (6) and (7)

$$E[X(t)] = p\, \lambda t^{\beta} \tag{8}$$

$$\text{Var}[X(t)] = p\, \lambda t^{\beta} \tag{9}$$

Similarly, for the function given in eq. (3) or simply function 2, we obtain from eqs. (6) and (7)

$$E[X(t)] = p\, \frac{\eta}{\theta} [1 - e^{-\theta t}] \tag{10}$$

$$\text{Var}[X(t) = p\, \frac{\eta}{\theta} [1 - e^{-\theta t}] \tag{11}$$

To estimate the parameters employed in function 1 and function 2, the following two approaches are employed.

(1) Least square estimation with respect to the mean, which has the following form;

$$\text{Minimize} \quad \sum_{i=1}^{n} [(X(t_i) - X_{est}(t_i)]^2$$

where

n = total number of data points,

$X(t_i)$ = observed sugar concentration at time t_i,

$X_{est}(t_i)$ = estimated mean value of the sugar concentration at time t_i.

For function 1, it has the form

$$X_{est}(t_i) = p\,\lambda t_i^{\beta} \tag{12}$$

and for function 2,

$$X_{est}(t_i) = p\,\frac{\eta}{\theta}\,[1 - e^{-\theta t_i}] \tag{13}$$

For function 1, the following constraints are imposed;

$$0 \leq p \leq 1 \tag{14}$$

$$0 \leq \lambda \leq 10 \tag{15}$$

$$0 \leq \beta \leq 1 \tag{16}$$

and for function 2, the following constraints are imposed;

$$0 \leq p \leq 1 \tag{17}$$

$$0 \leq \eta \leq 10 \tag{18}$$

$$0 \leq \beta \leq 10 \tag{19}$$

(2) Maximum likelihood estimation which has the form

$$\text{Maximize} \quad \prod_{i=1}^{n} p_i \tag{20}$$

where p_i is the probability of occurrence of the i-th data point; it is obtained as follows (Mood et al., 1979);

$$p_i = \frac{e^{-m(t_i)} (m(t_i))^{\left(\frac{X(t_i)}{p}\right)}}{\left(\frac{X(t_i)}{p}\right)!} \tag{21}$$

For function 1,

$$m(t_i) = \lambda t_i^{\beta}$$

and therefore, the objective function to be maximized is

$$\prod_{i=1}^{n} p_i$$

with

$$p_i = \frac{e^{-(\lambda t_i^{\beta})} (\lambda t_i^{\beta})^{\left(\frac{X(t_i)}{p}\right)}}{\left(\frac{X(t_i)}{p}\right)!}, \quad i = 1, 2, \ldots, n \tag{22}$$

The constraints imposed are the same as before [see eqs. 14-16]
For function 2

$$m(t_i) = \frac{n}{\theta}[1 - e^{-\theta t_i}]$$

and therefore, the objective function to be maximized is

$$\prod_{i=1}^{n} p_i$$

with

$$p_i = \frac{e^{-[\frac{n}{\theta}\{1 - e^{-\theta t_i}\}]} \left[\frac{n}{\theta}\{1 - e^{-\theta t_i}\}\right]^{\left(\frac{X(t_i)}{p}\right)}}{\left(\frac{X(t_i)}{p}\right)!} \qquad (23)$$

The constraints imposed are the same as before [see eqs. 17-19]. Note that in these maximum likelihood estimations the values of the ratio $\frac{X(t_i)}{p}$ have been rounded off to the nearest integer to estimate the corresponding probability via the Poisson distribution. These optimization problems have been solved using an adaptive random search technique for non-linear objective functions (Fan et al., 1975; Chen and Fan, 1976); the results are tabulated in Table 2.

RESULTS AND DISCUSSION

Using the parameter values obtained via a nonlinear adaptive random search technique, the mean values for the sugar concentration have been computed for different time periods of hydrolysis. Figure 2 shows the resultant estimates of sugar concentration plotted against the hydrolysis time for the Weibull process (function 1). For comparison, the experimental data are also plotted in the figure. It can be seen that the least square mean estimates predicted in the experimental results substantially better than the maximum likelihood estimates. Naturally, both the estimates seem to predict the experimental results fairly well. Notice that both of them tend to underestimate the results up to the hydrolysis time of 12 hours, after which they tend to overestimate the results.

Figure 3 represents a similar graph for the exponential process function 2 . In this case, the lease square mean estimates appear to predict the experimental results fairly well. These estimates are lower than the experimentally determined values up to the hydrolysis time of about 2 hours, after which they overestimate the experimental results. Due to the multimodal nature of the functional (objective) surface, we have failed to obtain reasonable estimates for the parameters using the maximum likelihood estimate. This can be seen from Fig. 3, where the maximum likelihood estimates tend to deviate substantially from the experimental results.

To compare the predictive ability of the models, namely, the Weibull and exponential processes, the estimates obtained from these models are plotted along with the experimental data in Fig. 4. It can be seen that the both models approximate experimental results reasonably well. In general, however, the Weibull model tends to underestimate the experimental results while the exponential model tends to overestimate. After the hydrolysis time

of about 12 hours, the Weibull model appears to overestimate while the exponential model tends to underestimate. On the basis of the parameter estimates obtained using both the methods, least square estimation and maximum likelihood estimation, the values of estimated means and variances can be obtained for both Weibull and exponential process. These values are tabulated in Table 3. It can be seen that for the Weibull process, the estimates of mean and variance obtained by the least square method do not differ widely from those obtained by the maximum likelihood method. For the exponential process, such comparison cannot be made because the estimates obtained by the maximum likelihood method appear to be unreasonable.

CONCLUSIONS

Two different non-homogeneous Poisson models, namely, Weibull and exponential, are proposed to describe the behavior of enzymatic hydrolysis of wheat straw as a renewal reward process. Two different methods, namely, least square estimation and maximum likelihood estimation have been used for determination of the model parameters. The computation has been performed using a non-linear adaptive random search technique.

It has been shown that both the models, Weibull and exponential, represent the hydrolysis process fairly well. Of the two different estimation methods, the least square estimation method has yielded parameter values that can predict the experimental results reasonably well according to either the Weibull or exponential model. Although the maximum likelihood estimate yielded valid parameter estimates for the Weibull model, it failed to yield reasonable parameter values for the exponential model.

REFERENCES

1. Chen, H. T. and L. T. Fan, "Multiple Minima in a Fluidized Reactor-Heater System," AIChE J., 22, 680-685 (1976).

2. Fan, L. T., H. T. Chen, and D. Aldis, "An Adaptive Random Search Procedure for Large Scale Industrial and Process Systems Synthesis," Proceedings of Symposium on Computers in the Design and Erection of Chemical Plants, pp. 279-291, Karlovy Vary, Czechoslovakia, Aug. 31 - Sept. 4, 1975.

3. Fan, L. T., M. M. Gharpuray, and Y. H. Lee, "Evaluation of Pretreatments for Enzymatic Conversion of Agricultural Residues," Biotechnol. Bioeng. Symp. no. 11, 29 (1981).

4. Lee, Y. H., L. T. Fan, and L. S. Fan, "Kinetics of Hydrolysis of Insoluble Cellulose by Cellulase," Adv. Biochem. Eng., 17, 131 (1980).

5. Lee, Y. H., "Enzymatic Hydrolysis of Insoluble Cellulose, a Kinetic Study," Ph.D. Dissertation, Kansas State Univ., 1981.

6. Mood, A. M., F. A. Graybill, and D. C. Boes, "Introduction to the Theory of Statistics," McGraw Hill, New York, 1974.

7. Ross, S. M., "Introduction to Probability Models," p. 236, Academic Press, New York (1980).

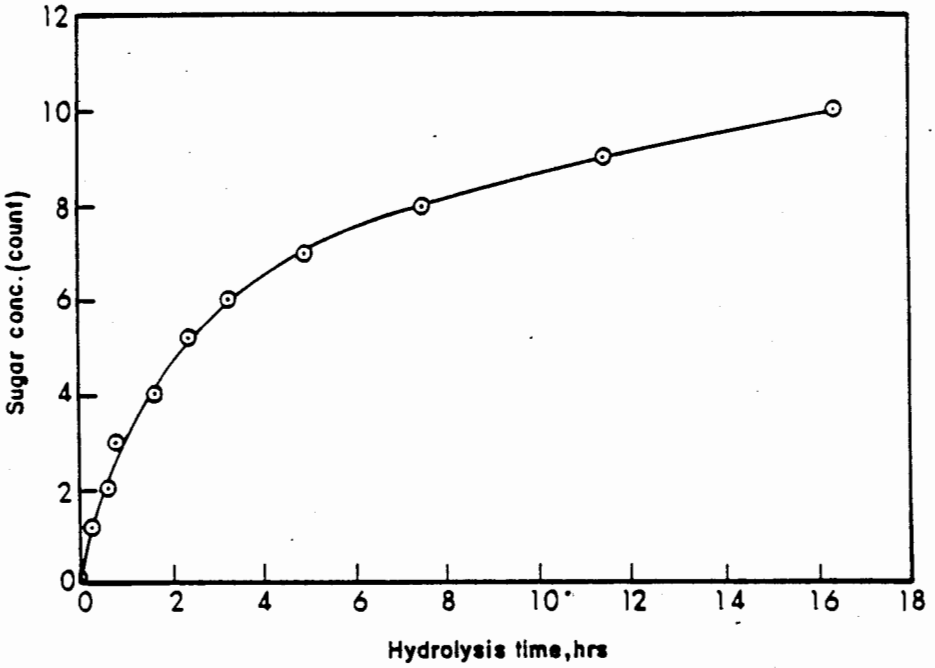

Fig. 1. A typical curve representing the progress of enzymatic hydrolysis of wheat straw.

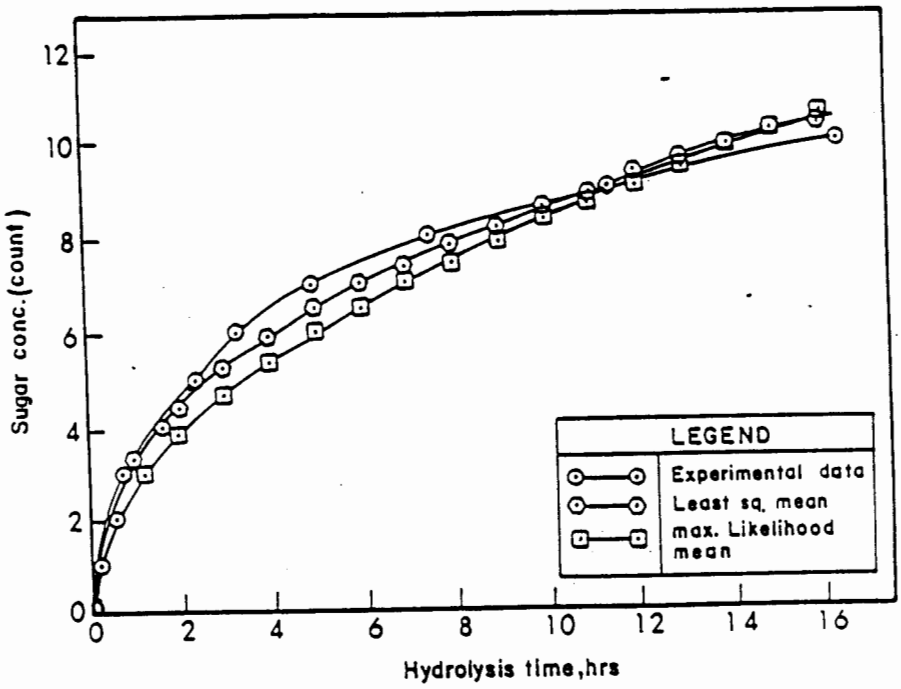

Fig. 2. Comparison of the Weibull process estimation with the experimental data.

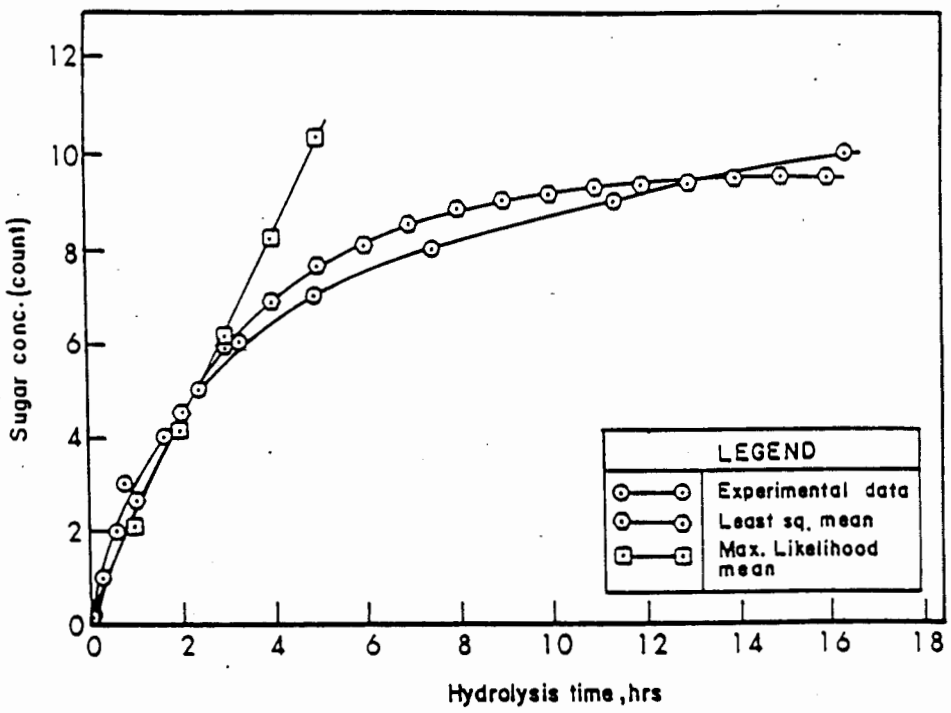

Fig.3. Comparison of the exponential process estimation with the experimental data.

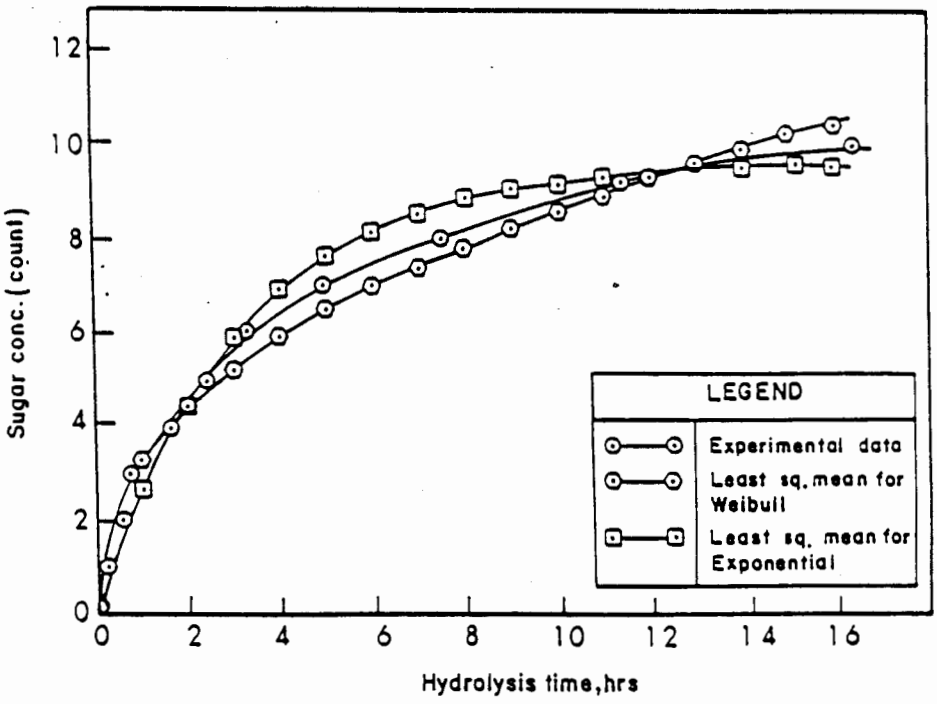

Fig. 4. Comparison between the means estimated by the Weibull process and the exponential process.

Table 1. Experimental data for enzymatic hydrolysis of wheat straw

obs. no.	sugar conc. count*	hydrolysis time, hrs.
1	1	0.25
2	2	0.6
3	3	0.75
4	4	1.65
5	5	2.4
6	6	3.3
7	7	4.95
8	8	7.5
9	9	11.4
10	10	16.4

*each count = 2.5 g/ℓ

Table 2. Estimated Values of the model parameters.

		Least Square Method	Maximum Likelihood M.
WEIBULL Proc.	λ	3.9197	3.02974
	β	0.4133	0.48758
	p	0.8472	0.8997
Expo. PROCESS	η	7.2779	10.0000
	θ	0.3222	0.0005
	p	0.4141	0.2054

Table 3. Mean and Variance estimates from the models.

	Estimates	Least square	MLE
Weibull Proc.	Mean E[X(t)]	$3.3207\ t^{0.4133}$	$2.726\ t^{0.48758}$
	Variance Var[X(t)]	$3.3207\ t^{0.4133}$	$2.726\ t^{0.48758}$
Expo. Process	Mean E[X(t)]	$9.354(1 - e^{-0.3222\ t})$	$4010(1 - e^{-0.0005\ t})$
	Variance Var[X(t)]	$9.354(1 - e^{-0.3222\ t})$	$4010(1 - e^{-0.0005\ t})$

List of Participants

Michael K. Dowd	Iowa State University
Chuck Glatz	
Zivko Nikalov	
Mike Meagher	
Peter J. Reilly	
Mike Sierks	
Etienne Selosse	
Bernard Tao	
Kate M. V. Baptie	Colorado State University
Jose L. Ibave	
Keith Lange	
Chih-Ming Li	
Jim Linden	
Lucas Alvarez-Martinez	
Ming Shiang	
Gred Sinton	
Larry E. Erickson	Kansas State University
Hyeon Yong Lee	
Mehmet D. Oner	
Snehal A. Patel	
R. Seeta	
Shahriar Alam	University of Missouri-Columbia
Rakesh K. Bajpai	
Yong Jayanata	
B. V. Mallu	
G. Natarajan	
Joey Patterson	
George Preckshot	
David Stevens	
Mark Yu	
Sam Watson (Energen Inc.)	
Oliver Sitton	University of Missouri-Rolla
Eric Dunlap	Washington University, St. Louis
Jeff Fowler	
Marilyn Mattione	
Morris Rosenberg	
Shao-Jian Ye	